A NUMERICAL STUDY ON COMBINED EFFECT OF DEFLECTOR PLATE, TWIST ANGLE OF BLADES, AND TIP SPEED RATIO ON THE PERFORMANCE OF SAVONIUS HYDROKINETIC TURBINE

A DISSERTATION

SUBMITTED IN PARTIAL FULFILLMENT OF THE REQUIREMENTS
FOR THE AWARD OF THE DEGREE
OF

MASTER OF TECHNOLOGY
IN
THERMAL ENGINEERING

Submitted by:
Souvik Samadder
2K20/THE/20

Under the supervision of
PROF. B. B. ARORA

DEPARTMENT OF MECHANICAL ENGINEERING
DELHI TECHNOLOGICAL UNIVERSITY
(Formerly Delhi College of Engineering)
Bawana Road, Delhi-110042

MAY, 2022

DELHI TECHNOLOGICAL UNIVERSITY
(Formerly Delhi College of Engineering)
Bawana Road, Delhi-110042

CANDIDATE'S DECLARATION

I, Souvik Samadder, 2K20/THE/20 student of M. Tech. Thermal Engineering, hereby declare that the project Dissertation titled "A numerical study on combined effect of deflector plate, twist angle of blades, and tip speed ratio on the performance of savonius hydrokinetic turbine" which is submitted by me to the Department of Mechanical Engineering, Delhi Technological University, Delhi in partial fulfillment of the requirement for the award of the degree of Master of Technology, carried out under the supervision of **Prof. B. B. Arora**, is original and not copied from any source without proper citation. This work has not previously formed the basis for the award of any Degree, Diploma Associateship, Fellowship or other similar title or recognition.

Place: Delhi **SOUVIK SAMADDER**

Date: 25/05/2022 **2K20/THE/20**

DEPARTMENT OF MECHANICAL ENGINEERING
DELHI TECHNOLOGICAL UNIVERSITY
(Formerly Delhi College of Engineering)
Bawana Road, Delhi-110042

CERTIFICATE

I hereby certify that the Project Dissertation titled "A numerical study on combined effect of deflector plate, twist angle of blades, and tip speed ratio on the performance of savonius hydrokinetic turbine" which is submitted by Souvik Samadder, 2K20/THE/20, Department Of Mechanical Engineering, Delhi Technological University, Delhi in partial fulfillment of the requirement for the award of the degree of Master of Technology, is a record of the project work carried out by the student under my supervision. To the best of my knowledge this work has not been submitted in part or full for any Degree or Diploma to this University or elsewhere.

Place: Delhi
Date: 25/05/2022

PROF. B. B. ARORA
SUPERVISOR
Professor,
Department of Mechanical Engineering,
Delhi Technological University, Delhi
Bawana Road, Delhi-110042

ABSTRACT

Savonius Hydrokinetic Turbine (SHT) is a small-scale renewable energy source that is a sustainable solution for remote areas and rural electrification. The current research work establishes a numerical study on combined effect of deflector plate (no deflector, deflector at 90°, deflector at 45°), twist angle of blades (0°, 12.5°, 25°), and tip speed ratio (0.5 to 1.5) on the turbine efficiency in terms of power coefficient (C_p) using CFD simulation considering a realizable k-ε turbulence model. A total of 99 simulations were performed considering all the above different conditions. To validate the results, simulations were compared with the results of a previous study having no deflector plate. It has been identified that SHT with blade twist angle of 12.5° and deflector plate at 90° produces highest power coefficient as 0.364 at tip speed ratio of 0.9 and 0.5 m/s water velocity. Similarly, SHT having a blade twist angle of 25° with deflector plate at 90° yields the highest torque coefficient as 0.454 at a TSR of 0.5. It was observed that C_p increases by an average 15% for SHT having blade twist and deflector plate as compared to SHT without blade twist and deflector plate.

ACKNOWLEDGEMENT

I would like to express my deepest appreciation to all those who provided me the possibility to work on this project. I owe a debt of gratitude to my mentor, **Professor B. B. Arora, Department of Mechanical Engineering, DTU**, for incorporating in the idea of a creative major project, helping me in undertaking this project and also for being there whenever I needed his assistance.

I'm also grateful to all my esteem **faculty members** of department of mechanical engineering, for their astute guidance, constant encouragement and sincere support for this project work. I feel proud and privileged in expressing my deep sense of gratitude to all those who have helped me in presenting this project.

I would also like to thanks **Mr. Ashutosh Mishra, Research Scholar, DTU,** for helping and guiding throughout my research work.

I also wish to thank all my **classmates** for their support and encouragement.

Last but never the least, I thank my respected **parents** for always being with me, in every sense.

SOUVIK SAMADDER

2K20/THE/20

CONTENTS

LIST OF TABLES

LIST OF FIGURES

LIST OF SYMBOLS, ABBRIVATIONS AND NOMENCLATURE

C_p = Coefficient of Power

C_t = Coefficient of Torque

ρ = density of water [kg/m^3]

V = free stream velocity [m/s]

A = swept area of turbine [m^2]

ω = rotational speed of turbine [rad/s]

R = radius of the turbine [m]

T = average moment generated on the turbine [Nm]

TSR = Tip Speed Ratio

SHT = Savonius Hydrokinetic Turbine

k = turbulent kinetic energy

ε = dissipation rate of turbulent kinetic energy

u_j = velocity components

x_j = Cartesian coordinate

t = time

μ = viscosity

Coeff. = Coefficient

μ_t = turbulent viscosity

σ_k = constant of k-ε turbulence model

G_k = production of turbulent kinetic energy because of velocity difference

G_b = production of turbulent kinetic energy because of buoyancy

Y_M = impact of altering dilatation in compressible turbulence to the total dispersal rate

$\acute{\Omega}_{ij}$ = rotational tensor observed in a reference outline with the angular velocity ω_k

CHAPTER 1

INTRODUCTION

Lately, the growing global energy need, the increasing reliability and cost of fossil fuels, and the unforeseen environmental threats associated with the consumption of fossil fuels have significantly increased the demand for renewable energy [1]. Global electricity demand increased by 81% from 13,152 TWh in 2000 to 23,845 TWh in 2019 and is anticipated to increase by another 58% by 2040 [2]. Global CO2 emission has increased by 61% in 31 years from 20.5 Gt in 1990 to 33.0 Gt in 2021 [3]. These crises have led researchers to search for new renewable sources to fulfill energy demand, decrease the dependency on petroleum derivatives, and reduce carbon emission that harm the environment. Nonetheless, the global renewable energy capacity has shown substantial growth of more than 170% from 1,135 GW in 2009 to 3,064 GW in 2021 [4]. Fig. 1.1 shows that, hydropower contributed the highest

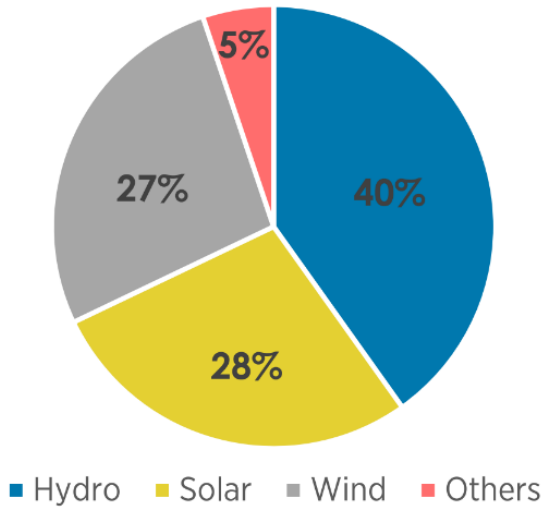

Fig. 1.1. Global renewable generation capacity by energy source at the end of

proportion of worldwide total energy capacity, with an total range of 1230 GW (40%), after that solar energy with range of 849 GW (28%) and wind energy with range 825 GW (27%), respectively [4]. The left out sources estimates at 160 GW (5%), consisting of bioenergy, marine energy, and geothermal [4]. Among renewable energy sources, hydropower is ample, inexpensive, and has maximum potential for electricity production in world [5]. However, conventional largescale hydropower systems are not taken into account as environmentally friendly energy generation systems since they need development of huge water reservoir and dam, which may severely impact environment and local ecosystem [6].

Hydrokinetic turbine is a type of hydropower system that produces energy sustainably with less environmental effect. The HKT technology operates similarly to wind turbine, with the distinction of water as operational fluid. It creates power by directly capturing the kinetic energy of water, obviating the need for penstock and dam. [7]. A micro hydrokinetic turbine can act as a small-scale renewable energy source which is a practical and sustainable answer to solve electricity crisis in rural and remote area which are unconnected to the power grid where the load requirement is less than 5kW [8]. We can find stream or canals with low or no water head near rural areas. In such a water flow, installing a traditional hydroelectric plant is impractical. However, a hydrokinetic energy system can utilize the energy of flowing water with low or no head [9].

Hydrokinetic technology can provide an appealing green energy source to decrease the necessity of fossil fuels and fulfill the electricity requirement. Hydrokinetic technology is seen as an affordable and environmentally friendly option for electrification in rural and those areas which are disconnected from grid [9]. The design and construction of a traditional Savonius rotor is basic, with an 'S' geometry rotor consisting two semi-circular rotors [10]. It works on the principle of differences in drag forces that exist among the returning and advancing blade, indicated in Fig. 1.2. Savonius hydrokinetic turbine was invented in 1931 by Finnish inventor Sigurd J. Savonius to harness wind energy [12]. In direction of fluid flow, a concave geometry is provided on advancing blade and convex geometry on returning blade, former

captures a fluid volume while later disperses the same. Concave geometry experiences greater drag as compared to convex geometry which results in a net positive torque. due to blade geometry. Since more the flowing fluid is collected on the concave portion, the pressure on that portion rises, moving the rotor with a net force and positive net torque. Numerous variables can influence rotor's performance for example number of blades, blade shape, tip speed ratio (TSR), end plate, aspect ratio, multi-staging, external improvement technique, and many more. [10,13].

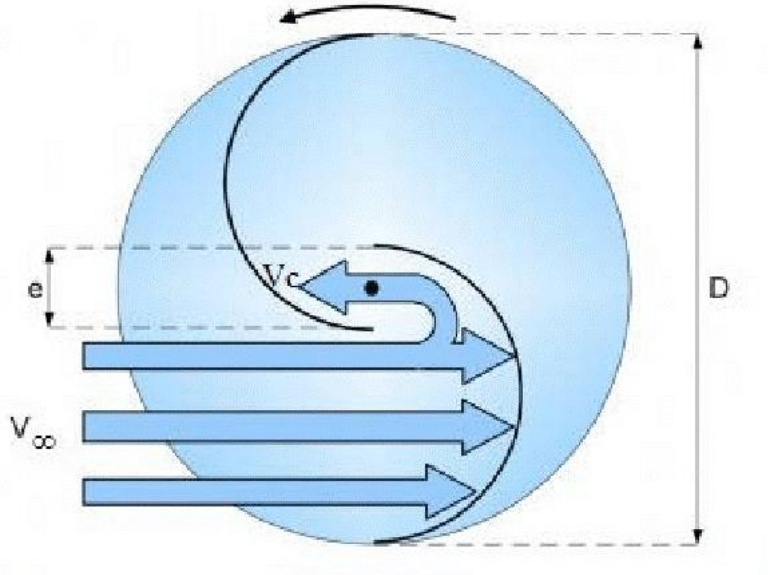

Fig 1.2. Savonius rotor working principle [11]

When we compare Savonius hydrokinetic turbine (SHT) to the conventional hydropower turbine, it begins rotation at a much low water speed. Despite benefits such as low manufacturing costs, greater torque during start-up, an easy construction, less rotational velocity, minimal noise production, and direction independence of water, SHT have less efficiency and substantial static torque fluctuation [14,15]. Several studies have been performed lately to increase the efficiency of SHT. These studies, which included theoretical, numerical, and experimental work, aimed to improve geometrical factors, blade design, and the employment of different improvement methods [16]. Savonius rotors having twisted blades have better effectiveness, smooth running, and start-up capacity than semicircular blade rotors [17]. Because of the longer moment arm, blades with angle

of twist yields greater moment as compared to a semicircular profile. Highest force operates center and vertical in a semicircular rotor, whereas most power is generated at the blade's tip in the case of twisted blade due to the twist in the blade. A blade with twist angle has a greater arm moment as result of these changes, and hence a larger power coefficient value [18]. Saha et al. [19] conducted experiments to investigate the effect of blade geometry on rotor performance, they evaluated the performance of Savonius rotors with 12.5° twist angle of blade and it was found that in all circumstances of single, two, and three-stage, the savonius rotor having twist showed improved performance compared to rotor having no twist. To summarise, a 2-stage system with angle of twist had highest power coefficient, $C_p = 0.31$. Kumar et al. [20] performed numerical analysis using CFD for optimization angle of twist of SHT and it was concluded that a SHT with 12.5° blade twist angle provides a highest power coefficient $C_p = 0.39$, at tip speed ratio of 0.9 for 2 m/s free stream velocity of water.

Since the beginning of study on Savonius rotor design, researchers have been interested in tip speed ratio. Mechanical design of turbine, that is number of blades and diameter of rotor, are significant parameters that effect tip speed ratio. If turbine blade rotates at low velocity, they cannot capture the majority of the water and will travel through the rotor with less water. However, if the turbine blade rotates at high velocity, it will constantly pass-through turbulent waters. There should be enough time between rotors passing by the same area for adjacent water to flow in and be harnessed, rather than the used, turbulent water [21]. According to the study of Sheldahl et al. [22], the coefficient of power for 2 and 3 blades of savonius wind turbine is optimal for TSR of 0.9 and 0.7, respectively. Zhao et al. [23] found that the maximum power coefficients for a helical Savonius rotor at tip speed ratio of 0.81 and 0.55 for 2 and 3-blade turbines. Kailash et al. [24] performed analysis of modified SHT and obtained a $C_{p,max}$ of 0.15 at tip speed ratio of 0.7. According to Kamoji. et al. [25], at maximum coefficient of power ($C_{p,max}$), tip speed ratio was determined as 0.69 for a modified Savonius turbine. Furthermore, Golecha et al. [26,27] put modified single-stage turbine having deflector plates in front of returning blade and two deflector plates in front of returning and advancing blades to the test in a water-based environment, and found that the tip speed ratio at max. power coefficient 0.82 for single deflector plate and 1.08 for two deflector plates.

Another performance enhancement technique of Savonius turbine is to utilise deflector, they eventually prevent and divert the fluid stream from striking the front of returning blade of the rotor and minimises drag on returning blade, resulting in a large increase in power output [28]. A deflector can be a useful device for enhancing the efficiency in both water and wind application [29], however they are required to be built and combined with the turbine before it can be practically used. The angle of deflector plate does not change in case of hydrokinetic application since the fluid stream in a river can be fairly anticipated as compared with wind [30]. Wind flow, on the other hand, can flow in any direction, complicating design integration [31]. Iio et al. [32] employed a level plate deflector to improve savonius rotor's power coefficient. The analysis illustrated that utilizing a single flat deflector enhanced the $C_{p,max}$= 0.47 by 80% in comparison to a rotor with no deflector. Golecha [26] performed an experiment to examine how a flat plate deflector arrangement affects performance of SHT, which Kamoji et al. [25] had previously investigated. In their research, they examined eight various deflector configurations placed at returning blade and discovered that power coefficient rose 50% to $C_{p,max}$=0.21 at TSR=0.82 when deflector plate angle was set to 101° [26].

Previous studies have shown individually that the variation of blade twist angle, tip speed ratio, and deflector plate angle can significantly improve the efficiency of Savonius hydrokinetic turbine (SHT) with respect to power coefficient (C_p). Many researches have been carried out in the case of wind turbine applications but there is a research gap in case of hydrokinetic applications considering a combination of these three design parameters as stated above. In the present work, a numerical investigation has been performed on Savonius hydrokinetic turbine rotor having a combination of 3 deflector plate configurations along with 3 varying blade twist angles at 11 different tip speed ratios (TSR) to check the practicality of combined effect of the deflector, blade twist, and TSR to improve the efficiency of turbine with respect to power and torque coefficient and to perform comparison of turbine for case of with or without deflector plate and blade twist.

CHAPTER 2

RESEARCH METHODOLOGY

2.1. PERFORMANCE PARAMETER

The Savonius Turbine's efficiency is measured by power and torque coefficient as stated below:

$$TSR = \frac{\omega R}{V} \tag{2.1}$$

$$C_t = \frac{T}{0.5\rho AV^2R} \tag{2.2}$$

$$C_p = \frac{T\,\omega}{0.5\rho AV^3} = \frac{T}{0.5\rho AV^2R}\frac{\omega R}{V} = C_t \times TSR \tag{2.3}$$

2.2. CONFIGURATIONS OF DEFLECTOR PLATE

Fig. 2.1 shows the 3 configurations of turbine and deflector plate used for analysis having 2 blades. First configuration design is considered without and deflector plate. Second design consists a deflector plate placed at 90˚ to the direction of liquid flow. Third design consists a deflector plate placed at 45˚ to the direction of liquid flow. Further analysis has been done by increasing the twist angle of blades viz. 0˚, 12.5˚ and 25˚.

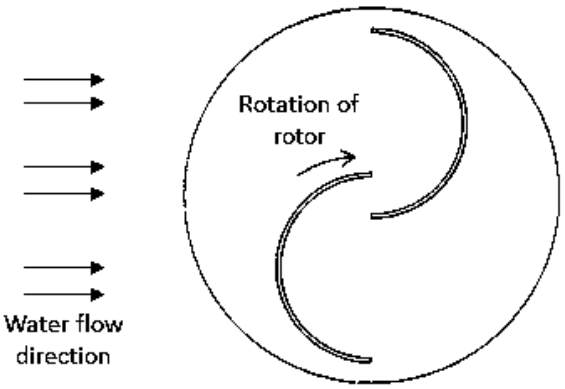

(a)

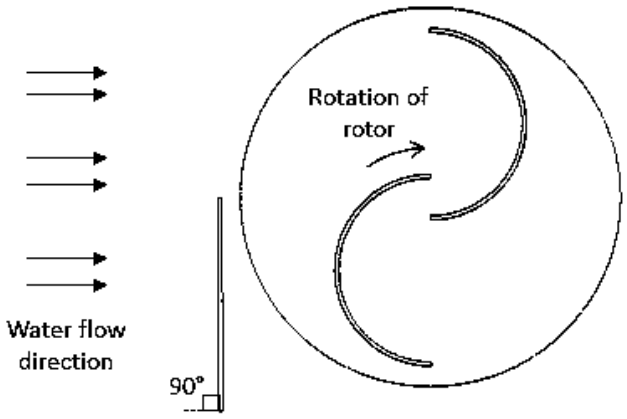

(b)

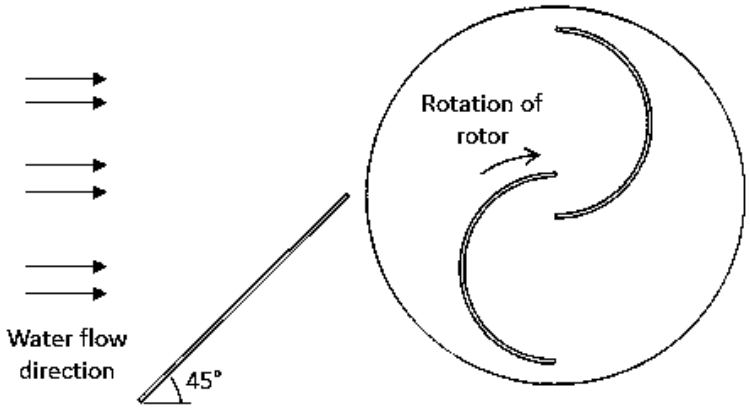

(c)

Fig. 2.1. Configurations of blades and deflector plate arrangement (a) no deflector plate (b) deflector plate at 90˚ (c) deflector plate at 45˚

2.3. DESIGN PARAMETERS

A two-blade Savonius turbine was modelled using SolidWorks considering various parameters as stated in Table 2.1.

Table 2.1. Design variables of savonius hydrokinetic turbine

Parameter	**Value**
Number of blades	2
Turbine diameter (D)	0.16 m
Turbine height (H)	0.25 m
Aspect ratio (H/D)	1.5625
Overlap ratio (e)	0.02 m

Fig. 2.2. shows show the schematic diagram of Savonius hydrokinetic turbine designed in SolidWoks

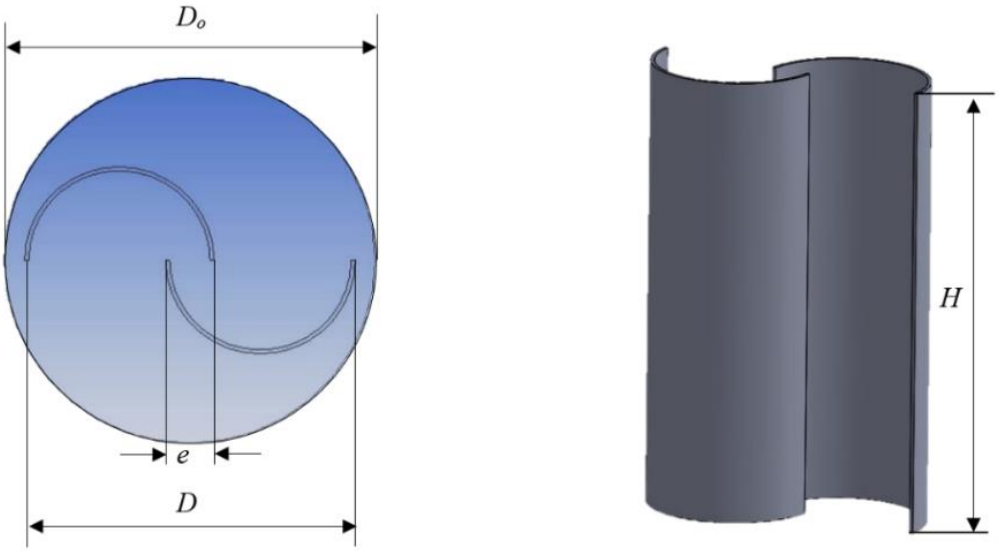

Fig. 2.2. Design parameters of Savonius hydrokinetic turbine

2.4. SAVONIUS HYDROKINETIC TURBINE DESIGN

Fig. 2.3. (a) - (b) depict side and top orientation of savonius turbine design modelled in SolidWorks based on the parameters in Table 2.1.

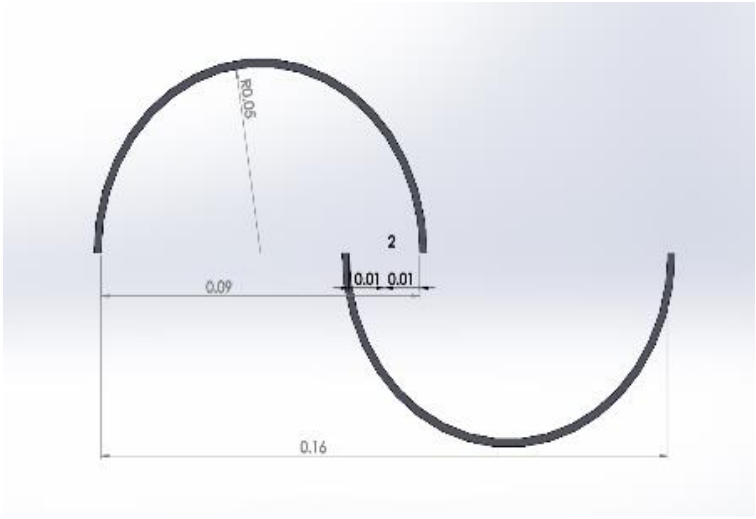

(a)

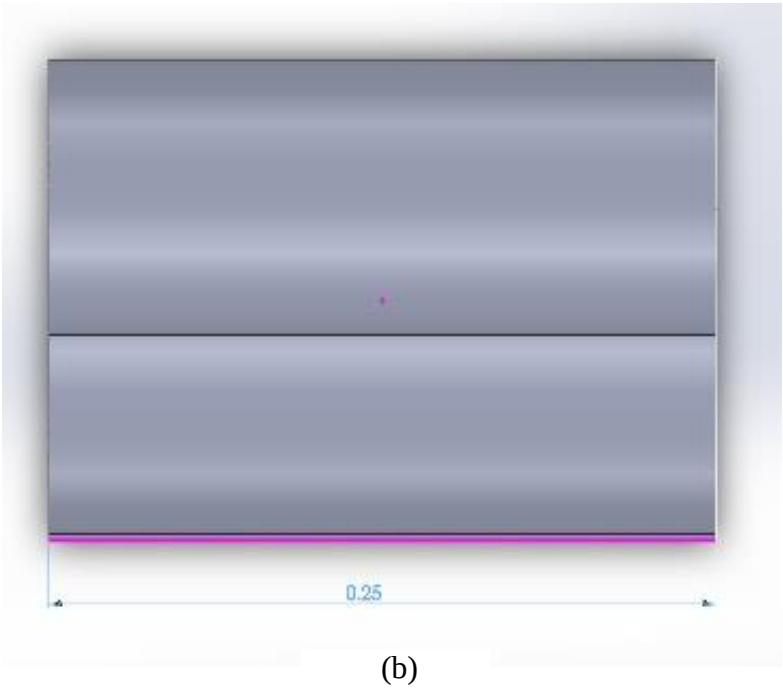

(b)

Fig. 2.3. (a) Turbine side view (b) Turbine top view

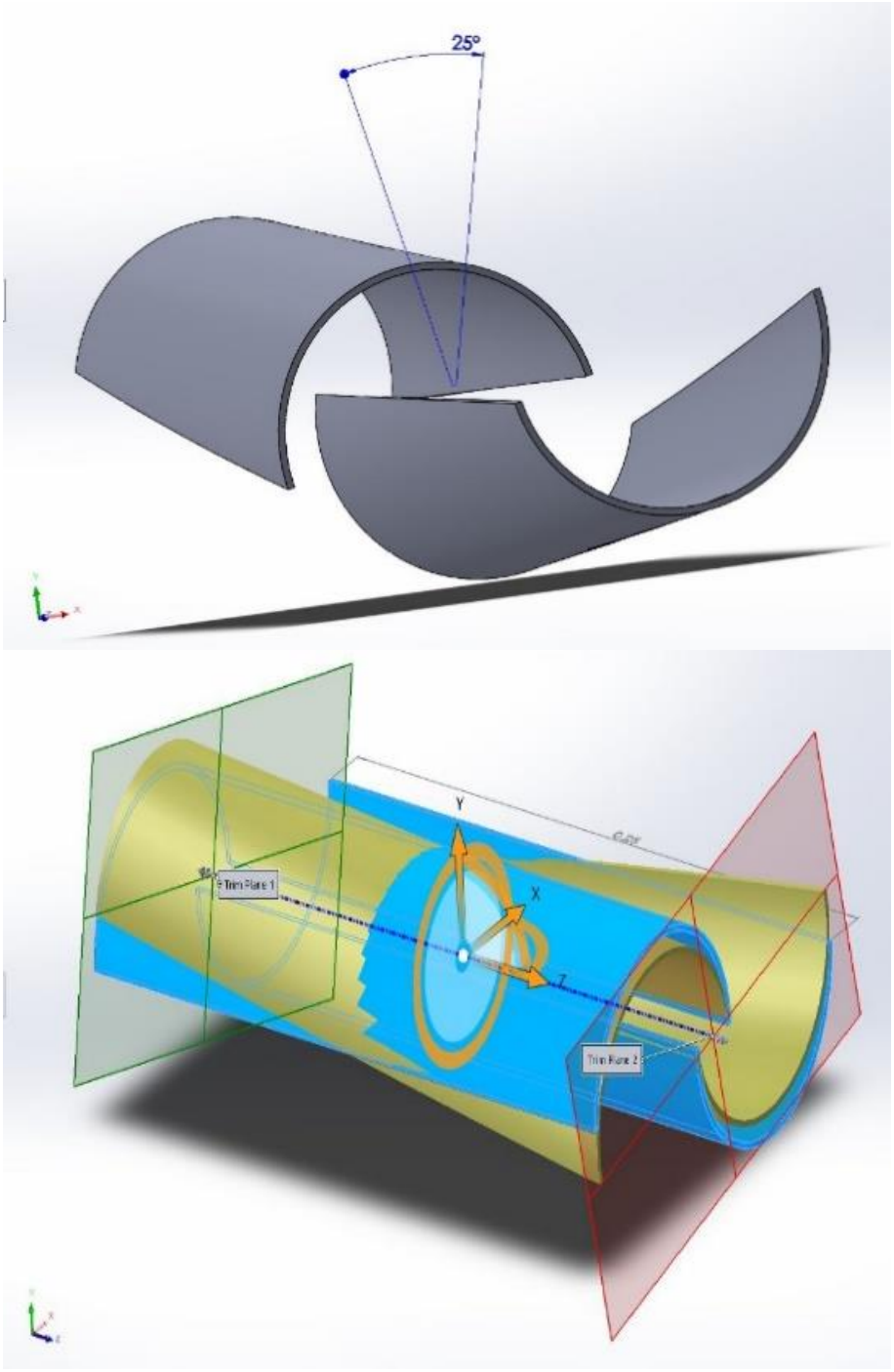

Fig. 2.4. Savonius hydrokinetic turbine with 25° twist angle of blades

Fig. 2.4 shows the isometric view of savonius turbine design with 25° twist angle of blades as modelled in SolidWorks. Similarly total 9 designs are modelled with 0°, 12.5°, 25° twist angle of blades and 3 different configuration of deflector plate. These designs are afterwards imported to ANSYS for simulations.

2.5 ROTATING ZONE

Rotating zone is the volume in the proximity of the turbine blades inside which rotation of blade takes place. Parameters considered for rotating zone are depicted in Table 2.2.

Table 2.2. Variables of rotating zone

Parameter	**Value**
Rotating zone diameter (D)	0.18 m
Rotating zone height (H)	0.27 m

2.6. STATOR ZONE

Stator zone or open channel flow is the volume where flow of water takes place. Free stream velocity in water channel considered in analysis is 0.5 m/s. Parameters for stator zone are indicated in Table 2.3.

Table 2.3. Parameters of open channel flow

Parameter	**Value**
Stator zone length	3 m
Stator zone height	0.6 m
Stator zone width	0.6 m
Blockage ratio	13.5

2.7. BOUNDARY CONDITIONS

Table 2.4. shows the various boundary conditions and boundary type taken into consideration in this study, and also depicted in Fig. 2.5. The velocity inlet on the left boundary is set to 0.5 m/s. The outflow condition is established at extreme right border. Channel's sidewall and bottom wall are designated as slip boundaries. Symmetry is given to the channel's top. Free surface effects aren't taken into account in this analysis because the turbine is thought to run at a depth that minimises the surface impact. The Savonius turbine, which is located inside the rotating zone, has a rotating wall condition (no-slip wall). The angular velocity of rotation zone is taken depending on tip speed ratio. As a result, several simulations are performed with different TSRs and free flow velocity.

Table 2.4. Boundary conditions

Boundary	**Boundary type**	**Boundary condition**
Inlet	Velocity Inlet	0.5 m/s, constant
Outlet	Outflow	Outflow
Side, bottom, top wall	Free slip	Fixed
Turbine	No slip wall	According to TSR

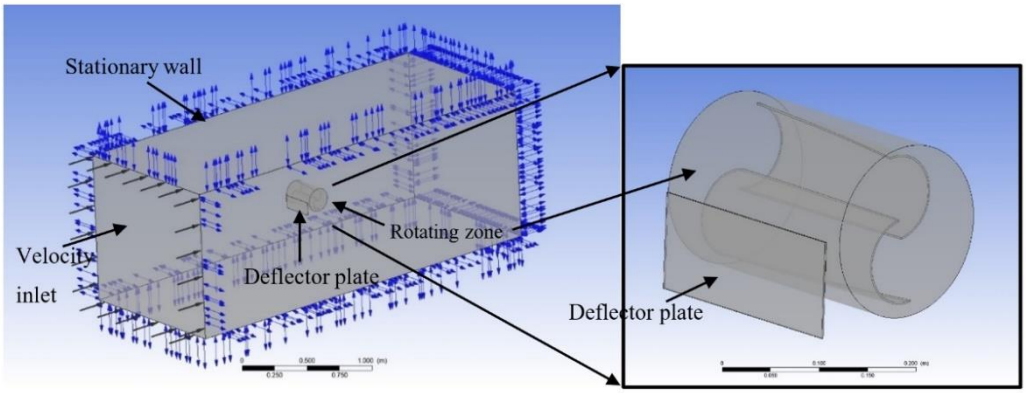

Fig. 2.5. Boundary conditions for CFD analysis

2.8. MESHING

Meshing has been done in Ansys Mesh System. For CFD investigations, a large flow domain is desired, but it must be constrained according to the computational load and the type of the flow issue being handled [33]. Computational subdomain was meshed using non-conformal unstructured lattice with tetrahedral elements. Because the mesh quality has a significant impact on the accuracy of CFD outcomes, an unstructured grid allows greater flexibility for automatic mesh generation in complex geometries. Fig. 2.6. shows the meshed model for rotor and stator zone of 0° blade twist. Number of elements for rotor zone is 4,62,451 and maximum skewness is 0.79637. Number of elements for rotor zone is 4,64,189 and maximum skewness is 0.79985.

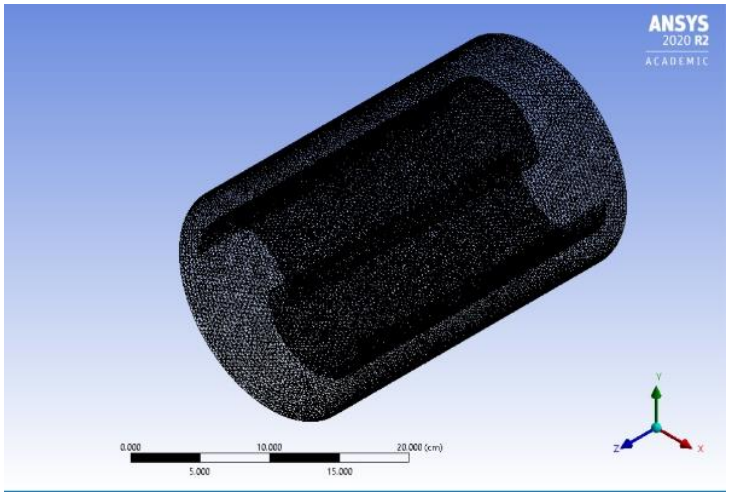

(a)

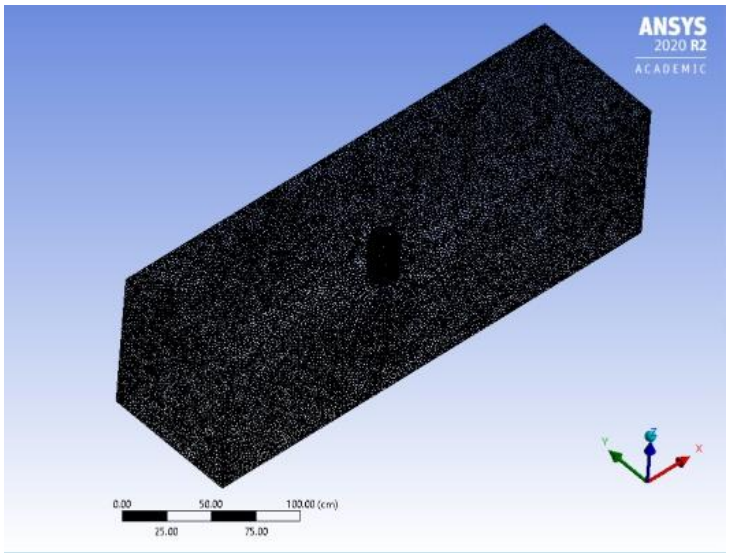

(b)

Fig. 2.6. (a) Mesh for Rotor Zone of 0° blade twist (b) Mesh for Stator Zone of 0° blade twist

CHAPTER 3

SIMULATION PROCEDURE

Flow solver used in present study is ANSYS FLUENT, which was utilised to resolve unsteady incompressible Navier-Stokes equation which are resolved with finite volume method to represent the flow fields. The condition with relevant boundary conditions are specified and resolved in order to achieve a numerical result.

3.1. TURBULENCE MODEL

Turbulence must be taken into account while modelling water flow. For modelling turbulence, a variety of models are available, and the model used is determined by the flow shape and Reynolds number. In the research by Mohamed et al. [34] it was suggested that Realizable k-ε turbulence model is better to simulate the rotating behavior of blades or air foil, flow through the channel, a boundary layer or separated flows. As a result, the Realizable k- ε model was used to represent the rotation of rotor blades in present study. This model includes a novel turbulent viscosity formulation and a new dissipation rate transport equation which derives accurate solutions for transfer of mean-square vorticity variations. Furthermore, it doesn’t consider the anticipated link between strain rate and Reynolds stress tensor.

The conditions for Realizable k- ε model are as follows [35]:

$$\frac{\partial}{\partial t}(pk) + \frac{\partial}{\partial x_j}(pku_j) = \frac{\partial}{\partial x_j}\left[\left(\mu + \frac{\mu_t}{\sigma_k}\right)\frac{\partial k}{\partial x_j}\right] + G_k + G_b - \rho\varepsilon - Y_M + S_k \quad (3.1)$$

$$\frac{\partial}{\partial t}(p\varepsilon) + \frac{\partial}{\partial x_j}(p\varepsilon u_j) = \frac{\partial}{\partial x_j}\left[\left(\mu + \frac{\mu_t}{\sigma_\varepsilon}\right)\frac{\partial \varepsilon}{\partial x_j}\right] + \rho G_k S_\varepsilon + \rho C_2 \frac{\varepsilon^2}{k+\sqrt{\vartheta\varepsilon}} + C_{1\varepsilon}\frac{\varepsilon}{k}C_3 C_b + S_\varepsilon \quad (3.2)$$

where,

$$C_1 = max\left[0.43, \frac{\eta}{\eta+5}\right], \eta = S\frac{k}{\varepsilon} \; and \; S = \sqrt{2S_{ij}S_{ij}} \quad (3.3)$$

If there should be an occurrence of normal k-ε model, C_μ is constant while for Realizable k-ε model, it differs and determined utilizing Equation (3.2) [35]:

$$C_\mu = \frac{1}{A_o + A_s\frac{kU^*}{\varepsilon}} \quad (3.4)$$

where,

$$U^* = \sqrt{S_{ij}S_{ij} + \acute{\Omega}_{ij}\acute{\Omega}_{ij}} \quad (3.5)$$

and

$$\acute{\Omega}_{ij} = \Omega_{ij} - 2\varepsilon_{ijk}\omega_k \quad (3.6)$$

$$\Omega_{ij} = \acute{\Omega}_{ij} - 2\varepsilon_{ijk}\omega_k \quad (3.7)$$

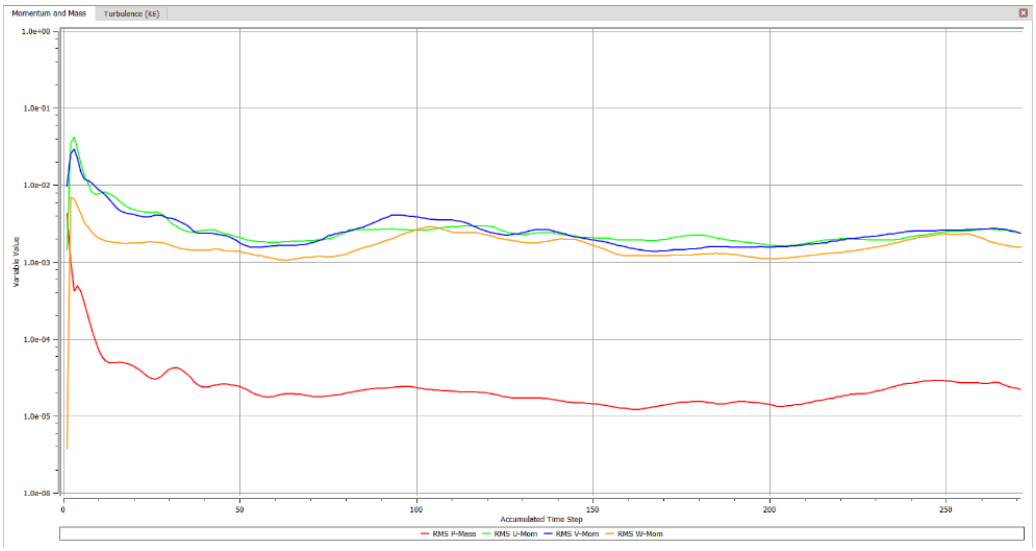

Fig. 3.2. Plot for Momentum and Mass Kinetic Energy v/s Timestep

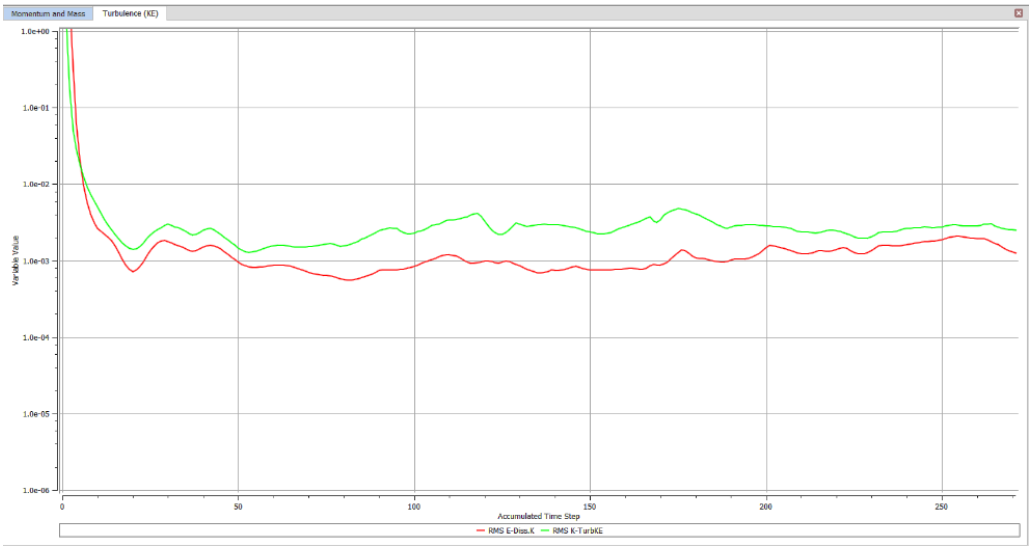

Fig. 3.1. Plot for Turbulence v/s Timestep

CHAPTER 4

RESULTS AND DISCUSSION

A total of 99 simulations were performed in this study for different tip speed ratio (TSR) values ranging from 0.5 to 1.5 and for blade twist ranging for 0˚, 12.5˚ and 25˚ for 3 different deflector plate configurations. Simulation results were achieved for all of the parameter values investigated

4.1. CONTOURS

4.1.1. Velocity Contours

At the blade's tip, a high speed zone has been observed., as shown in Fig 4.1. Low speed zone (wake zone) is noticed behind rotor blades due to turbine rotation as shown in Fig 4.1. The flow velocity in the wake zone is substantially reduced. The flow velocity is periodically raised at the higher and lower ends of the wake zone, resulting in a "periodic high speed zone."

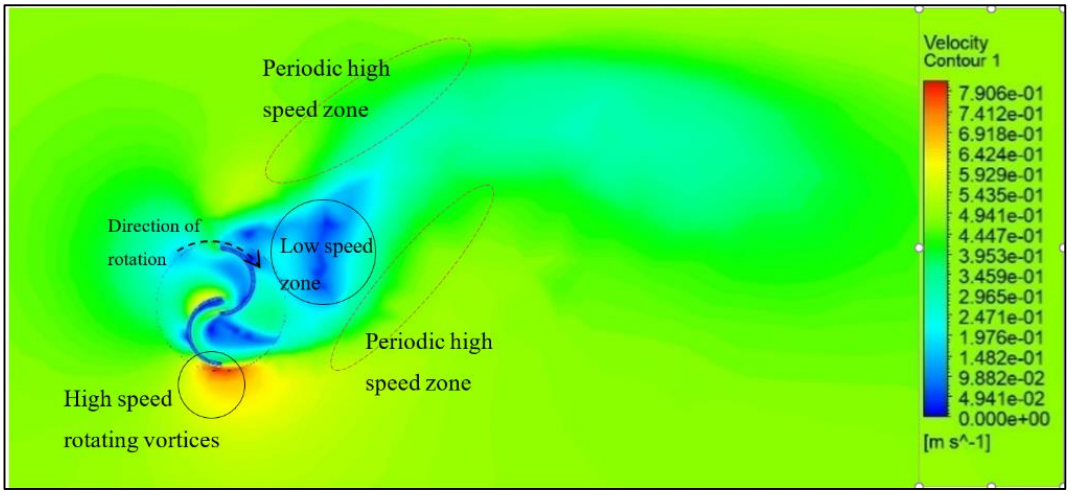

Fig. 4.1. Velocity contour for **0° blade twist at TSR of 0.7** and 0.5 m/s water velocity

4.1.2. Pressure Contours

Pressure contour plots are used to anticipate pressure differences in various places close to turbine blades in flow domain. Blue and red colours show the minimum and maximum pressure values in pressure contours, respectively. Fig. 4.2 shows that high pressure zone is created near the advancing blade whereas low

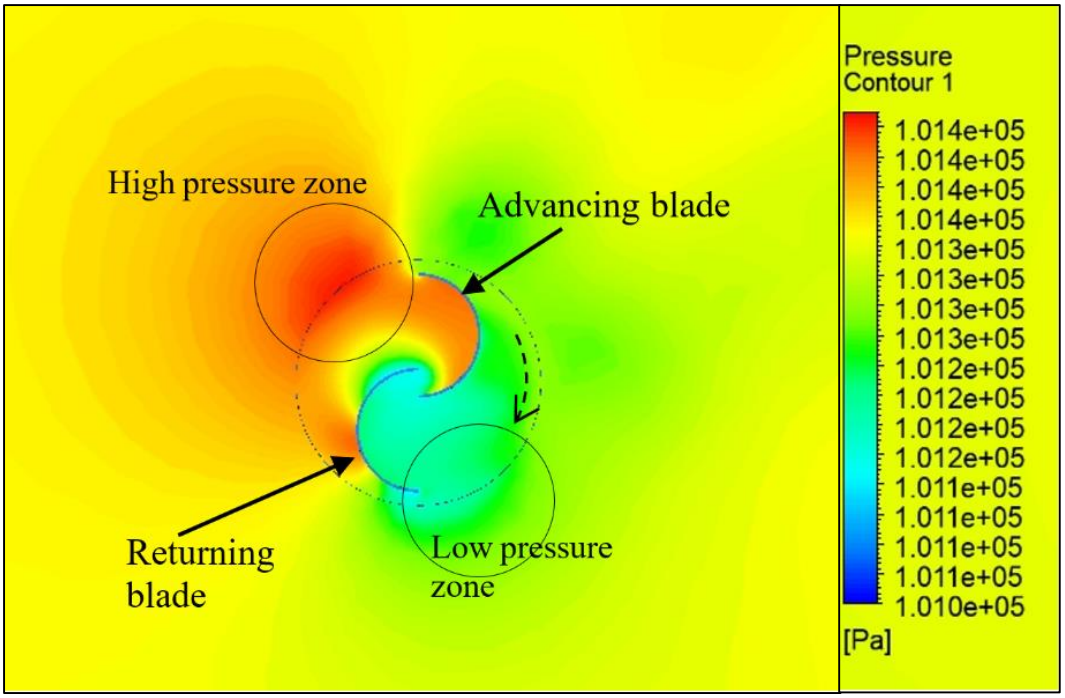

Fig. 4.2. Pressure contours for **0° blade twist at 0.7 TSR** and 0.5 m/s velocity

pressure zone is created near returning blade. Thus, these two pressure zones produce a pressure drop across the rotor and causes the blades to rotate which in turn produces power by energy abstraction by Savonius hydrokinetic turbine from the flowing fluid.

4.2. CONTOURS FOR 0° TWIST ANGLE OF BLADES

4.2.1. Velocity Contours for 0° blade twist angle without deflector

Fig. 4.3. (a)-(k) illustrates, velocity contour plots which depicts the changes in velocity across different places around the SHT having blade twist angle 0° without deflector plate at TSR ranging from 0.5 - 1.5.

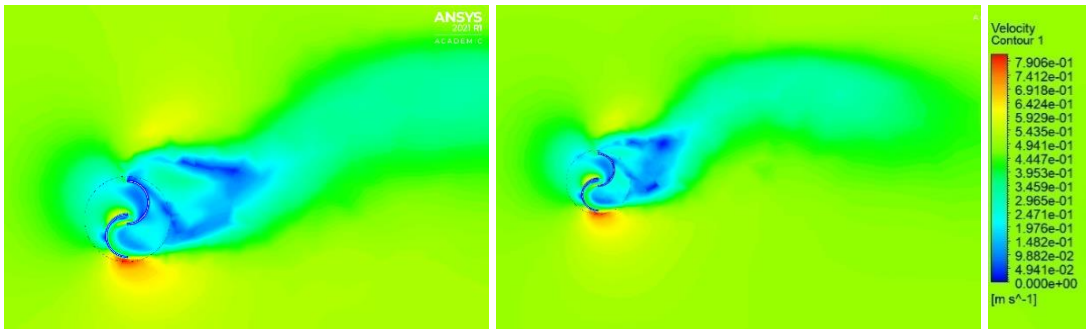

(a) 0.5 TSR (b) 0.6 TSR

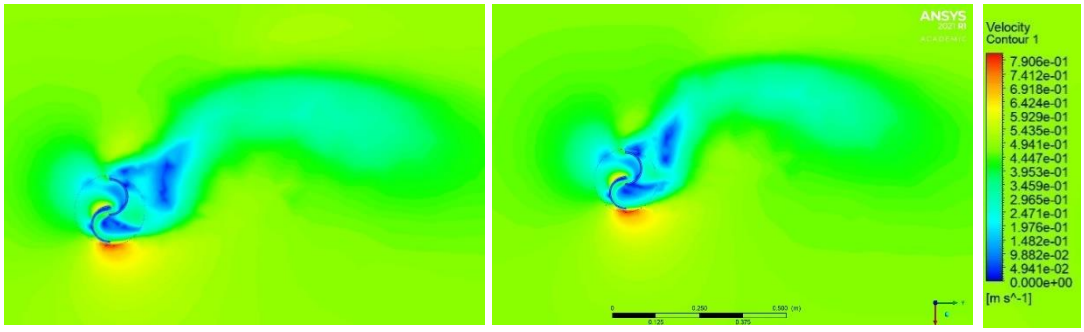

(c) 0.7 TSR (d) 0.8 TSR

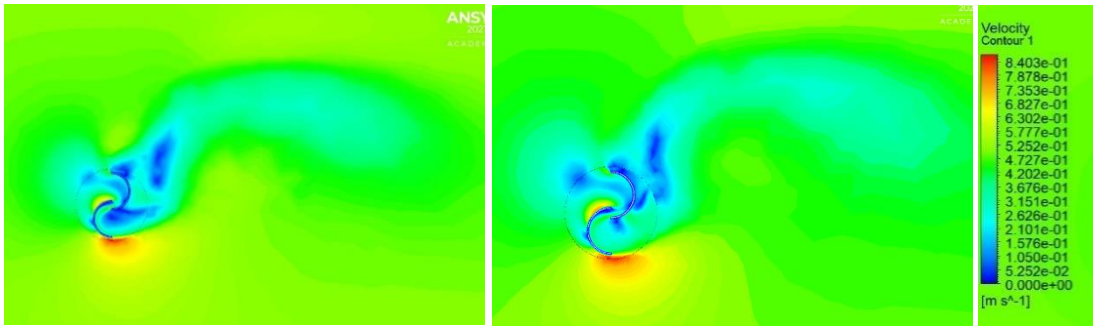

(e) 0.9 TSR (f) 1.0 TSR

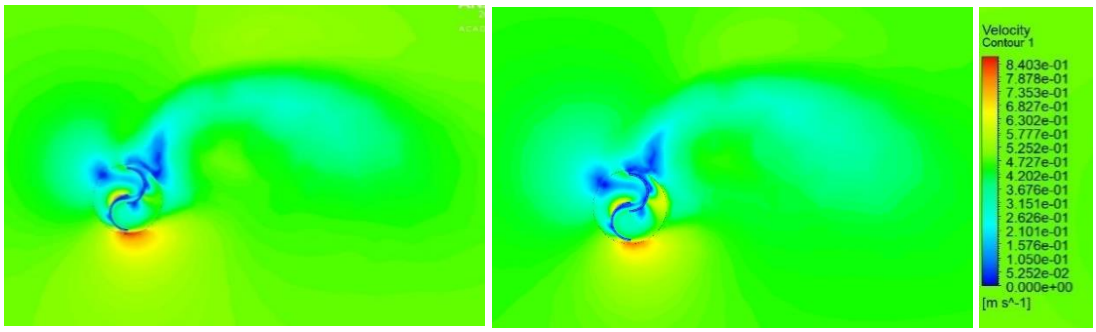

(g) 1.1 TSR (h) 1.2 TSR

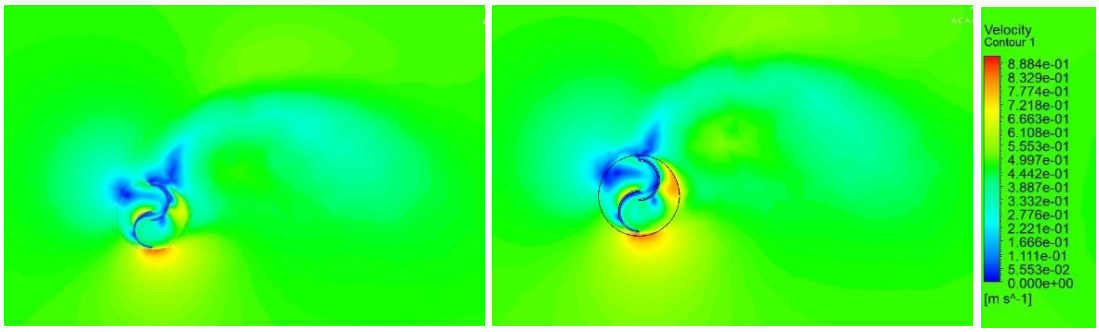

(i) 1.3 TSR (j) 1.4 TSR

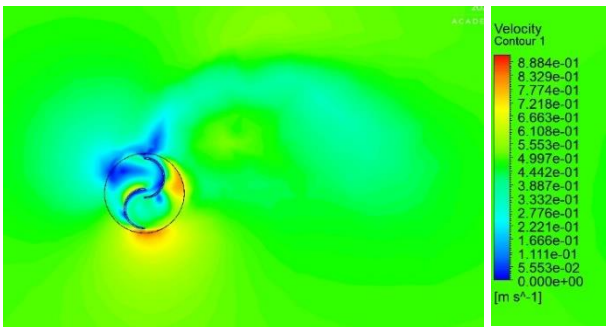

(k) 0.7 TSR

Fig. 4.3. (a) – (k) Velocity contours for **0° blade twist angle without deflector plate** at TSR ranging from 0.5 - 1.5

4.2.2. Pressure Contours for 0° blade twist angle without deflector

Fig. 4.4. (a) – (k) depicts pressure contour of rotor for 0° twist angle without deflector plate at TSR ranging from 0.5 – 1.5 and 0.5 m/s water velocity. We can observe that pressure decreases on rotor from upstream to downstream.

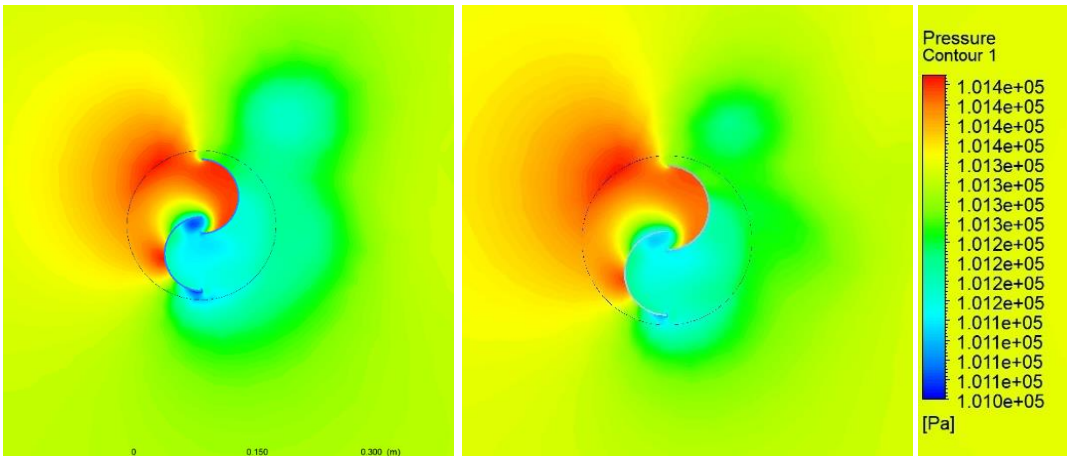

(a) 0.5 TSR (b) 0.6 TSR

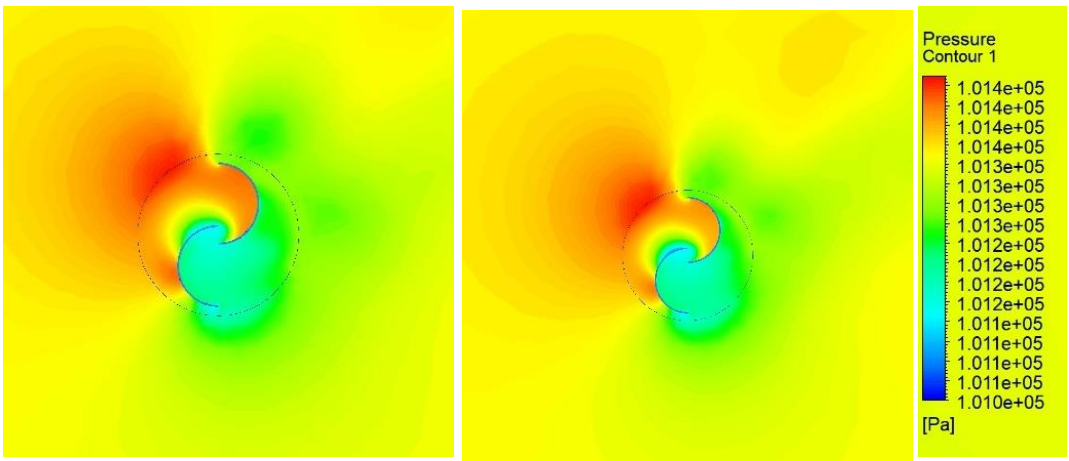

(c) 0.7 TSR (d) 0.8 TSR

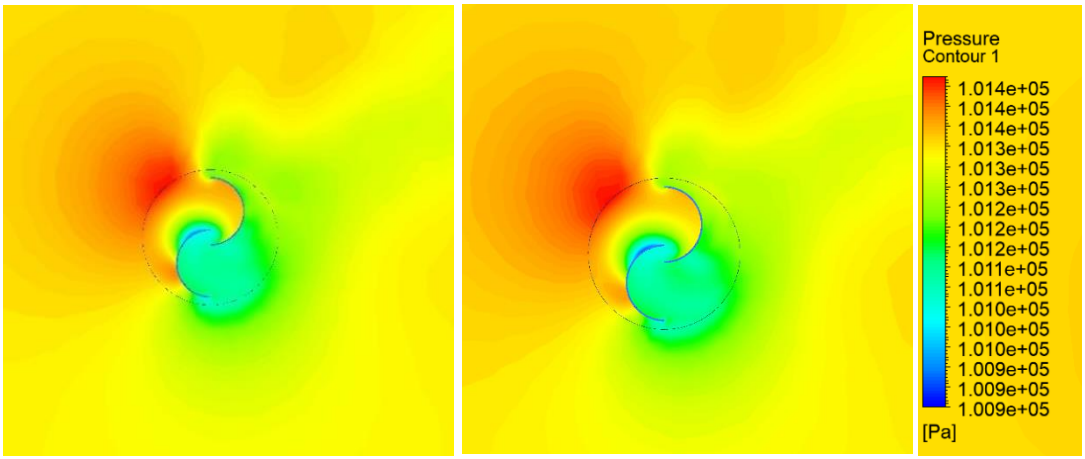

(e) 0.9 TSR (f) 1.0 TSR

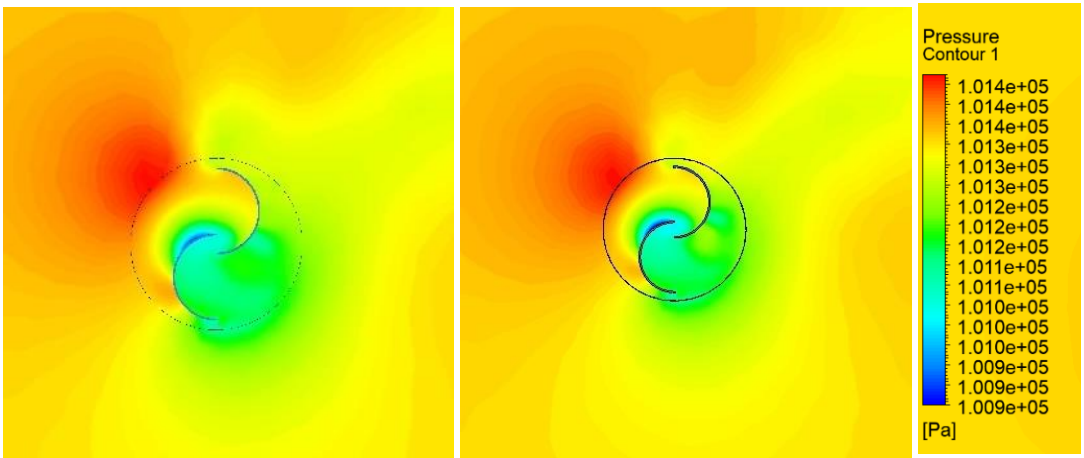

(g) 1.1 TSR (h) 1.2 TSR

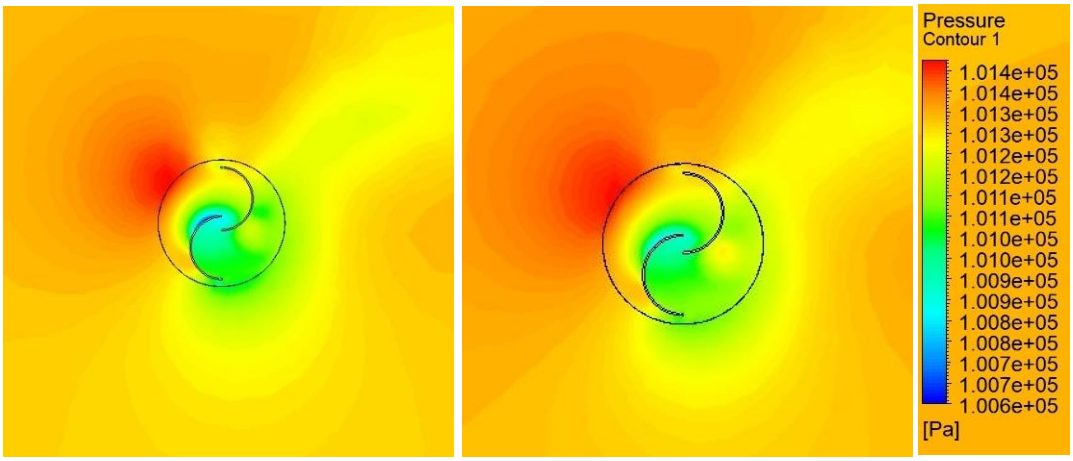

(i) 1.3 TSR (j) 1.4 TSR

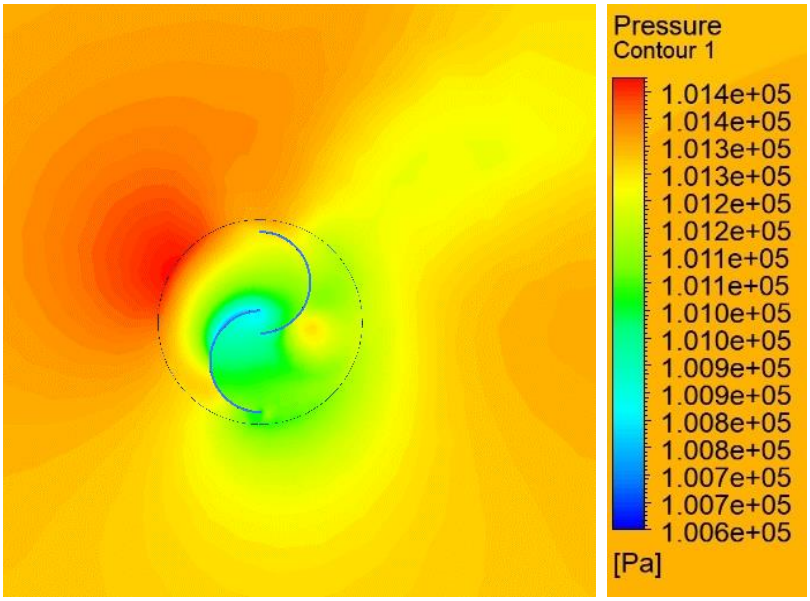

(k) 1.5 TSR

Fig. 4.4. (a) – (k) Pressure contours for **0° blade twist angle without deflector plate** at TSR ranging from 0.5 - 1.5

4.2.3. Velocity Contours for 0° blade twist angle with deflector plate at 90°

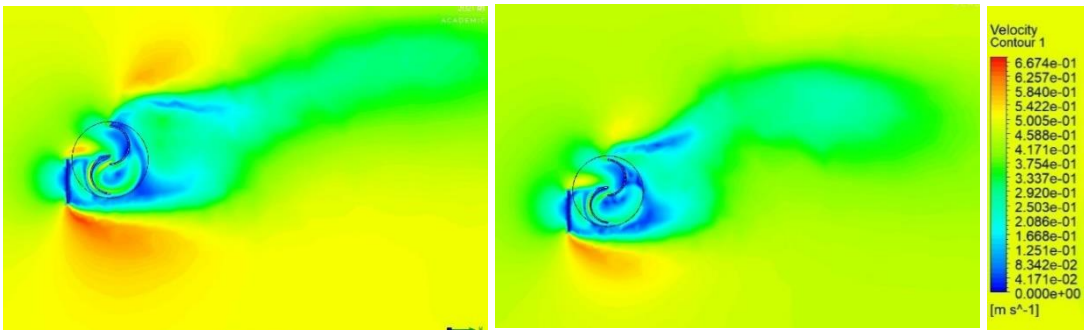

(a) 0.5 TSR (b) 0.7 TSR

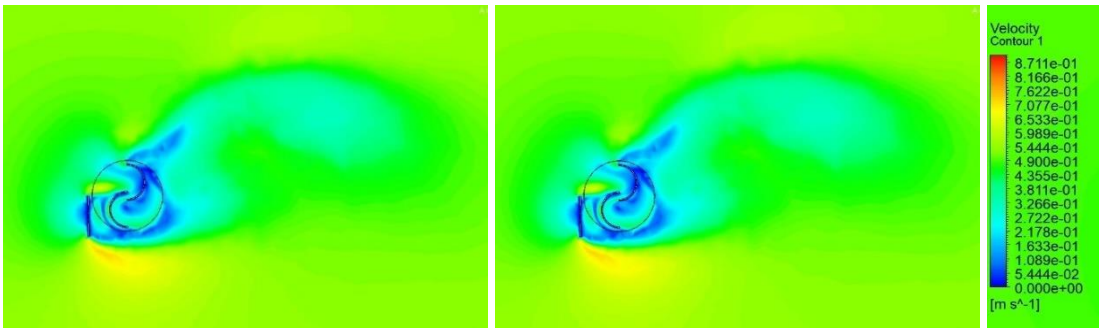

(c) 0.9 TSR (d) 1.1 TSR

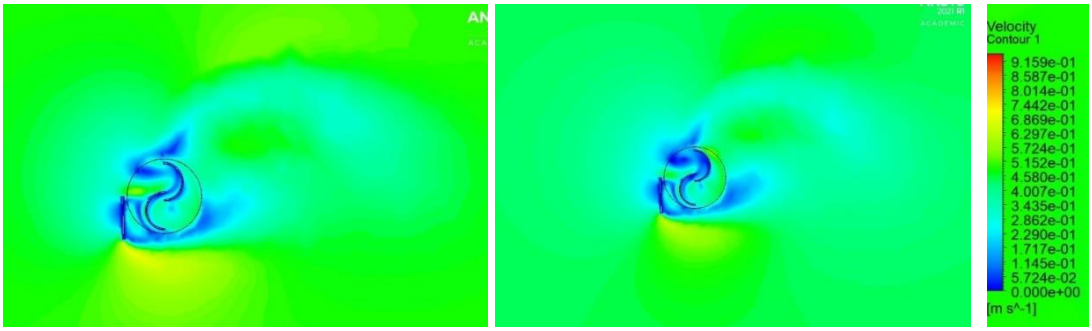

(e) 1.3 TSR (f) 1.5 TSR

Fig. 4.5. (a) – (k) Velocity contours for **0° blade twist angle with deflector plate at 90°** at TSR ranging from 0.5 - 1.5

4.2.4. Pressure Contours for 0° blade twist angle with deflector plate at 90°

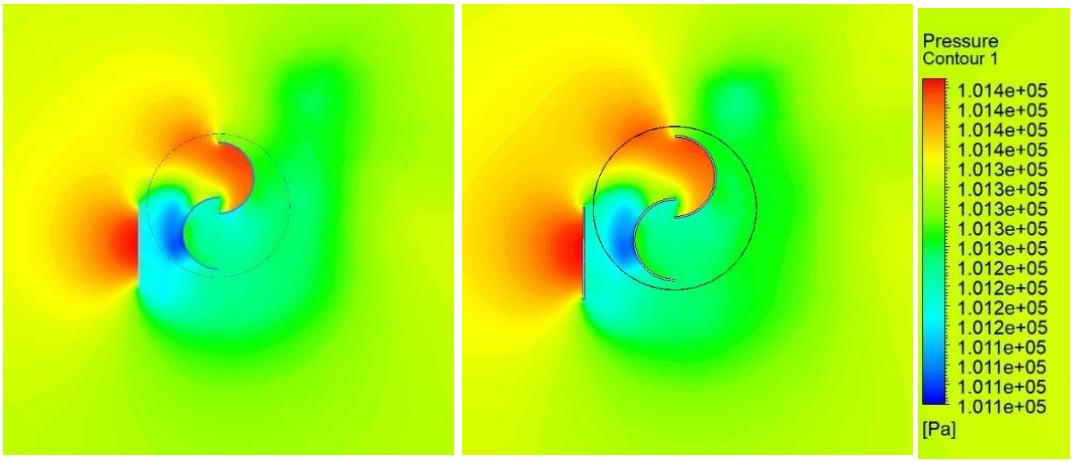

(a) 0.5 TSR (b) 0.6 TSR

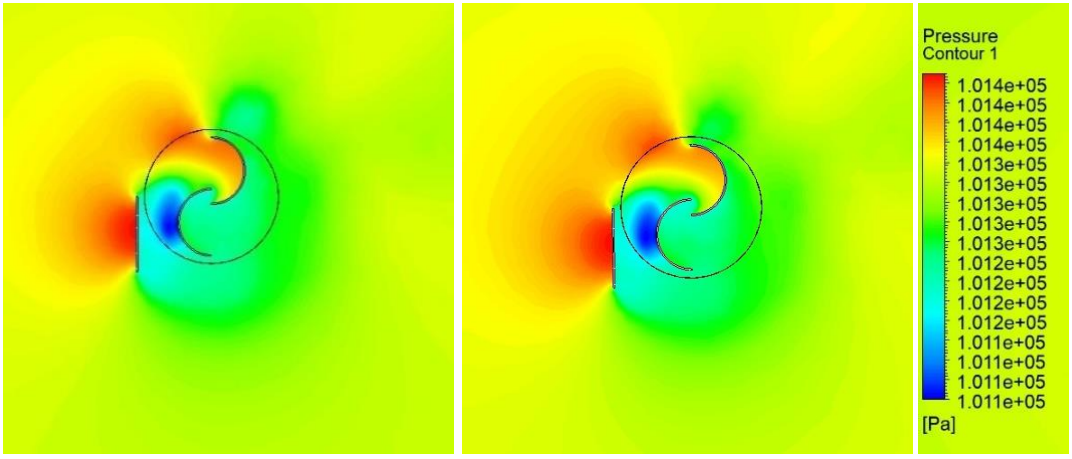

(c) 0.7 TSR (d) 0.8 TSR

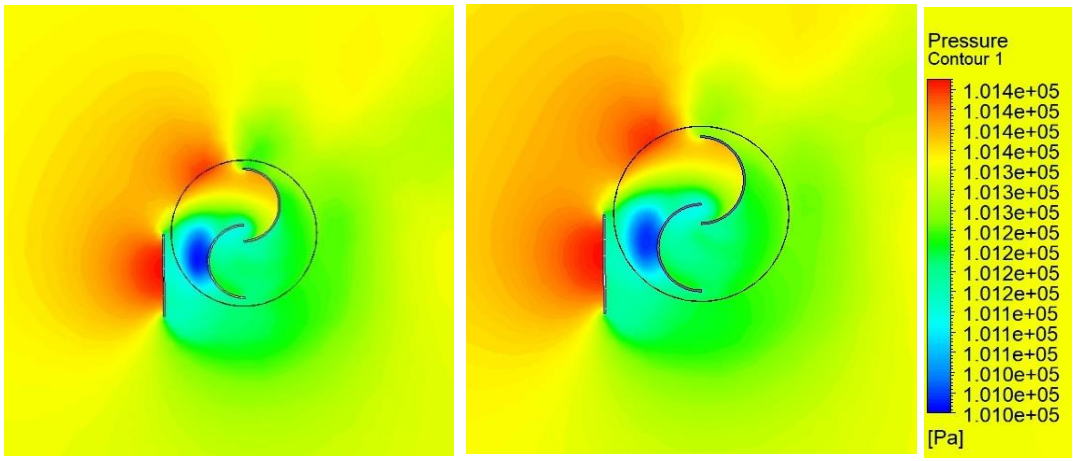

(e) 0.9 TSR (f) 1.0 TSR

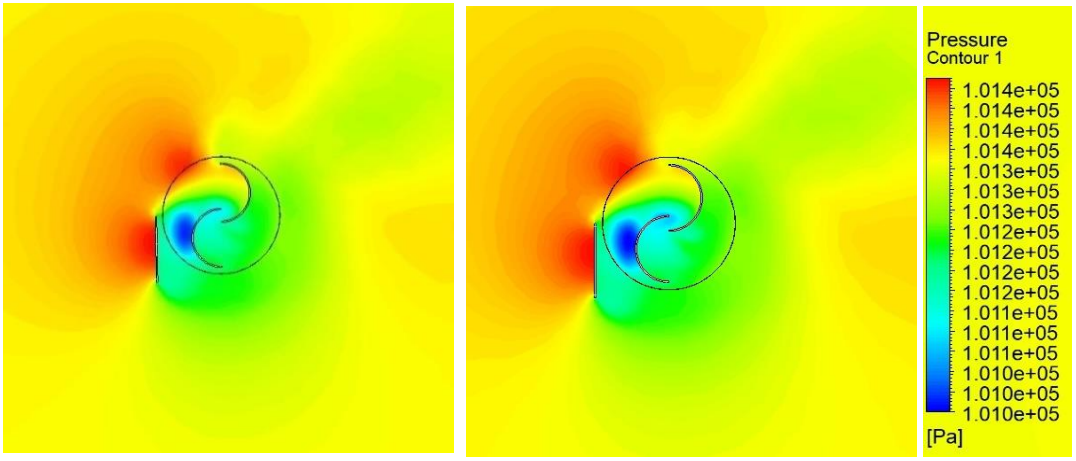

(g) 1.1 TSR (h) 1.2 TSR

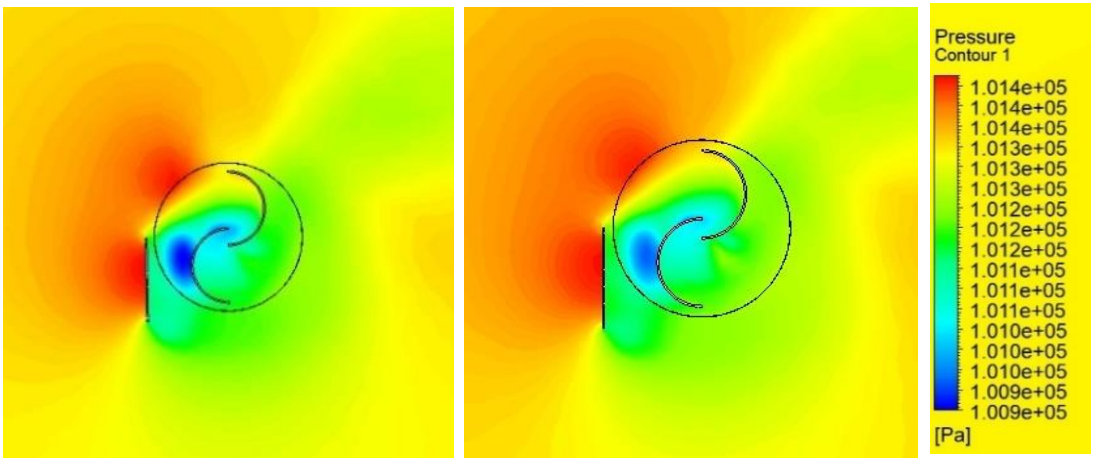

(i) 1.3 TSR (j) 1.4 TSR

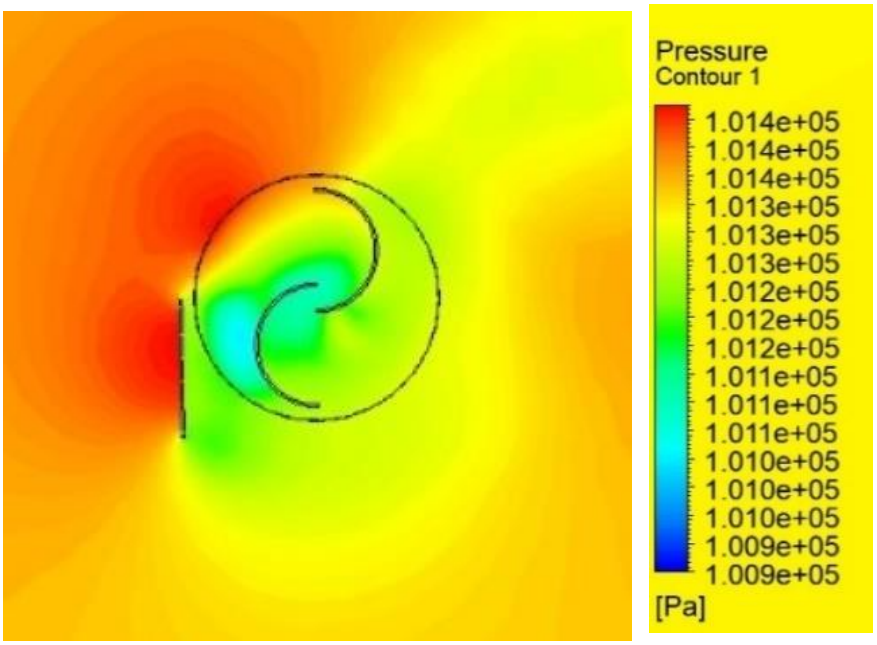

(k) 1.5 TSR

Fig. 4.6. (a) – (k) Pressure contours for **0° blade twist angle with deflector plate at 90°** at TSR ranging from 0.5 - 1.5

4.2.5. Velocity Contours for 0° blade twist angle with deflector plate at 45°

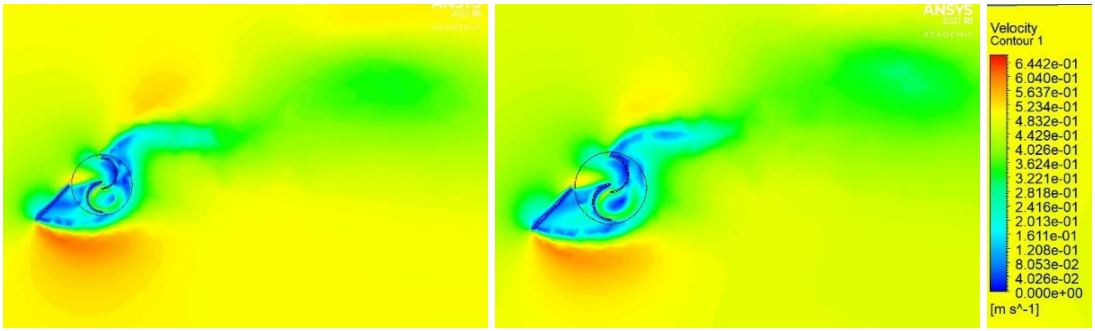

(a) 0.5 TSR (b) 0.6 TSR

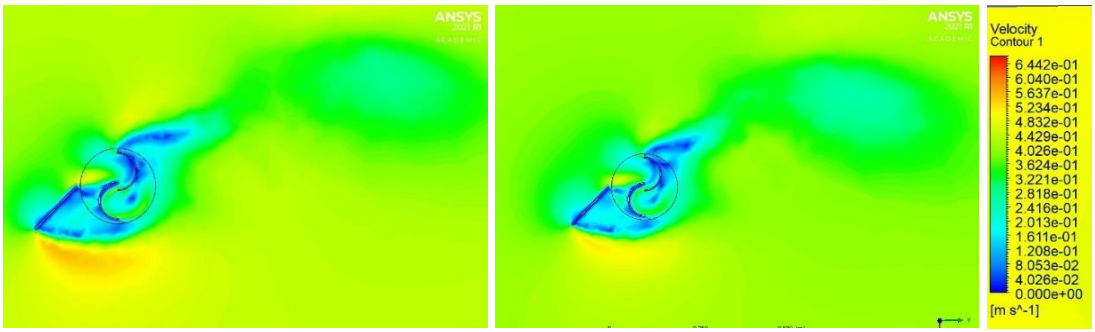

(c) 0.7 TSR (d) 0.8 TSR

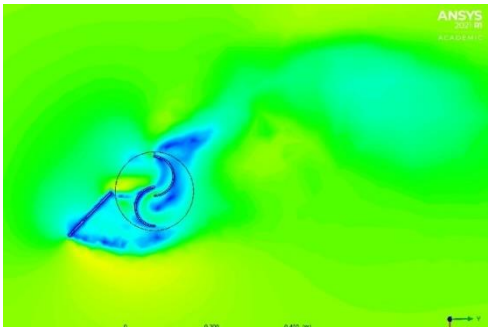

(e) 0.9 TSR

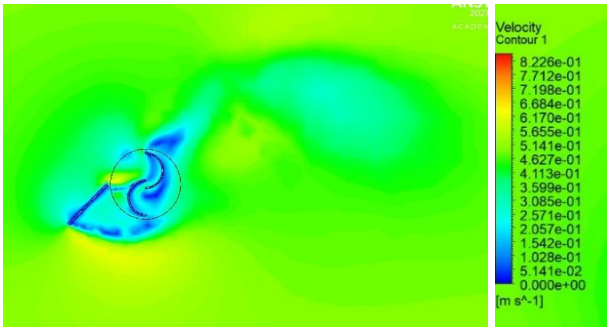

(f) 1.0 TSR

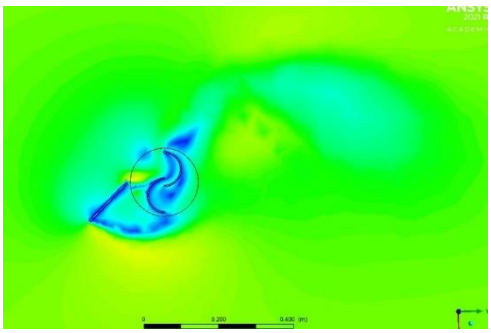

(g) 1.1 TSR

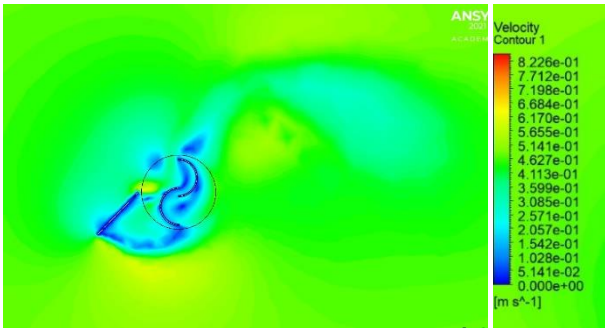

(h) 1.2 TSR

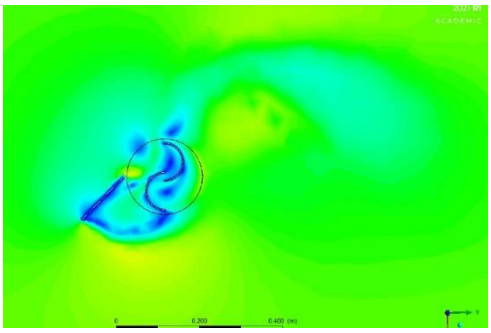

(i) 1.3 TSR

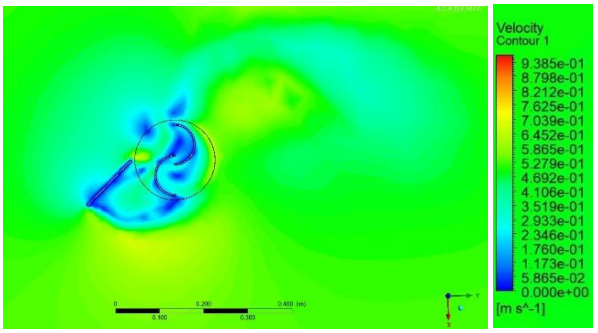

(j) 1.4 TSR

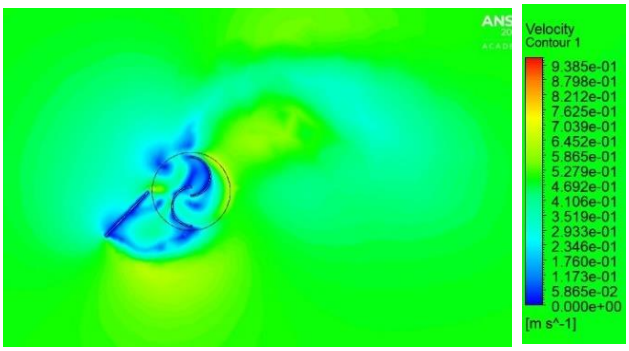

(k) 1.3 TSR

Fig. 4.7. (a) – (k) Velocity contours for **0° blade twist angle with deflector plate at 45°** at TSR ranging from 0.5 - 1.5

4.2.6. Pressure Contours for 0° blade twist angle with deflector plate at 45°

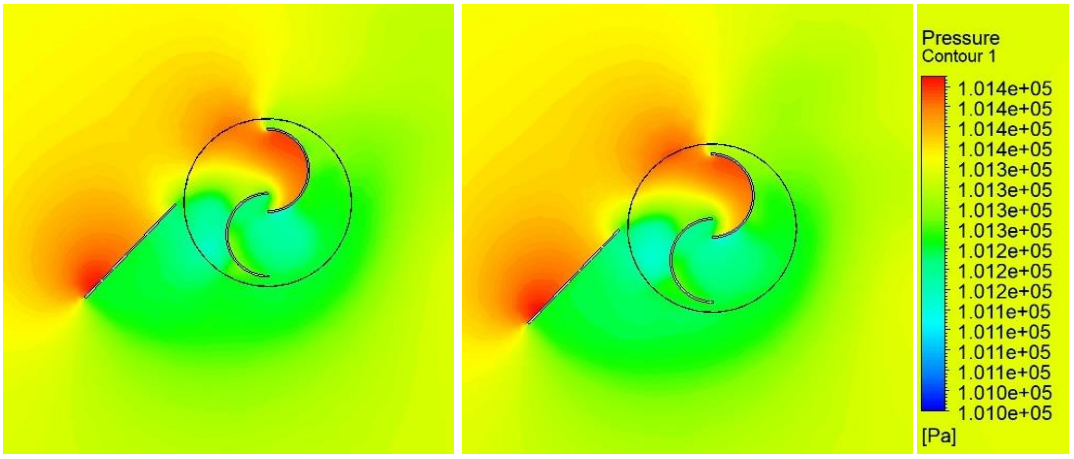

(a) 0.5 TSR (b) 0.6 TSR

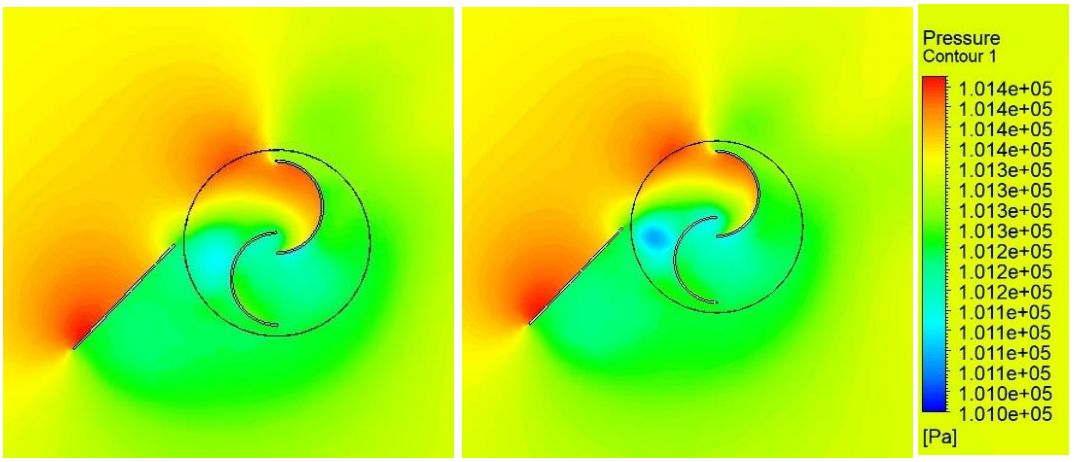

(c) 0.7 TSR (d) 0.8 TSR

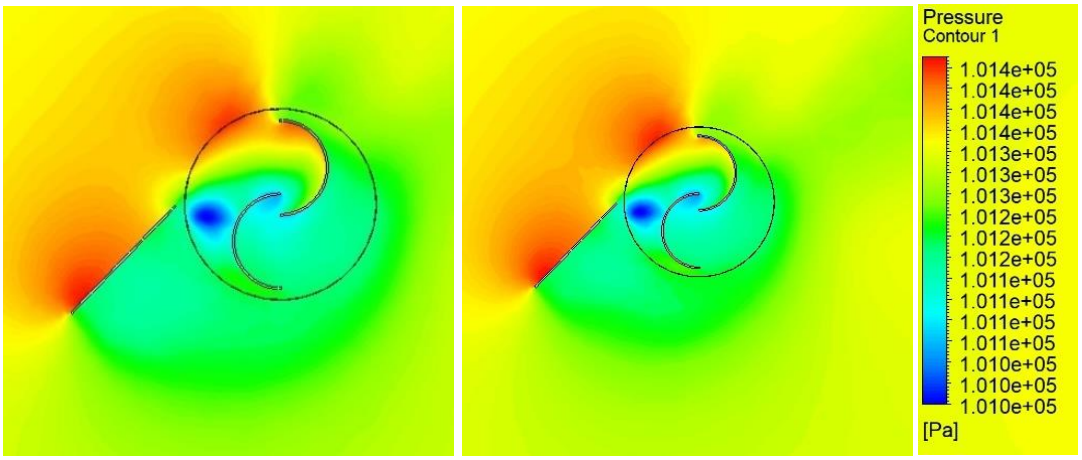

(e) 0.9 TSR (f) 1.0 TSR

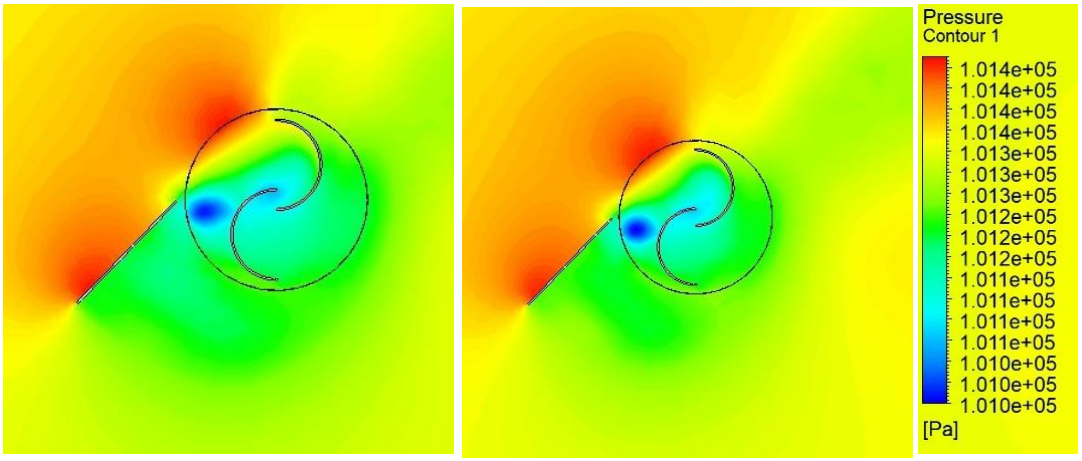

(g) 1.1 TSR (h) 1.2 TSR

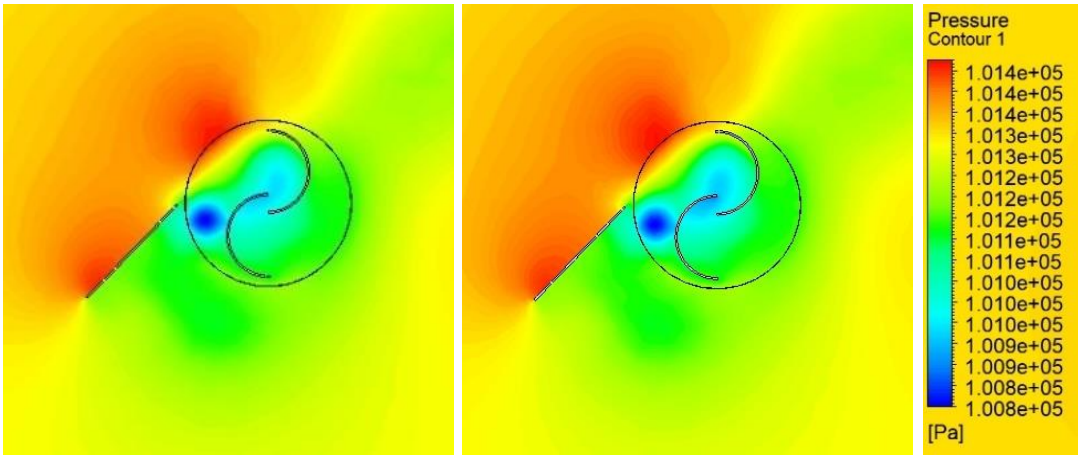

(i) 1.3 TSR (j) 1.4 TSR

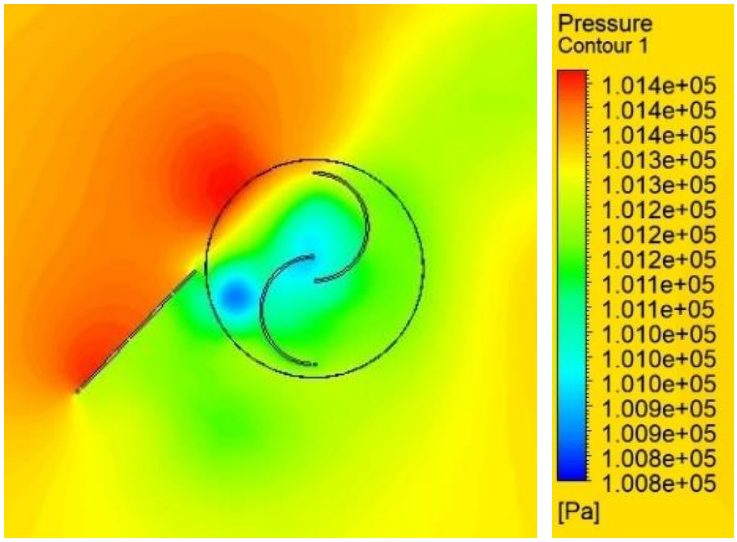

(k) 1.5 TSR

Fig. 4.8. (a) – (k) Pressure contours for **0° blade twist angle with deflector plate at 45°** at TSR ranging from 0.5 - 1.5

4.3. CONTOURS FOR 12.5° TWIST ANGLE OF BLADES

4.3.1. Velocity Contours for 12.5° blade twist angle without deflector

Fig. 4.9. (a)-(k) illustrates, velocity contour plots which depicts the changes in velocity across different places around the SHT having blade twist angle 12.5° without deflector plate at TSR ranging from 0.5 - 1.5.

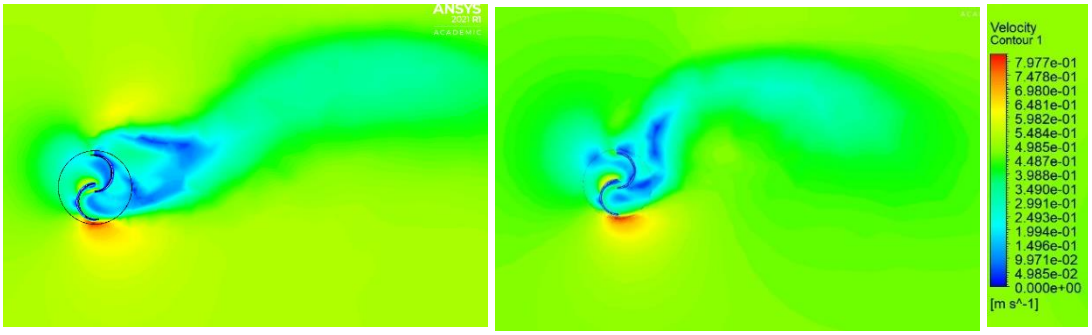

(a) 0.5 TSR (b) 0.6 TSR

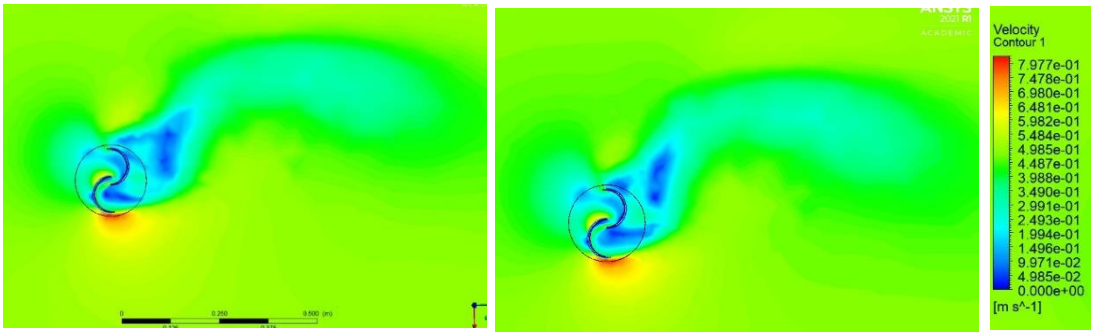

(c) 0.7 TSR (d) 0.8 TSR

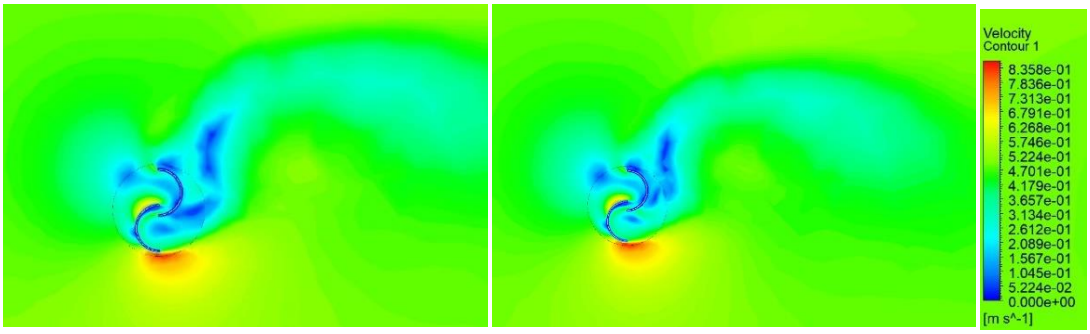

(e) 0.9 TSR (f) 1.0 TSR

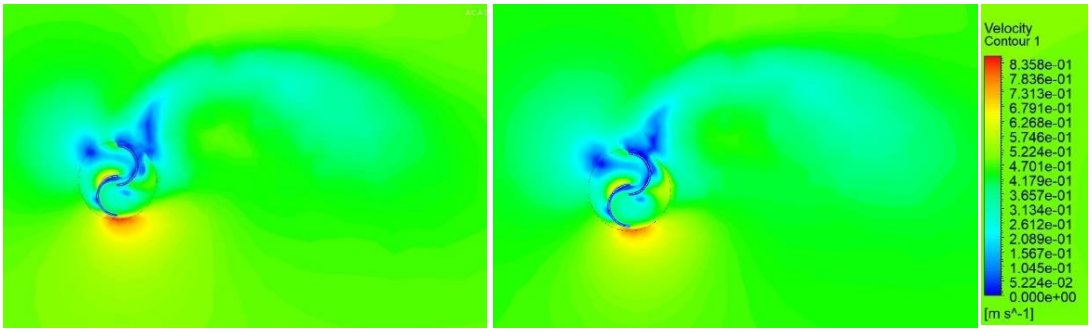

(g) 1.1 TSR (h) 1.2 TSR

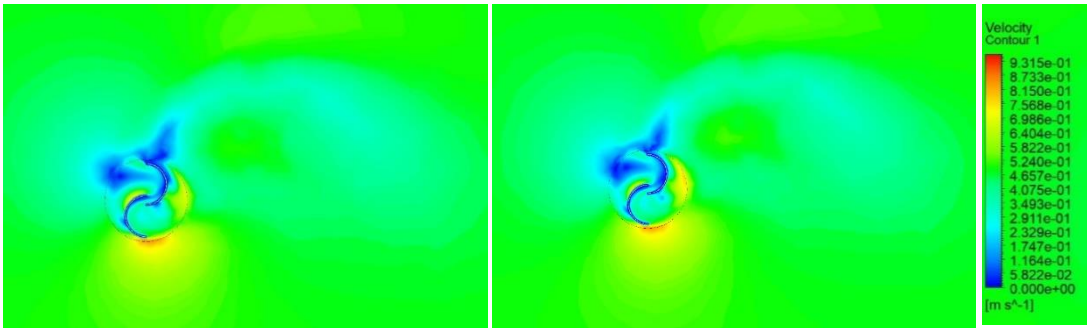

(i) 1.3 TSR (j) 1.4 TSR

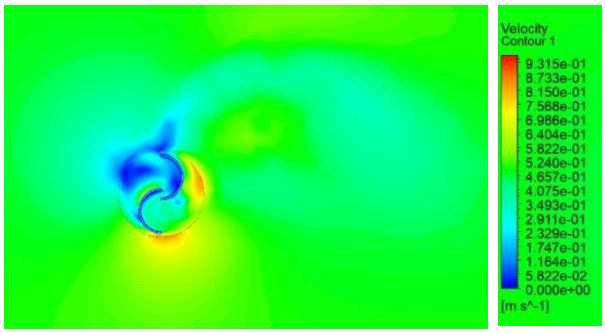

(k) 1.5 TSR

Fig. 4.9. (a) – (k) Velocity contours for **12.5° blade twist angle without deflector plate** at TSR ranging from 0.5 - 1.5

4.3.2. Pressure Contours for 12.5° blade twist angle without deflector

Fig. 4.10. (a) – (k) depicts pressure contour of rotor for 12.5° twist angle without deflector plate at TSR ranging from 0.5 – 1.5 and 0.5 m/s free stream velocity. We can observe that pressure decreases on rotor from upstream to downstream.

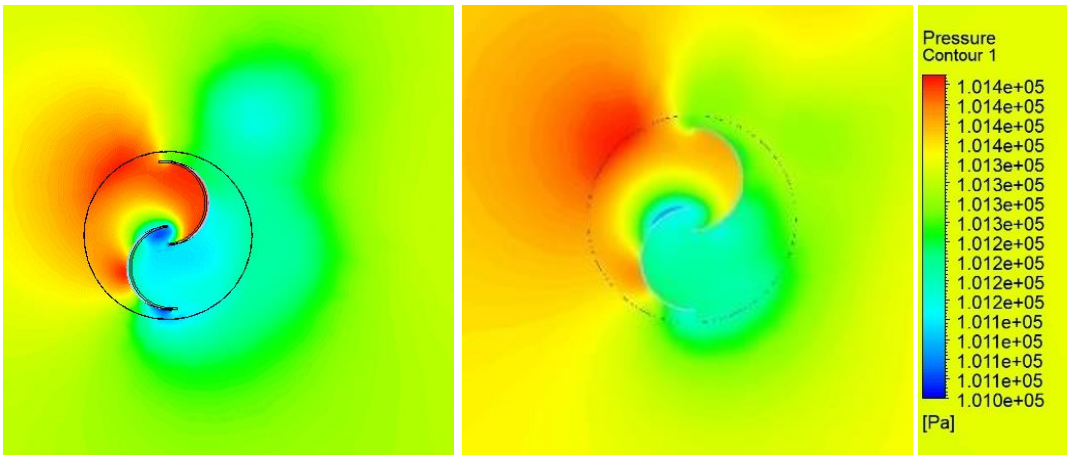

(a) 0.5 TSR (b) 0.6 TSR

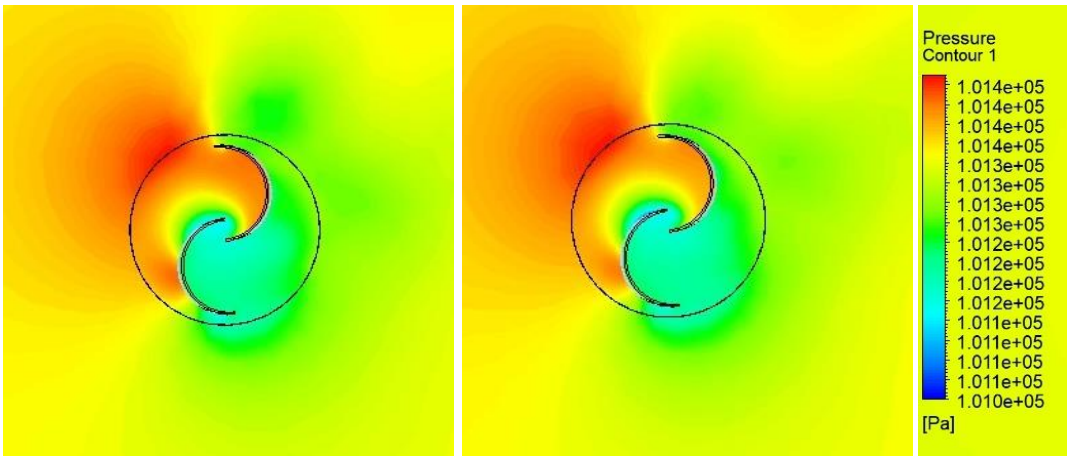

(c) 0.7 TSR (d) 0.8 TSR

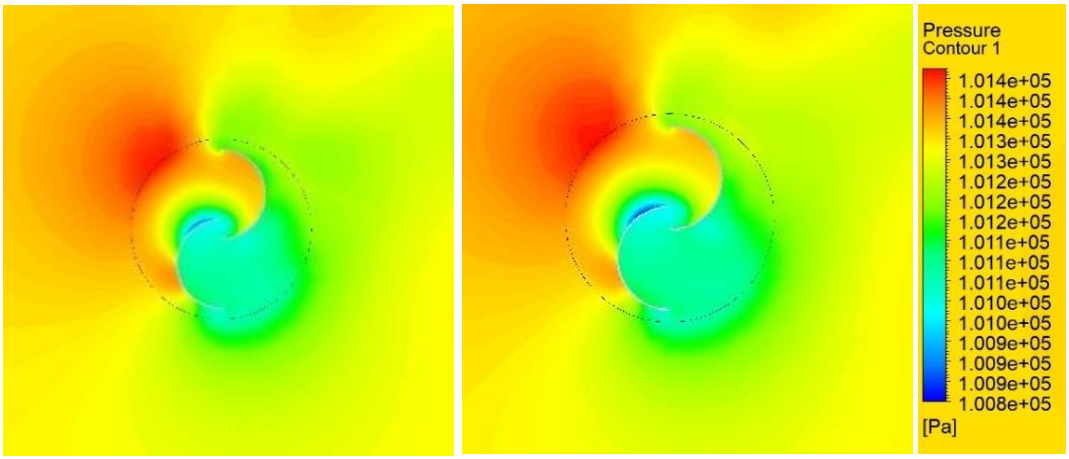

(e) 0.9 TSR (f) 1.0 TSR

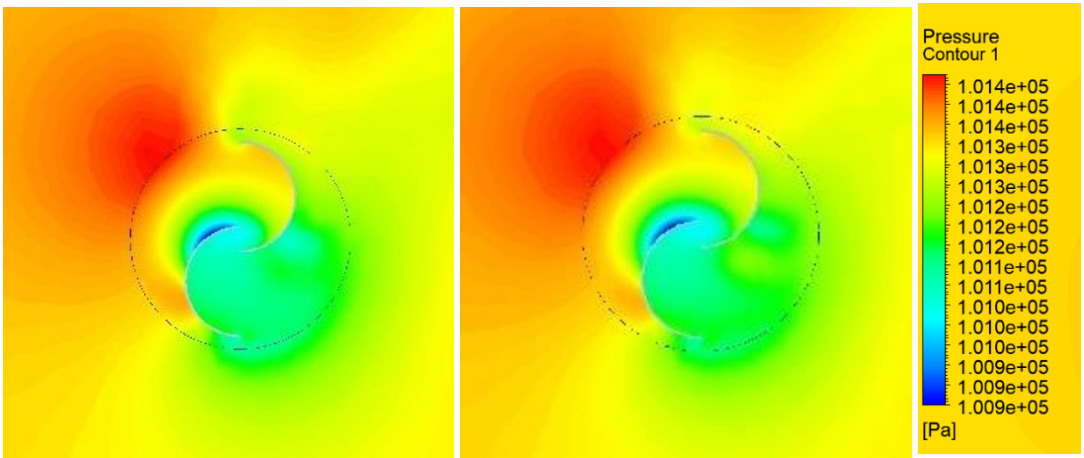

(g) 1.1 TSR (h) 1.2 TSR

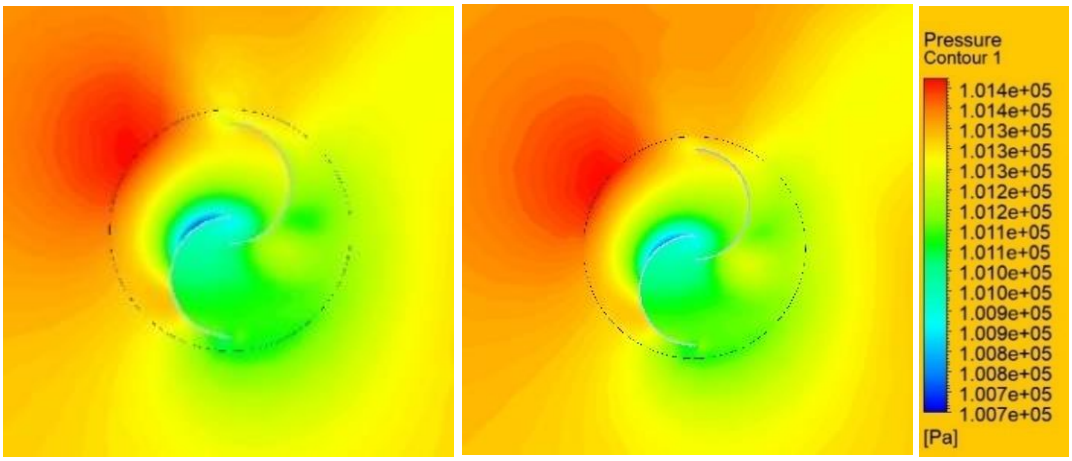

(i) 1.3 TSR (j) 1.4 TSR

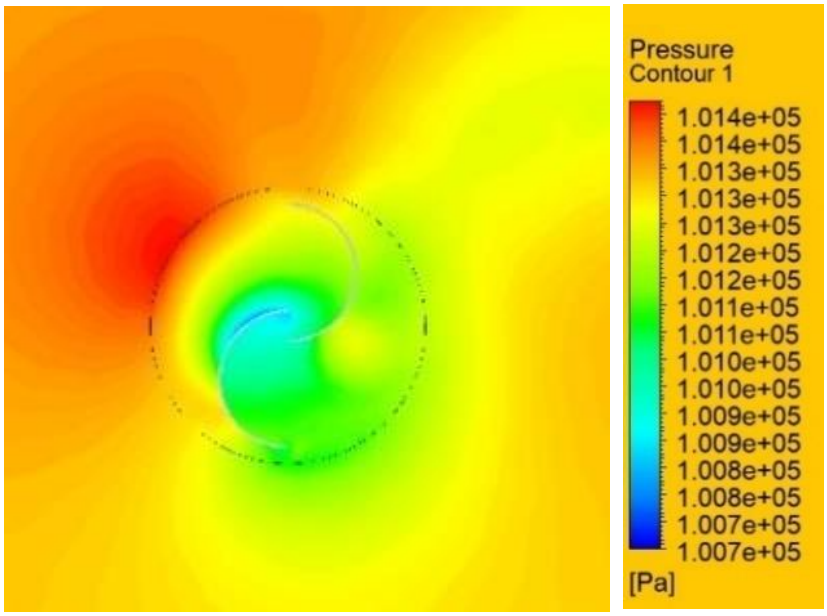

(k) 1.5 TSR

Fig. 4.10. (a) – (k) Pressure contours for **12.5° blade twist angle without deflector plate** at TSR ranging from 0.5 - 1.5

4.3.3. Velocity Contours for 12.5° blade twist angle with deflector at 90°

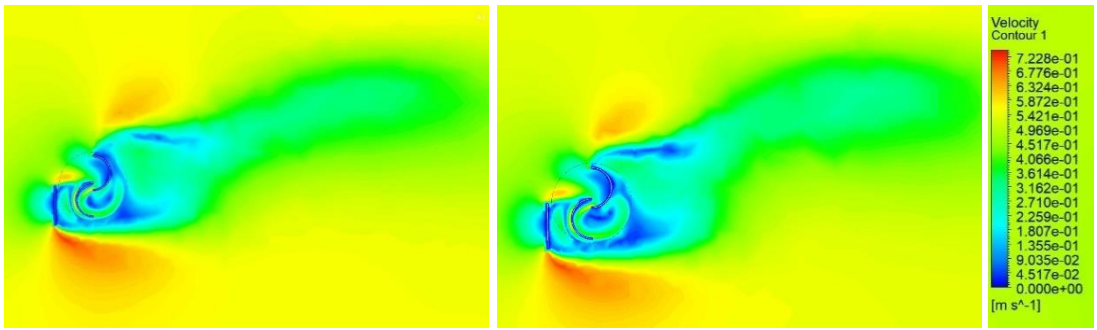

(a) 0.5 TSR (b) 0.6 TSR

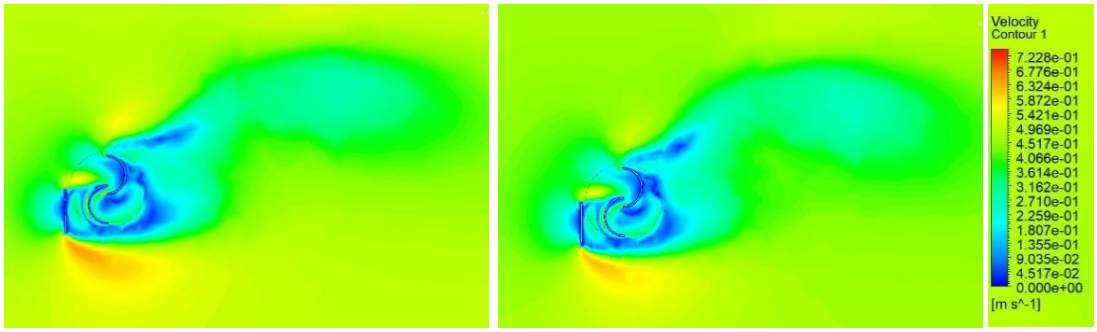

(c) 0.7 TSR (d) 0.8 TSR

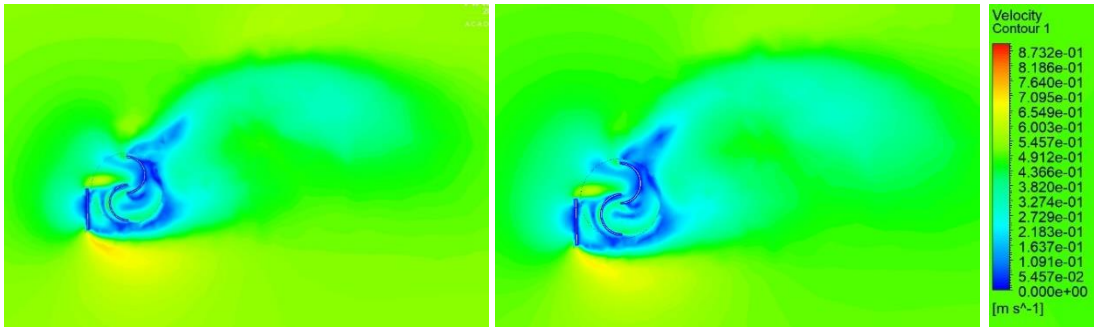

(e) 0.9 TSR (f) 1.0 TSR

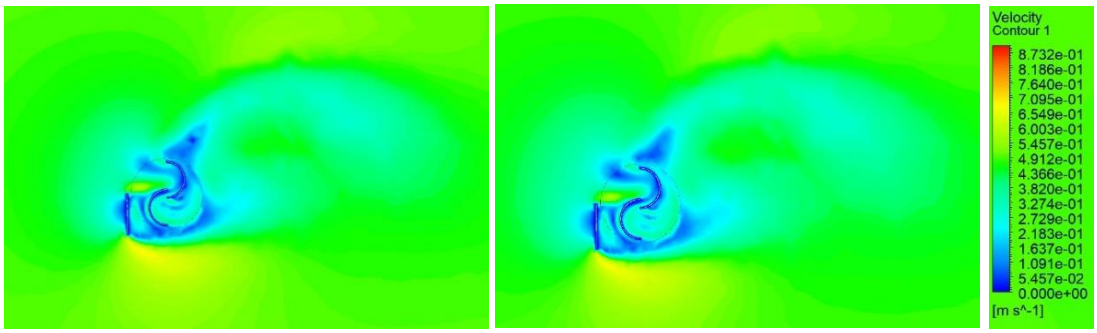

(g) 1.1 TSR (h) 1.2 TSR

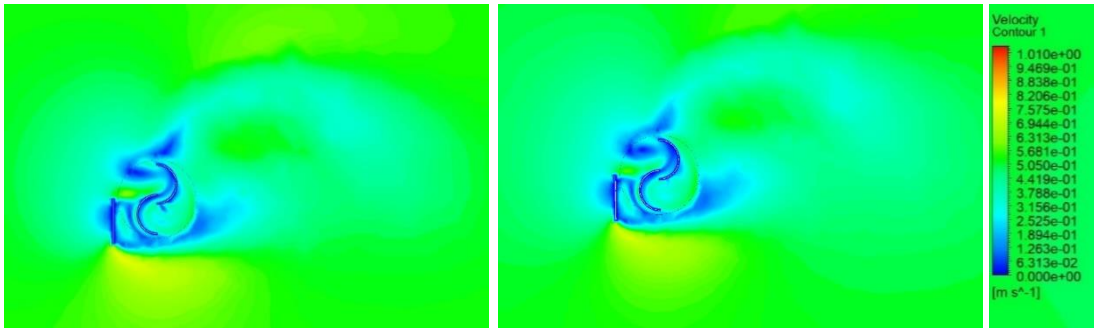

(i) 1.3 TSR (j) 1.4 TSR

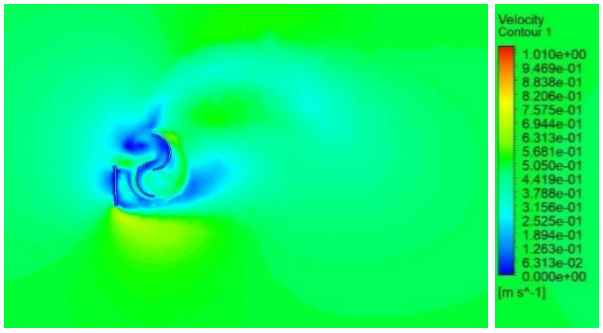

(j) 1.5 TSR

Fig. 4.11. (a) – (k) Velocity contours for **12.5° blade twist angle with deflector plate at 90°** at TSR ranging from 0.5 - 1.5

4.3.4. Pressure Contours for 12.5° blade twist angle with deflector at 90°

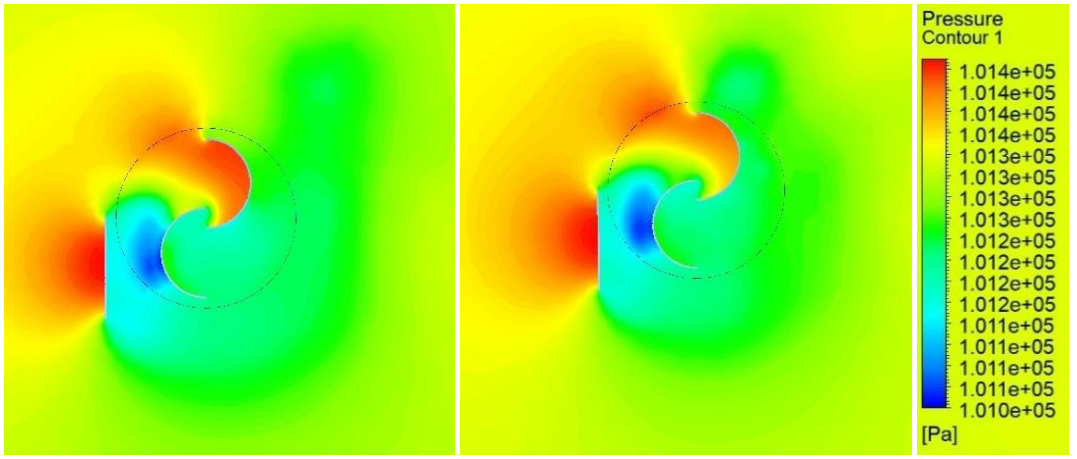

(a) 0.5 TSR (b) 0.7 TSR

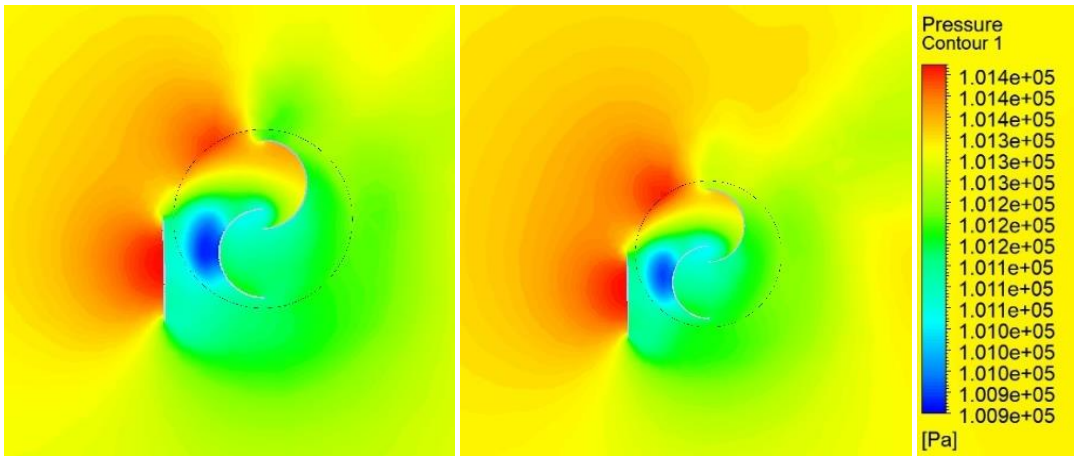

(c) 0.9 TSR (d) 1.1 TSR

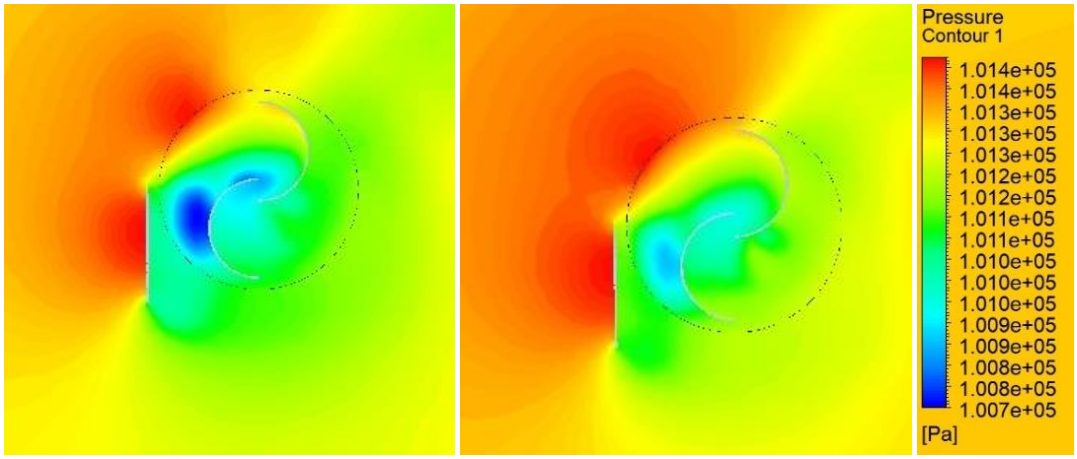

(e) 0.9 TSR (f) 0.9 TSR

Fig. 4.12. (a) – (f) Pressure contours for **12.5° blade twist angle with deflector plate at 90°** at TSR ranging from 0.5 - 1.5

4.3.5. Velocity Contours for 12.5° blade twist angle with deflector at 45°

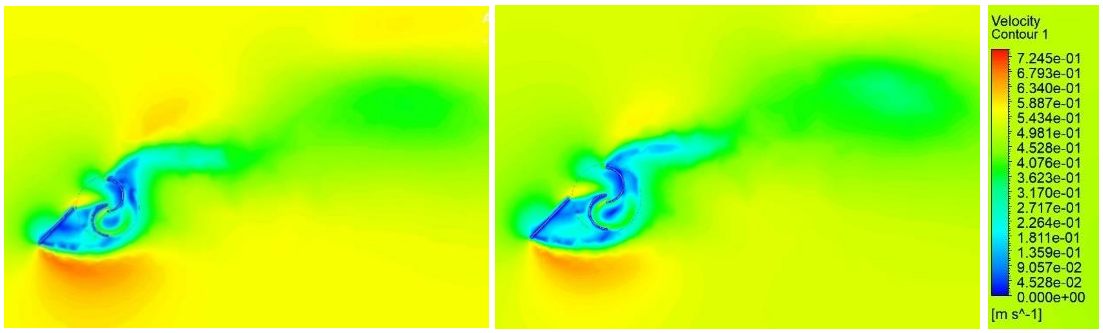

(a) 0.5 TSR (b) 0.6 TSR

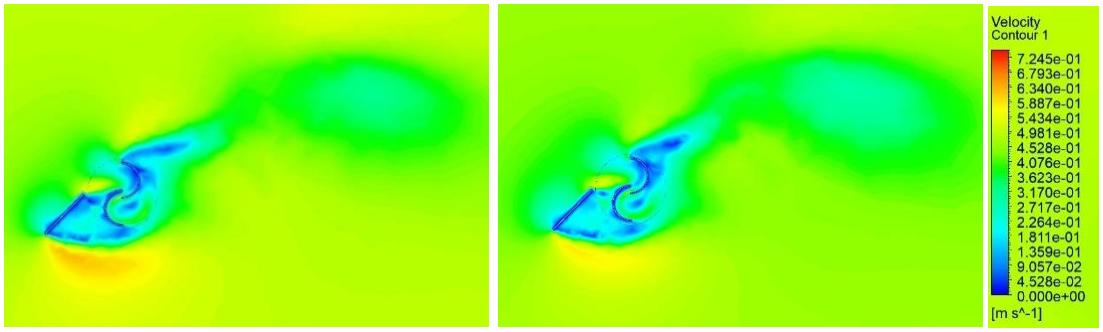

(c) 0.7 TSR (d) 0.8 TSR

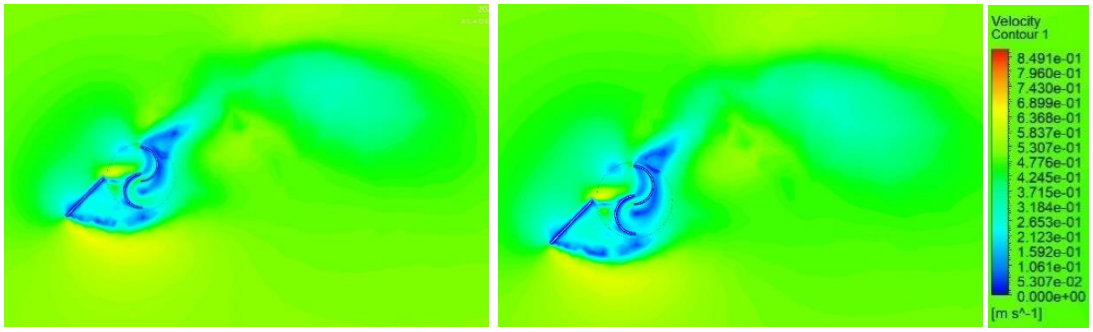

(e) 0.9 TSR (f) 1.0 TSR

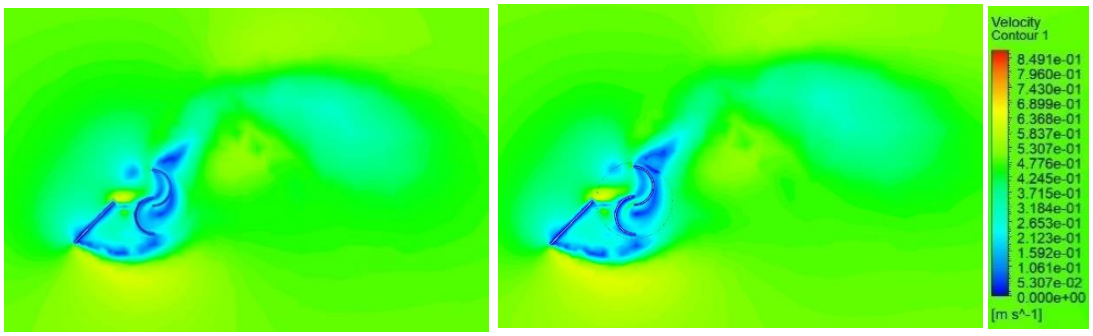

(g) 1.1 TSR (h) 1.2 TSR

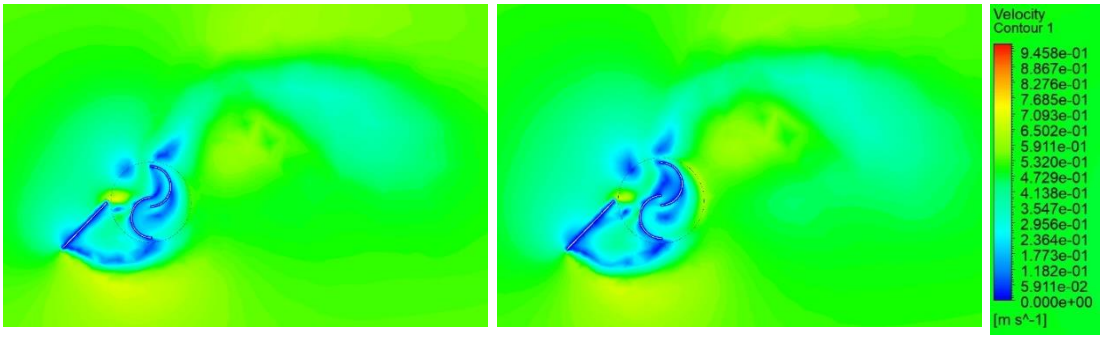

(i) 1.3 TSR (j) 1.4 TSR

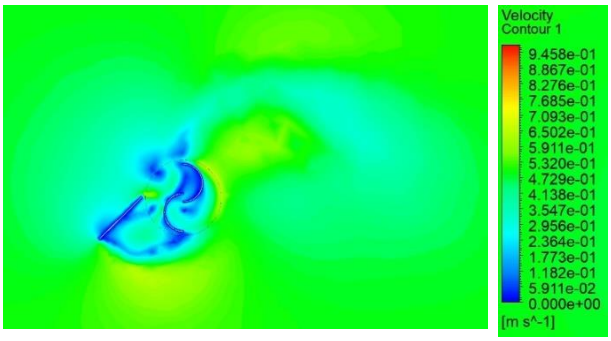

(k) 1.3 TSR

Fig. 4.13. (a) – (k) Velocity contours for **12.5° blade twist angle with deflector plate at 45°** at TSR ranging from 0.5 - 1.5

4.3.6. Pressure Contours for 12.5° blade twist angle with deflector at 45°

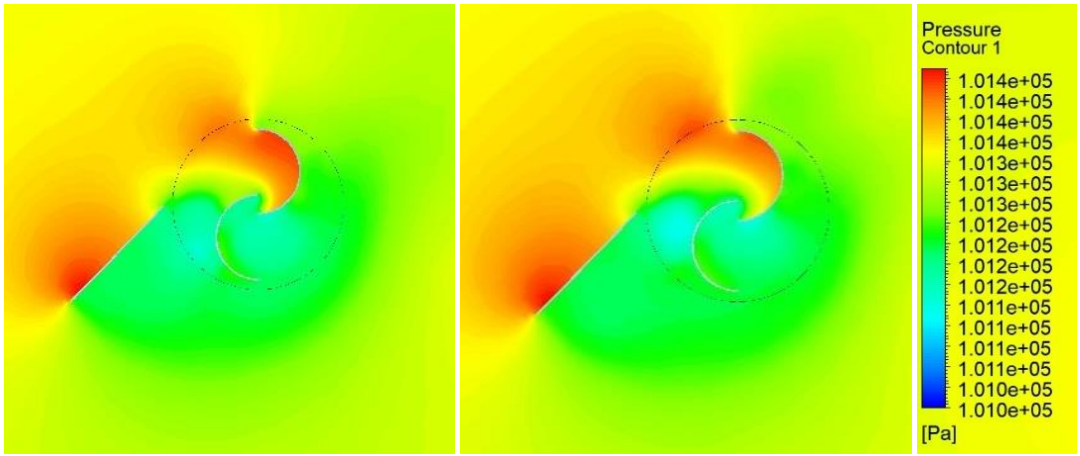

(a) 0.5 TSR (b) 0.7 TSR

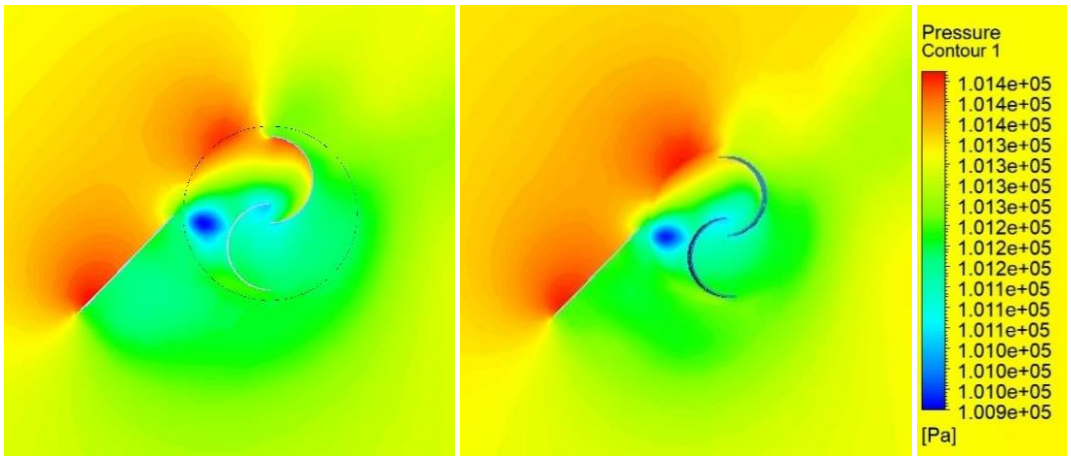

(c) 0.9 TSR (d) 1.1 TSR

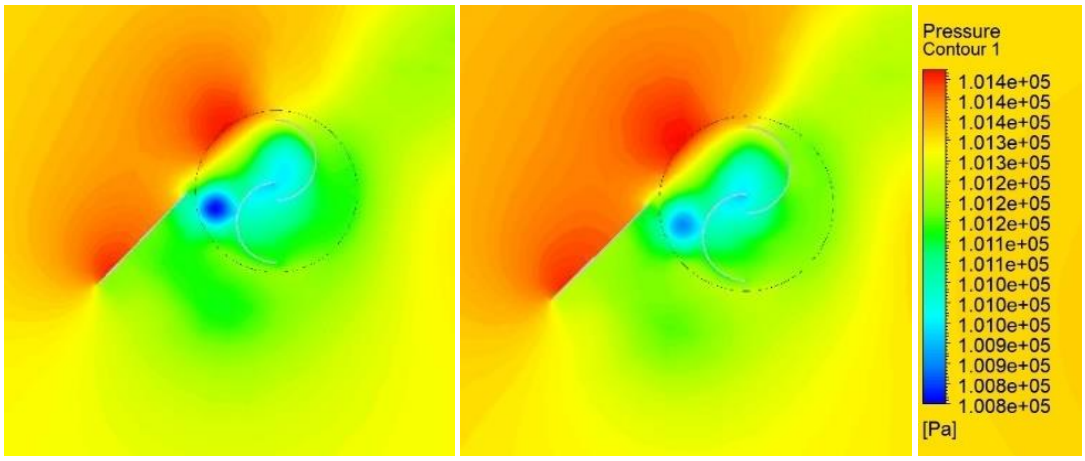

(e) 0.5 TSR (f) 0.5 TSR

Fig. 4.14. (a) – (f) Velocity contours for **12.5° blade twist angle with deflector plate at 45°** at TSR ranging from 0.5 - 1.5

4.4. CONTOURS FOR 25° TWIST ANGLE OF BLADES

4.4.1. Velocity Contours for 25° blade twist angle without deflector

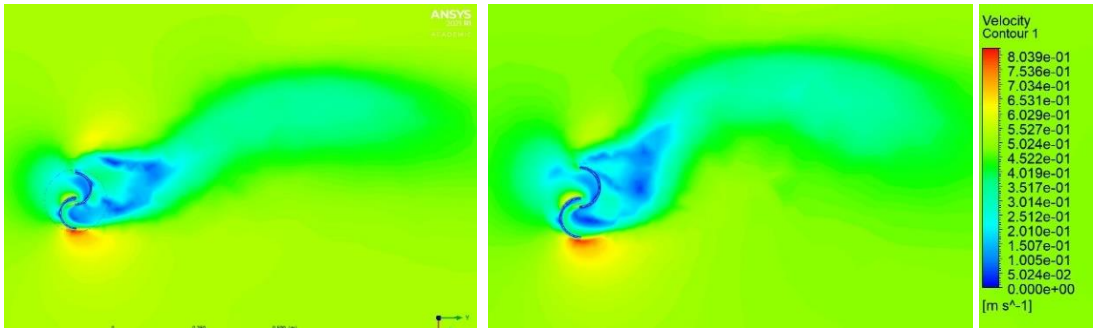

(a) 0.5 TSR (b) 0.7 TSR

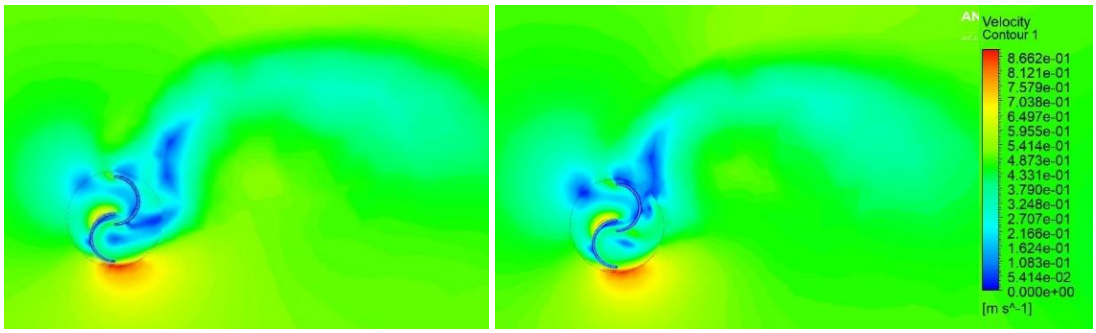

(c) 0.9 TSR (d) 1.1 TSR

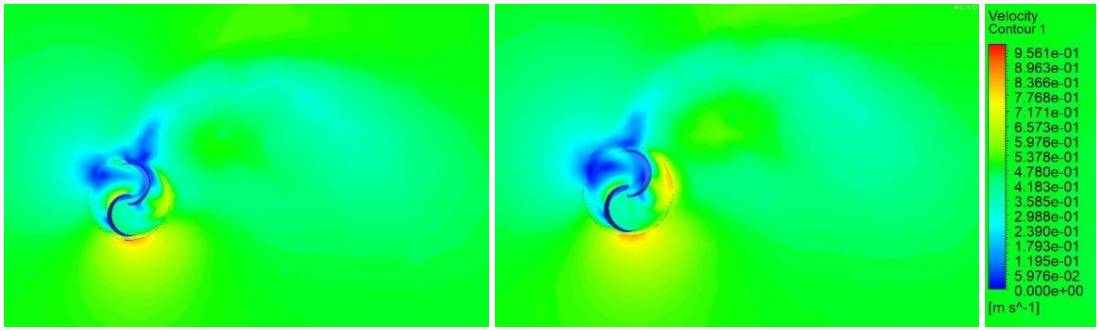

(e) 0.5 TSR (f) 0.5 TSR

Fig. 4.15. (a) – (f) Velocity contours for **25° blade twist angle with deflector plate at 45°** at TSR ranging from 0.5 - 1.5

4.4.2. Pressure Contours for 25° blade twist angle without deflector

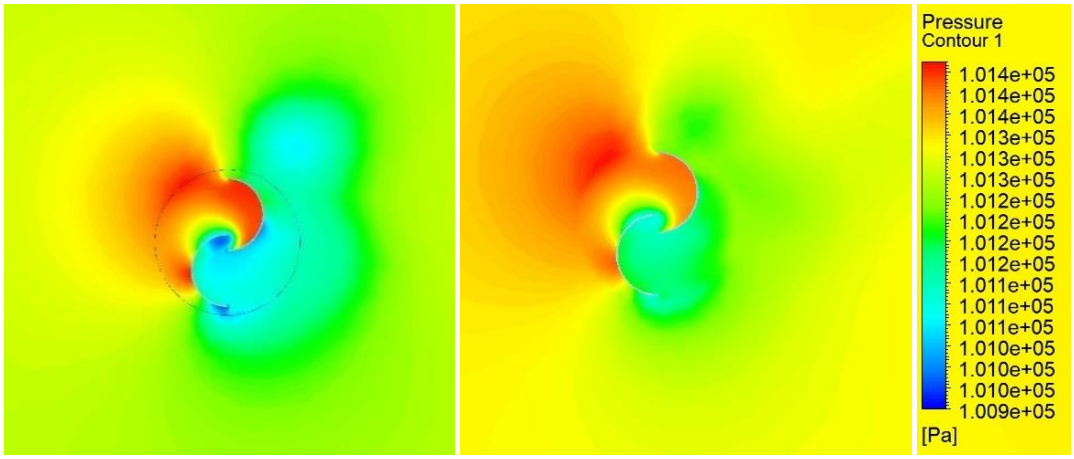

(a) 0.5 TSR (b) 0.7 TSR

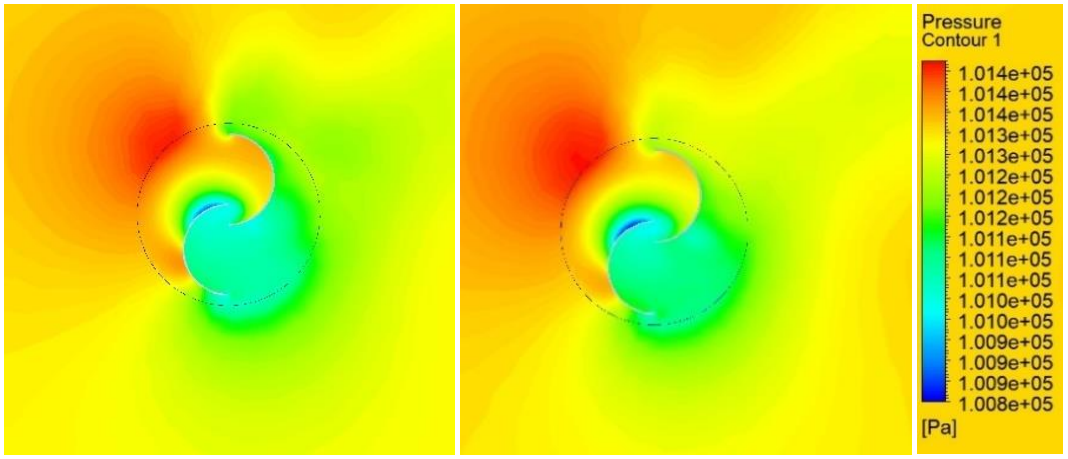

(c) 0.9 TSR (d) 1.1 TSR

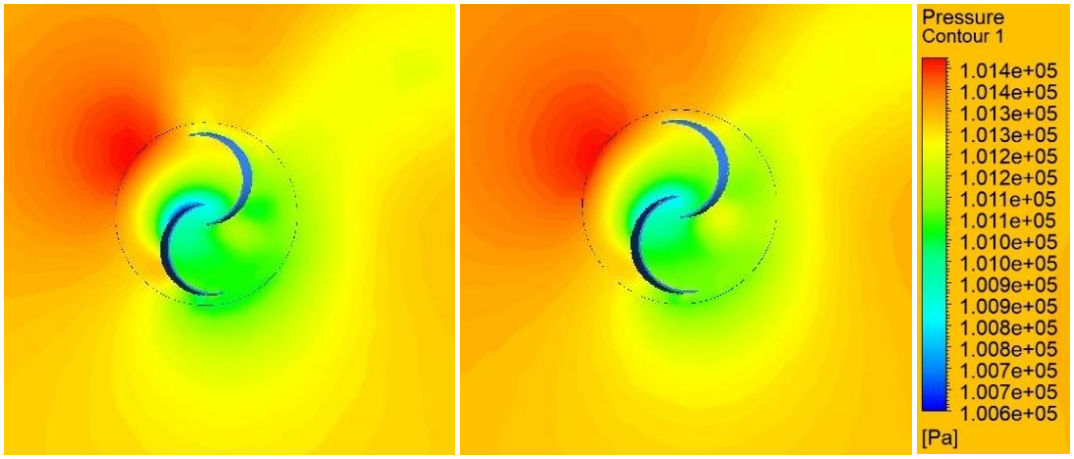

(e) 1.3 TSR (f) 1.5 TSR

Fig. 4.16. (a) – (f) Pressure contours for **25° blade twist angle without deflector plate** at TSR ranging from 0.5 - 1.5

4.4.3. Velocity Contours for 25° blade twist angle with deflector at 90°

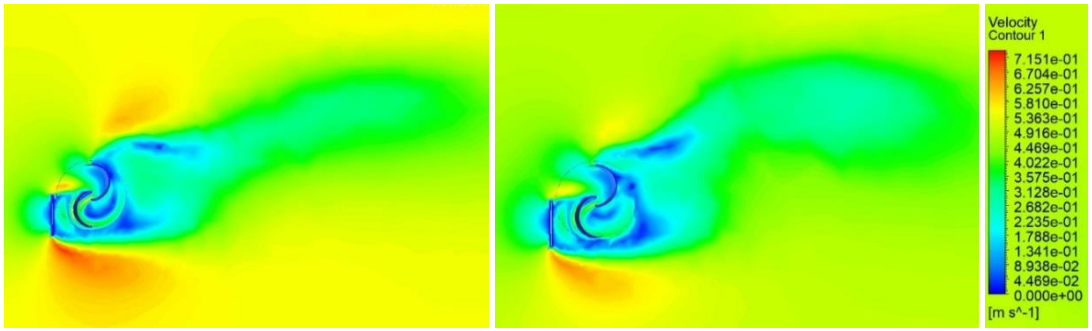

(a) 0.5 TSR (b) 0.7 TSR

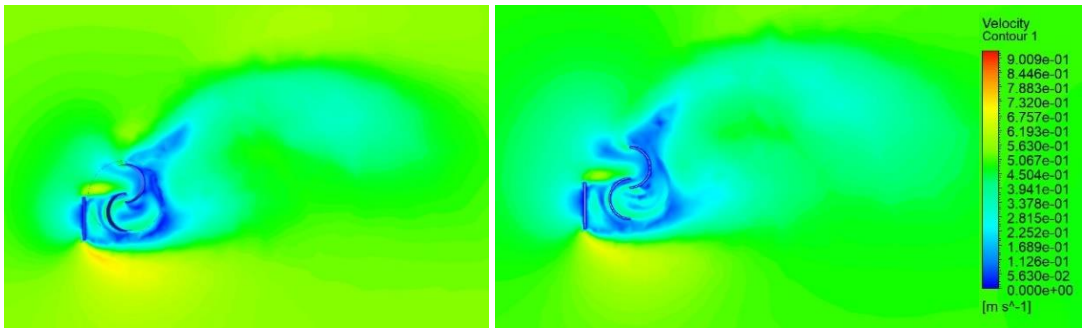

(c) 0.9 TSR (d) 1.1 TSR

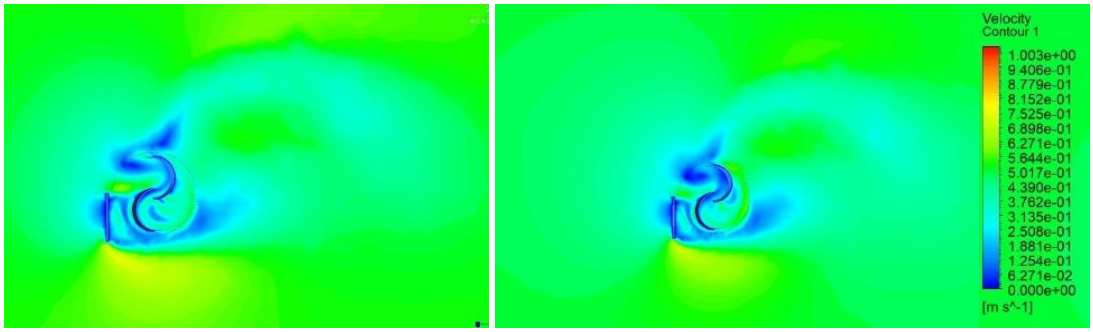

(e) 1.3 TSR (f) 1.5 TSR

Fig. 4.17. (a) – (f) Velocity contours for **25° blade twist angle with deflector plate at 90°** at TSR ranging from 0.5 - 1.5

4.4.4. Pressure Contours for 25° blade twist angle with deflector at 90°

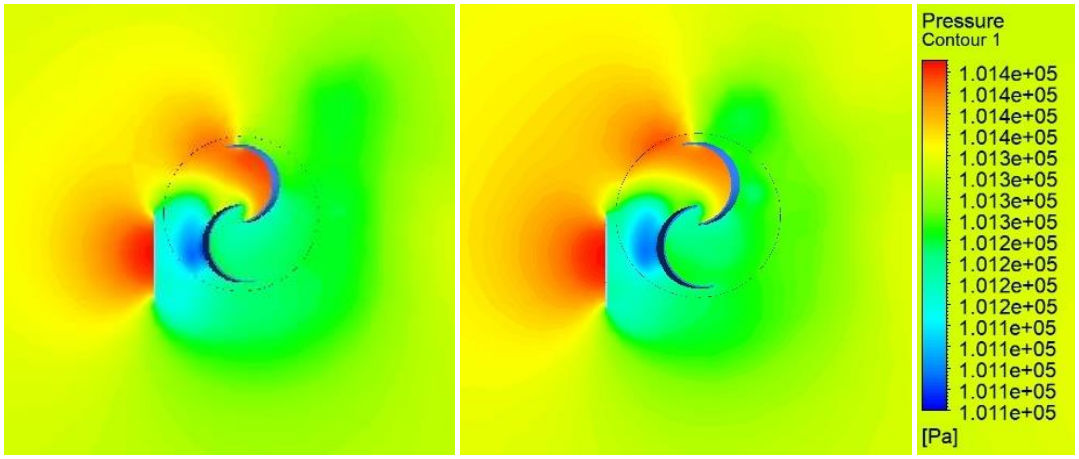

(a) 0.5 TSR (b) 0.7 TSR

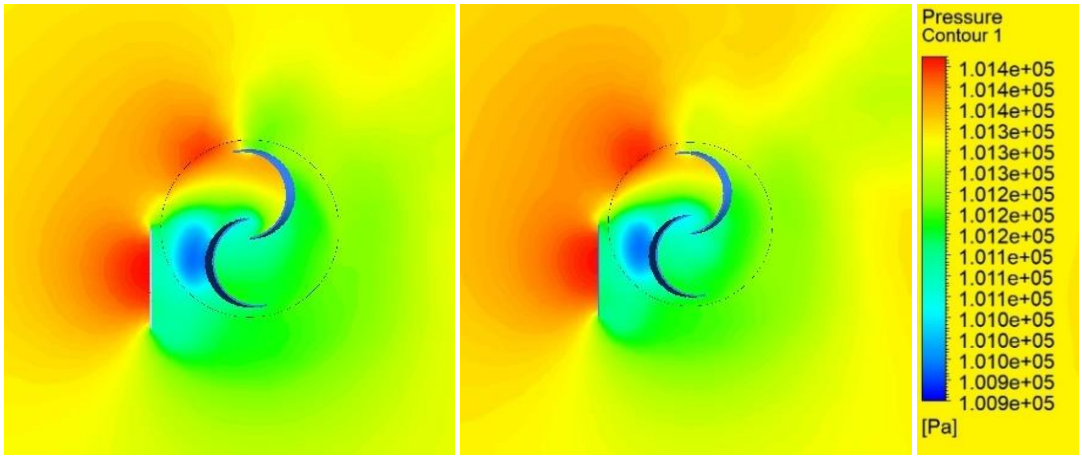

(c) 0.9 TSR (d) 1.1 TSR

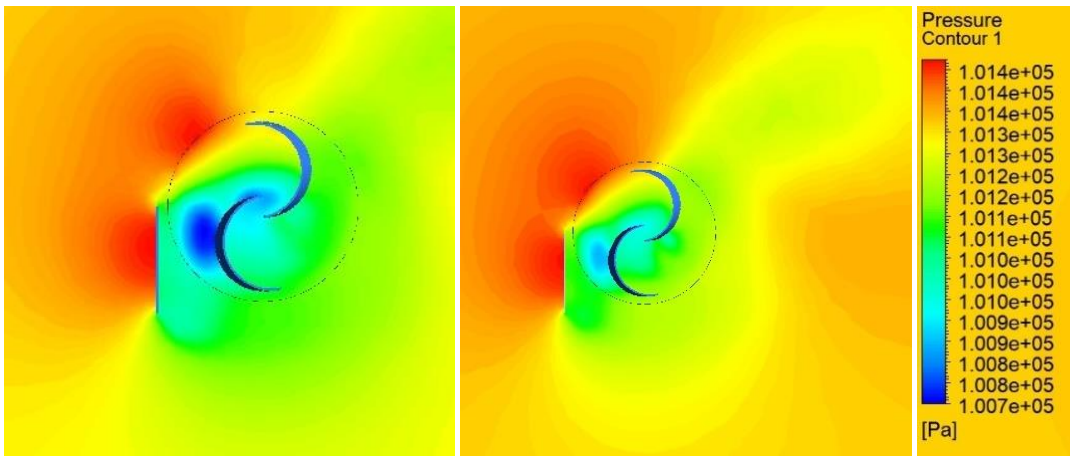

(e) 1.3 TSR (f) 1.5 TSR

Fig. 4.18. (a) – (f) Pressure contours for **25° blade twist angle with deflector plate at 90°** at TSR ranging from 0.5 - 1.5

4.4.5. Velocity Contours for 25° blade twist angle with deflector at 45°

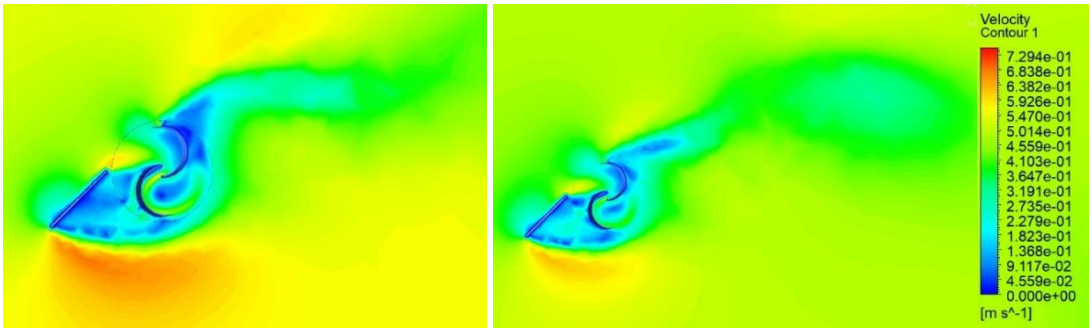

(a) 0.5 TSR (b) 0.7 TSR

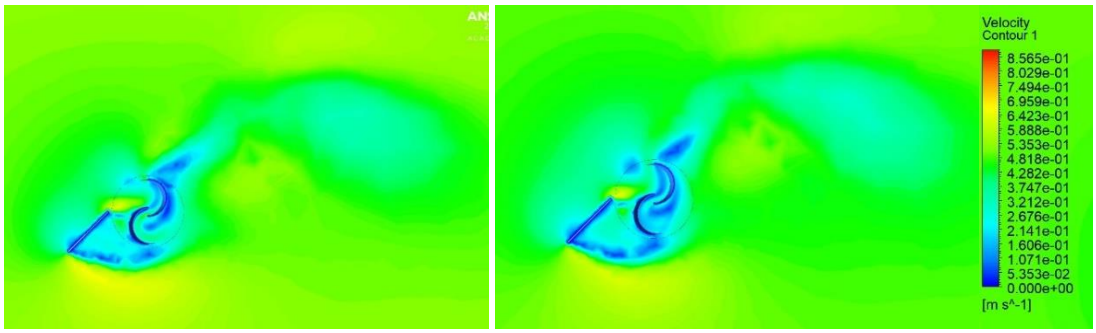

(c) 0.9 TSR (d) 1.1 TSR

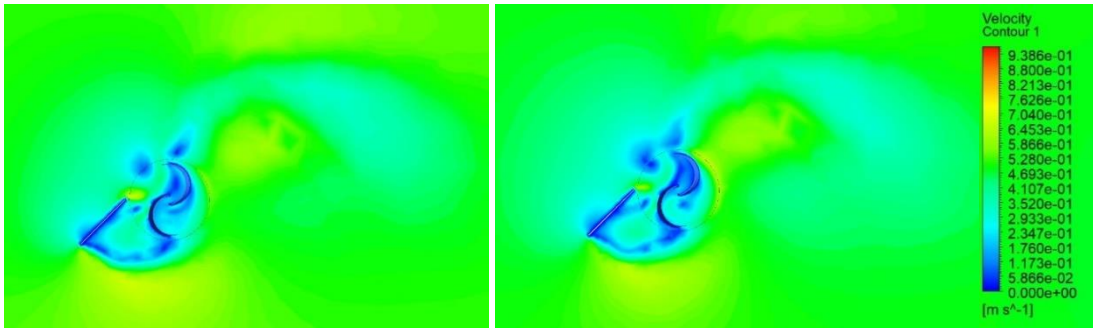

(e) 1.3 TSR (f) 1.5 TSR

Fig. 4.19. (a) – (f) Velocity contours for **25° blade twist angle with deflector plate at 45°** at TSR ranging from 0.5 - 1.5

4.4.6. Pressure Contours for 25° blade twist angle with deflector at 45°

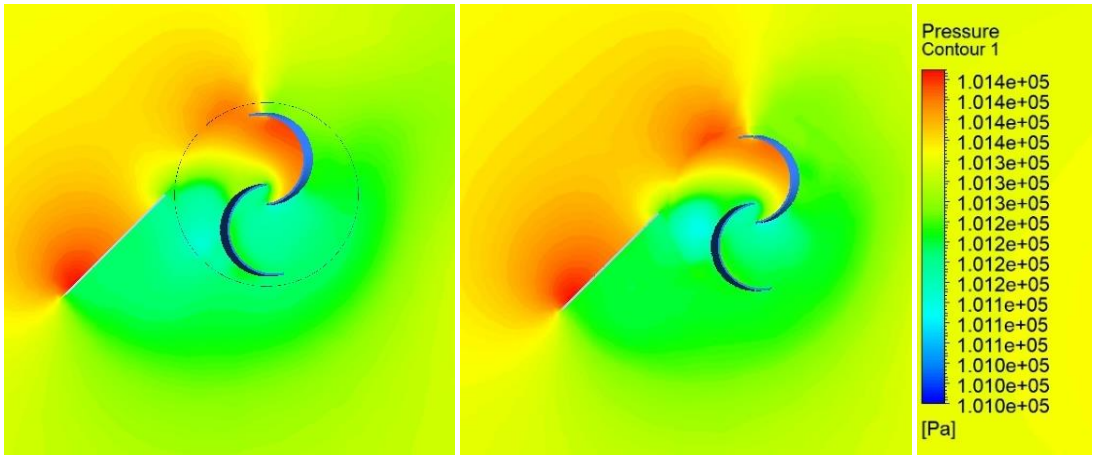

(a) 0.5 TSR (b) 0.7 TSR

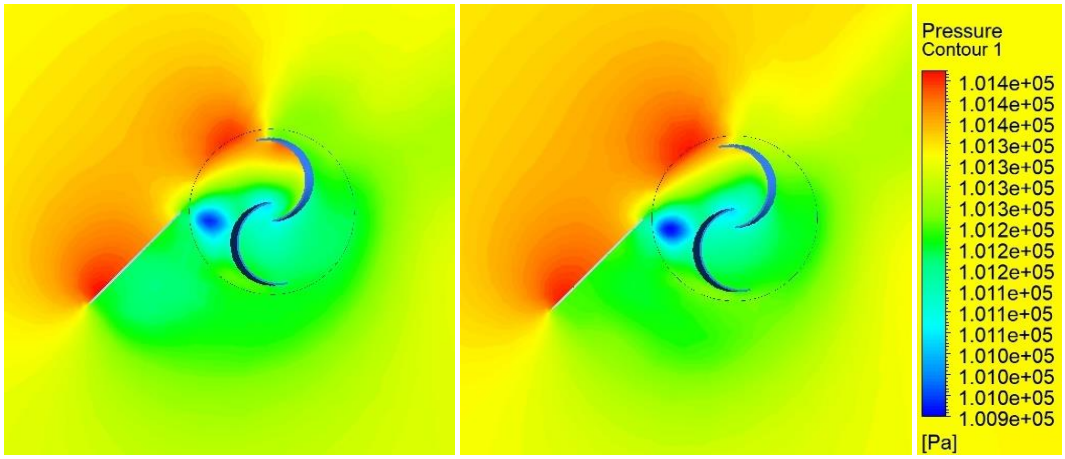

(c) 0.9 TSR (d) 1.1 TSR

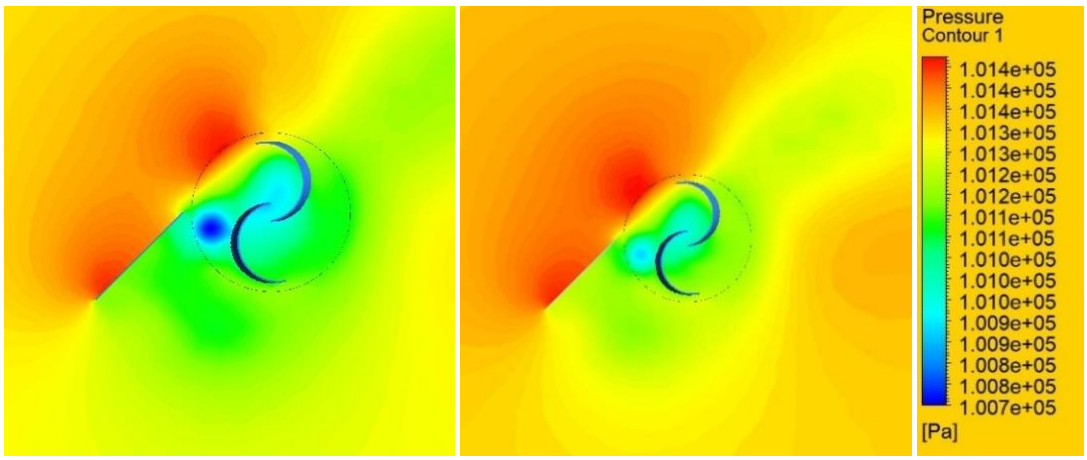

(e) 1.3 TSR (f) 1.3 TSR

Fig. 4.20. (a) – (f) Pressure contours for **25° blade twist angle with deflector plate at 45°** at TSR ranging from 0.5 - 1.5

4.5. STREAMLINES

4.5.1. Streamline for 0° twist angle of blades

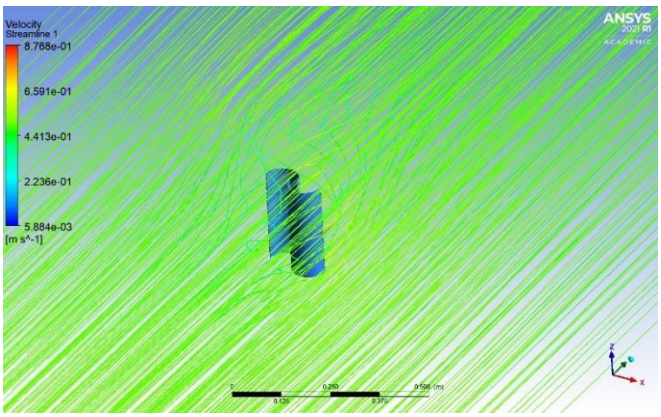

(a)

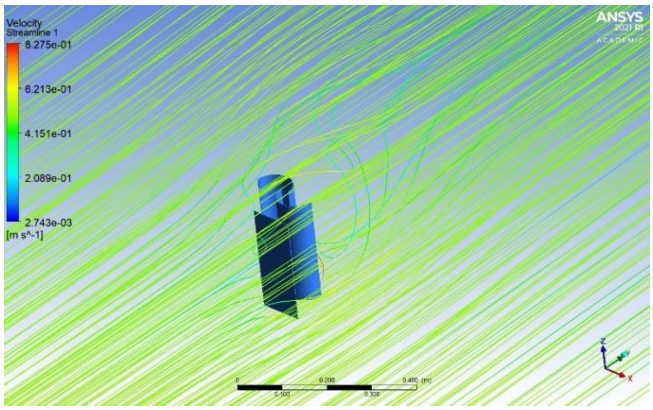

(b)

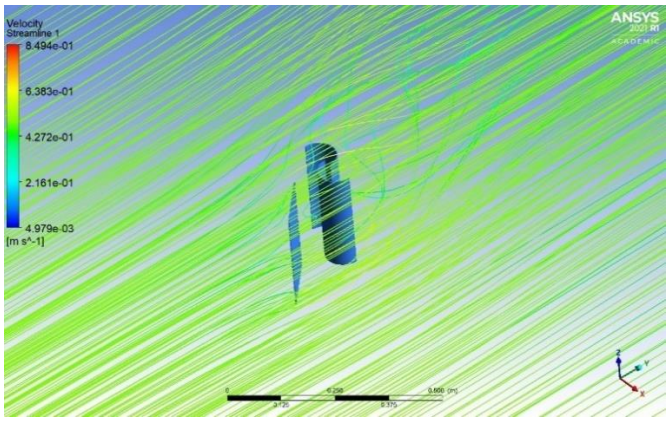

(c)

Fig. 4.21. Streamline for **0° twist angle** (a) no deflector (b) with deflector at 90° (c) with deflector at 45° at TSR = 0.7

4.5.2. Streamline for 12.5° twist angle of blades

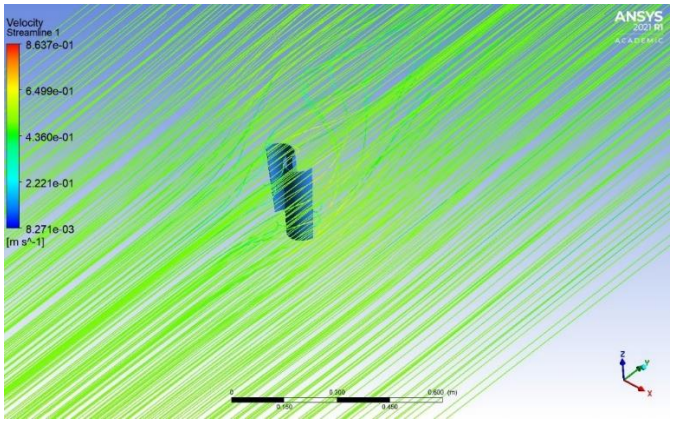

(a)

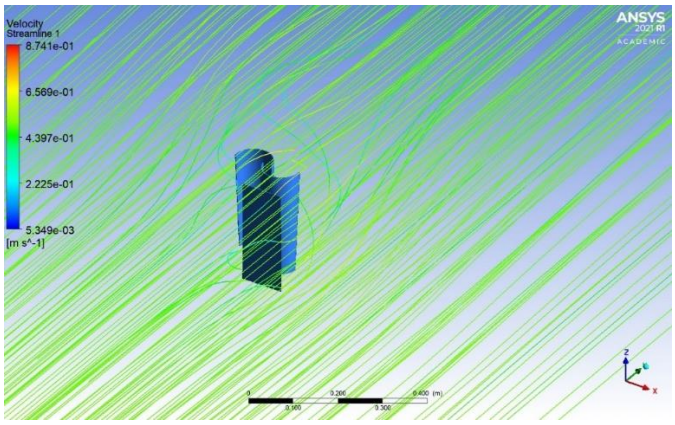

(b)

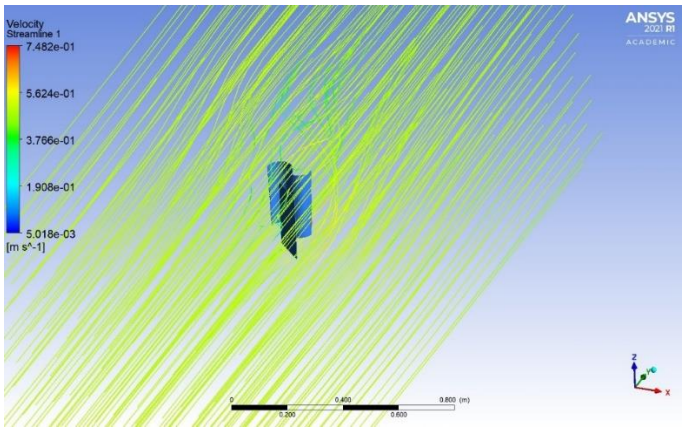

(c)

Fig. 4.22. Streamline for **12.5° twist angle** (a) no deflector (b) with deflector at 90° (c) with deflector at 45° at TSR = 0.7

4.5.3. Streamline for 25° twist angle of blades

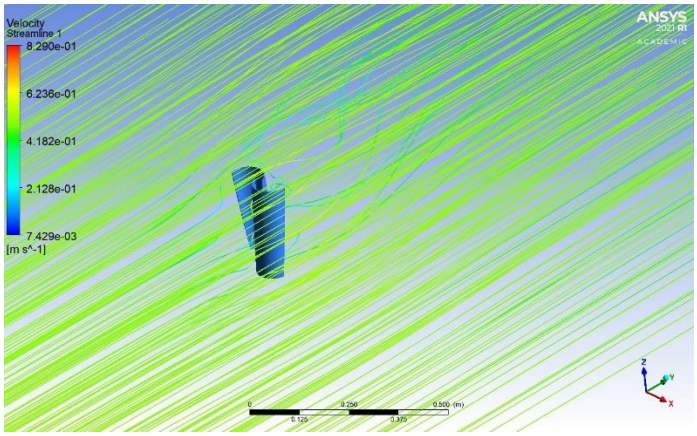

(a)

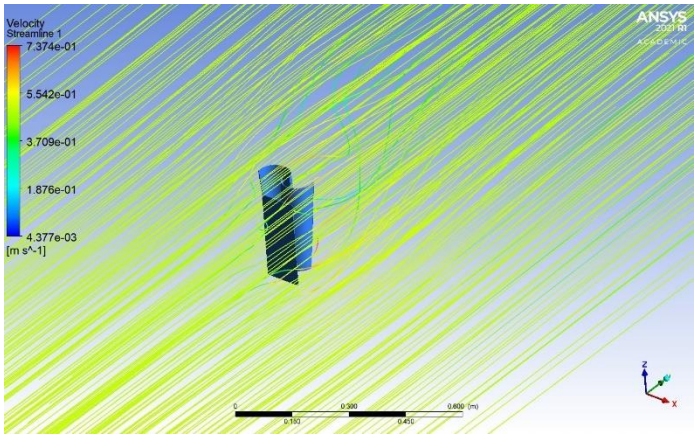

(b)

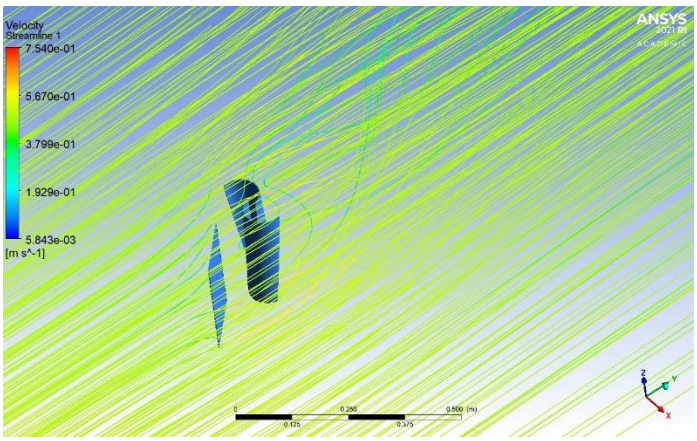

(c)

Fig. 4.23. Streamline for 25° twist angle (a) no deflector (b) with deflector at 90° (c) with deflector at 45° at TSR = 0.7

4.6. VARIATION OF POWER COEFF. (C_p) & TORQUE COEFF. (C_t) WITH RESPECT TO TIP SPEED RATIO

4.6.1. Variation for turbine with 0° twist angle of blades

Table 4.1. Power Coeff. (C_p) & Torque Coeff. (C_t) for **0° twist angle of blade without deflector plate** at equivalent tip speed ratio

Angular Speed (ω)	TSR	Torque (N-m)	C_p	C_t
3.125	0.5	0.061032	0.19130	0.153039368
3.75	0.6	0.061905	0.23284	0.155228686
4.375	0.7	0.058347	0.25604	0.146307422
5	0.8	0.057963	0.29068	0.145342277
5.625	0.9	0.05984	0.31735	0.150048897
6.25	1	0.054573	0.27368	0.136841775
6.875	1.1	0.039544	0.21815	0.099158225
7.5	1.2	0.037743	0.18171	0.094640421
8.125	1.3	0.020578	0.10062	0.05160005
8.75	1.4	-0.00182	-0.00639	-0.00456745
9.375	1.5	-0.01812	-0.06816	-0.04543982

Table 4.2. Power Coeff. (C_p) & Torque Coeff. (C_t) for **0° twist angle of blade with deflector plate at 90°** at equivalent tip speed ratio

Angular Speed (ω)	TSR	Torque (N-m)	C_p	C_t
3.125	0.5	0.180674	0.23784817	0.453044132
3.75	0.6	0.181108	0.28610341	0.454132397
4.375	0.7	0.175515	0.32347925	0.440107823

5	0.8	0.162699	0.342695988	0.407971414
5.625	0.9	0.14825	0.351294509	0.371740221
6.25	1	0.134457	0.343897041	0.337153962
6.875	1.1	0.123147	0.33967327	0.308793882
7.5	1.2	0.113936	0.325694684	0.285697091
8.125	1.3	0.101123	0.313156733	0.253568205
8.75	1.4	0.086417	0.303370662	0.21669333
9.375	1.5	0.063527	0.238943455	0.159295637

Table 4.3. Power Coeff. (C_p) & Torque Coeff. (C_t) for **0° twist angle of blade with deflector plate at 45°** at equivalent tip speed ratio

Angular Speed (ω)	**TSR**	**Torque (N-m)**	**C_p**	**C_t**
3.125	0.5	0.115904	0.188910732	0.290631896
3.75	0.6	0.117269	0.229362638	0.294054664
4.375	0.7	0.126179	0.287920988	0.31639669
5	0.8	0.126537	0.329986158	0.317294383
5.625	0.9	0.116075	0.340540998	0.291060682
6.25	1	0.089687	0.292359829	0.224892177
6.875	1.1	0.052433	0.188013445	0.131477934
7.5	1.2	0.023658	0.092544223	0.05932322
8.125	1.3	0.015392	0.065226881	0.038595787
8.75	1.4	0.015809	0.072146023	0.039640672
9.375	1.5	0.013341	0.065232585	0.033452608

Fig. 4.24. and 4.25. represents change in power coeff. and torque coeff. respectively at varying tip speed ratio for 0˚ angle of twist along with 3 configuration of deflector plate. We can observe from Fig.

4.24 and 4.25 that power coeff. and torque coeff. in case of turbine with deflector plate is higher than that of turbine without deflector plate which depicts that deflector plate is efficiently preventing the upstream water flow from striking the return blade, as a result minimizing drag and negative torque on blades and improving the self starting capacity of turbine. Now we will require less water velocity for turbine self start as compared to previous case of without any deflector plate.

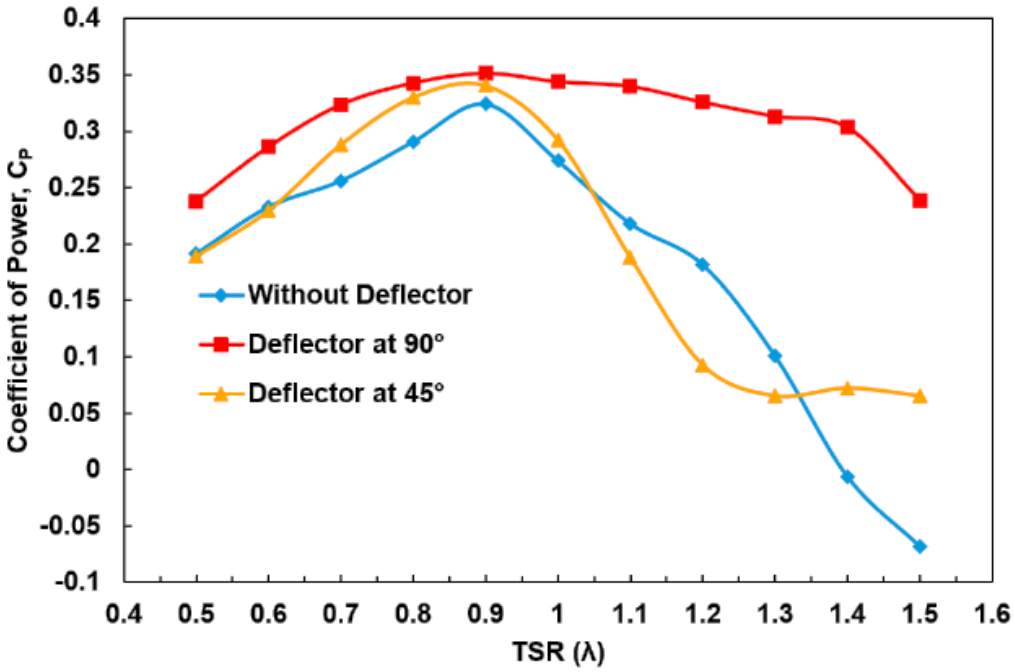

Fig. 4.24. Variation of **C_p** w.r.t. tip speed ratio for **0° twist angle of blade**

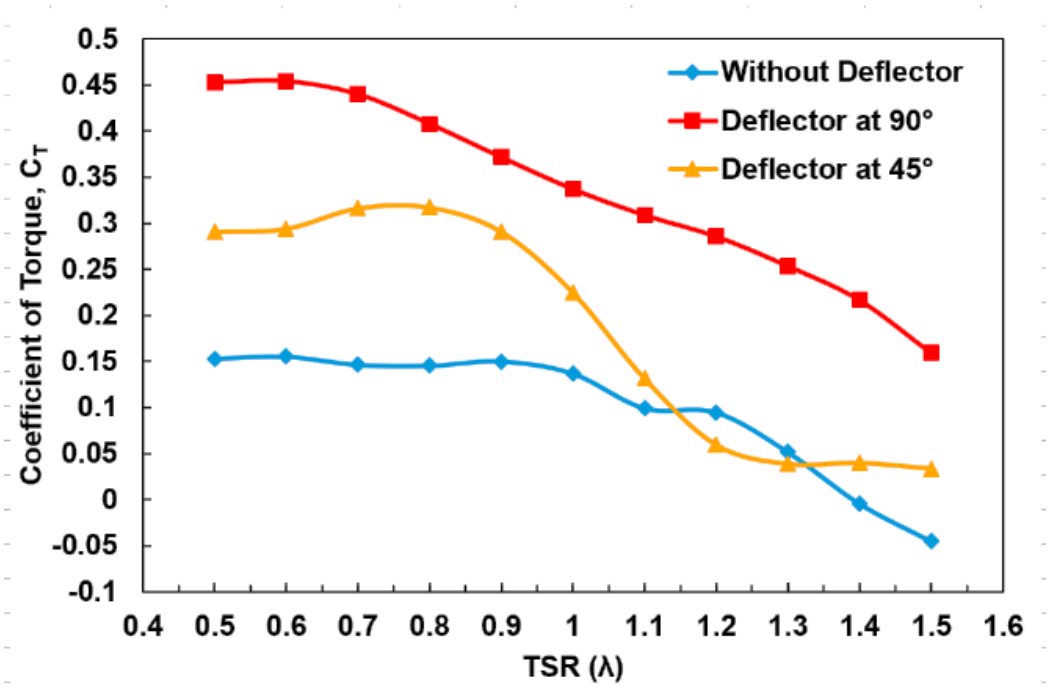

Fig. 4.25. Variation of **C_t** w.r.t. tip speed ratio for **0° twist angle of blade**

4.6.2. Variation for turbine with 12.5° twist angle of blades

Table 4.4. Power Coeff. (C_p) & Torque Coeff. (C_t) for **12.5° twist angle of blade without deflector plate** at equivalent tip speed ratio

Angular Speed (ω)	**Torque (N-m)**	**TSR**	**C_p**	**C_t**
3.125	0.061675	0.5	0.193314318	0.154651454
3.75	0.0647461	0.6	0.233787322	0.162352307
4.375	0.0598134	0.7	0.283468721	0.14998345
5	0.0577546	0.8	0.324398957	0.144820963
5.625	0.0581212	0.9	0.341032116	0.145740221
6.25	0.0539362	1	0.297541725	0.135246239
6.875	0.0438809	1.1	0.217864047	0.110032347
7.5	0.0337928	1.2	0.152525176	0.084736209
8.125	0.0168063	1.3	0.082177244	0.042142177
8.75	-0.00609605	1.4	-0.021400376	-0.01528598
9.375	-0.0222383	1.5	-0.083644559	-0.05576304

Table 4.5. Power Coeff. (C_p) & Torque Coeff. (C_t) for **12.5° twist angle of blade with deflector plate at 90°** at equivalent tip speed ratio

Angular Speed (ω)	**Torque**	**TSR**	**C_p**	**C_t**
3.125	0.180967	0.5	0.226889418	0.453778837
3.75	0.180029	0.6	0.270856068	0.45142678
4.375	0.180029	0.7	0.315998746	0.45142678
5	0.161434	0.8	0.35622347	0.404799398
5.625	0.146893	0.9	0.364654137	0.368337513
6.25	0.133343	1	0.334360582	0.334360582
6.875	0.12176	1.1	0.335847543	0.305315948
7.5	0.1119	1.2	0.33671013	0.280591775
8.125	0.0984427	1.3	0.320901479	0.246847292
8.75	0.0846691	1.4	0.297233551	0.212309679
9.375	0.0626035	1.5	0.235469534	0.156979689

Table 4.6. Power Coeff. (C_p) & Torque Coeff. (C_t) for **12.5° twist angle of blade with deflector plate at 45°** at equivalent tip speed ratio

Angular Speed (ω)	**Torque (N-m)**	**TSR**	**C_p**	**C_t**
3.125	0.114711	0.5	0.215730316	0.287640421
3.75	0.1203	0.6	0.253390171	0.301654965
4.375	0.125766	0.7	0.298016224	0.315361083
5	0.126542	0.8	0.329999198	0.317306921
5.625	0.115014	0.9	0.337428235	0.288400201
6.25	0.0911298	1	0.308488541	0.22851003

6.875	0.0570399	1.1	0.23599758	0.143028837
7.5	0.0299965	1.2	0.135390421	0.075216901
8.125	0.0184506	1.3	0.090217327	0.046265296
8.75	0.0155345	1.4	0.08180153	0.038953109
9.375	0.012005	1.5	0.067731319	0.030102808

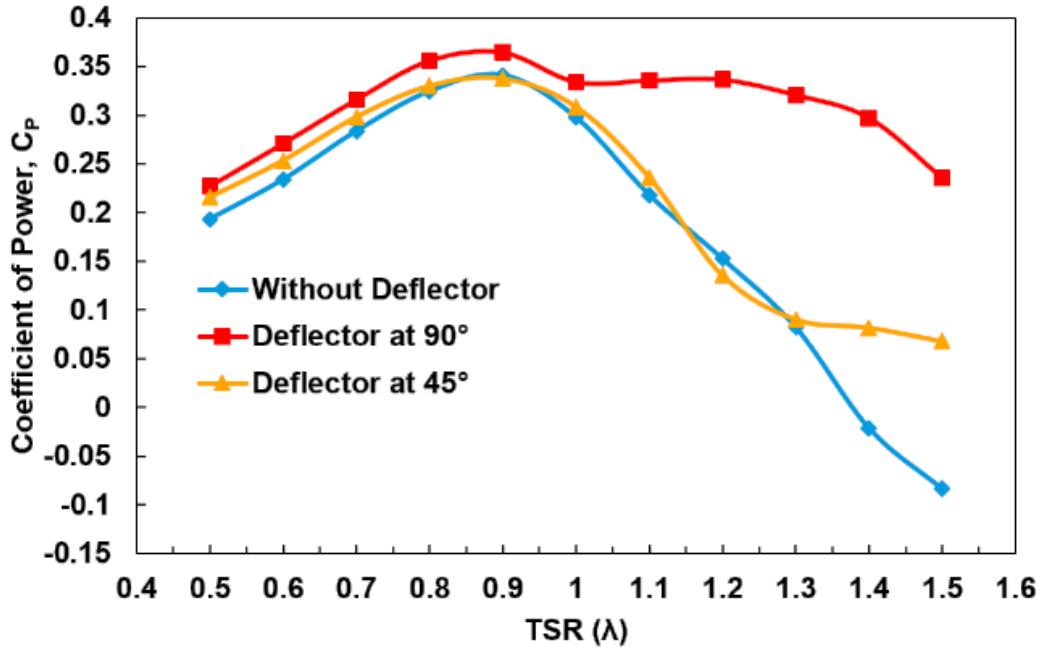

Fig. 4.26. Variation of C_p w.r.t. tip speed ratio for **12.5° twist angle of blade**

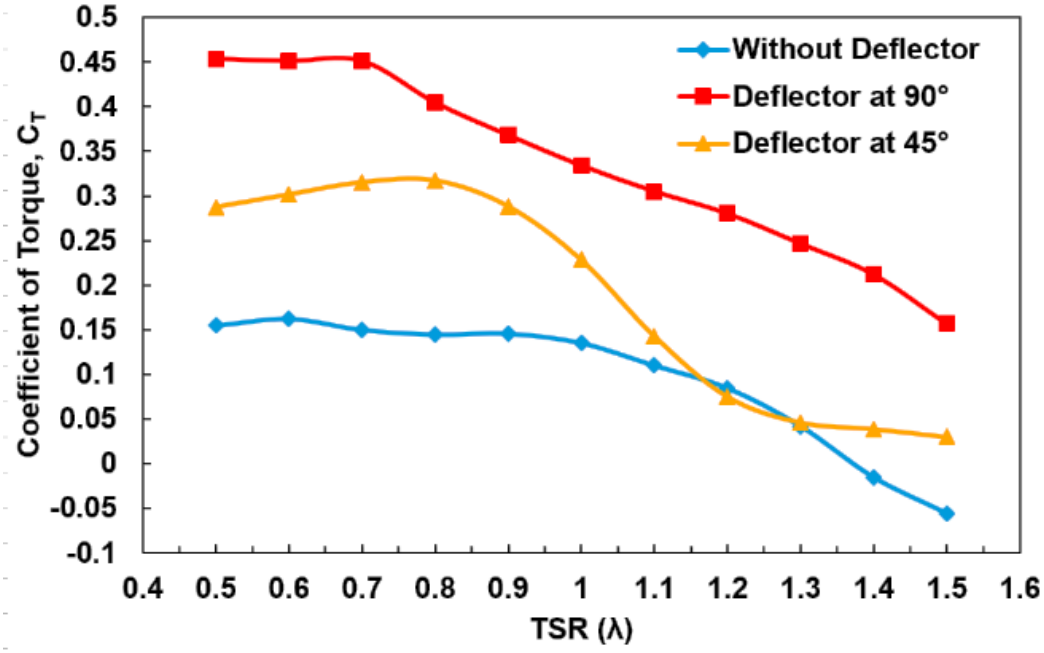

Fig. 4.27. Variation of C_t w.r.t. tip speed ratio for **12.5° twist angle of blade**

4.6.3. Variation for turbine with 25° twist angle of blades

Table 4.7. Power Coeff. (C_p) & Torque Coeff. (C_t) for **25° twist angle of blade without deflector plate** at equivalent tip speed ratio

Angular Speed (ω)	**Torque**	**TSR**	**C_p**	**C_t**
3.125	0.068285	0.5	0.171226179	0.171226179
3.75	0.0665108	0.6	0.210139438	0.166777332
4.375	0.0615943	0.7	0.23785161	0.154449097
5	0.0584313	0.8	0.269592758	0.146517803
5.625	0.0578606	0.9	0.287271785	0.14508676
6.25	0.0548974	1	0.234015998	0.137656469
6.875	0.0442713	1.1	0.19537986	0.111011284
7.5	0.0346286	1.2	0.166717432	0.086831996
8.125	0.01656	1.3	0.086371113	0.041524574
8.75	-0.00745332	1.4	-0.026165115	-0.01868937
9.375	-0.0236476	1.5	-0.088945336	-0.05929689

Table 4.8. Power Coeff. (C_p) & Torque Coeff. (C_t) for **25° twist angle of blade with deflector plate at 90°** at equivalent tip speed ratio

Ang. Speed (ω)	**Torque**	**TSR**	**C_p**	**C_t**
3.125	0.181168	0.5	0.238498495	0.454282849
3.75	0.178077	0.6	0.281315221	0.446532096
4.375	0.171024	0.7	0.315202207	0.42884654
5	0.15957	0.8	0.336105316	0.400125376
5.625	0.145199	0.9	0.344064832	0.364089769
6.25	0.131518	1	0.33638004	0.329784353

6.875	0.119503	1.1	0.336214559	0.299656469
7.5	0.109982	1.2	0.337557593	0.275782347
8.125	0.0978116	1.3	0.325221117	0.245264794
8.75	0.0858697	1.4	0.307477261	0.215320211
9.375	0.0655989	1.5	0.251670805	0.164490722

Table 4.9. Power Coeff. (C_p) & Torque Coeff. (C_t) for **25° twist angle of blade with deflector plate at 45°** at equivalent tip speed ratio

Ang. Speed (ω)	**Torque**	**TSR**	**C_p**	**C_t**
3.125	0.117954	0.5	0.17746339	0.295772317
3.75	0.124026	0.6	0.223918556	0.310997994
4.375	0.126821	0.7	0.267125476	0.31800652
5	0.125776	0.8	0.302770712	0.315386158
5.625	0.114395	0.9	0.309795888	0.286848044
6.25	0.0937265	1	0.282025577	0.235021314
6.875	0.0636604	1.1	0.210711454	0.15962989
7.5	0.0372468	1.2	0.134491956	0.093397192
8.125	0.0217393	1.3	0.085038385	0.054511785
8.75	0.0136707	1.4	0.057589709	0.034279589
9.375	0.00960105	1.5	0.043334729	0.02407485

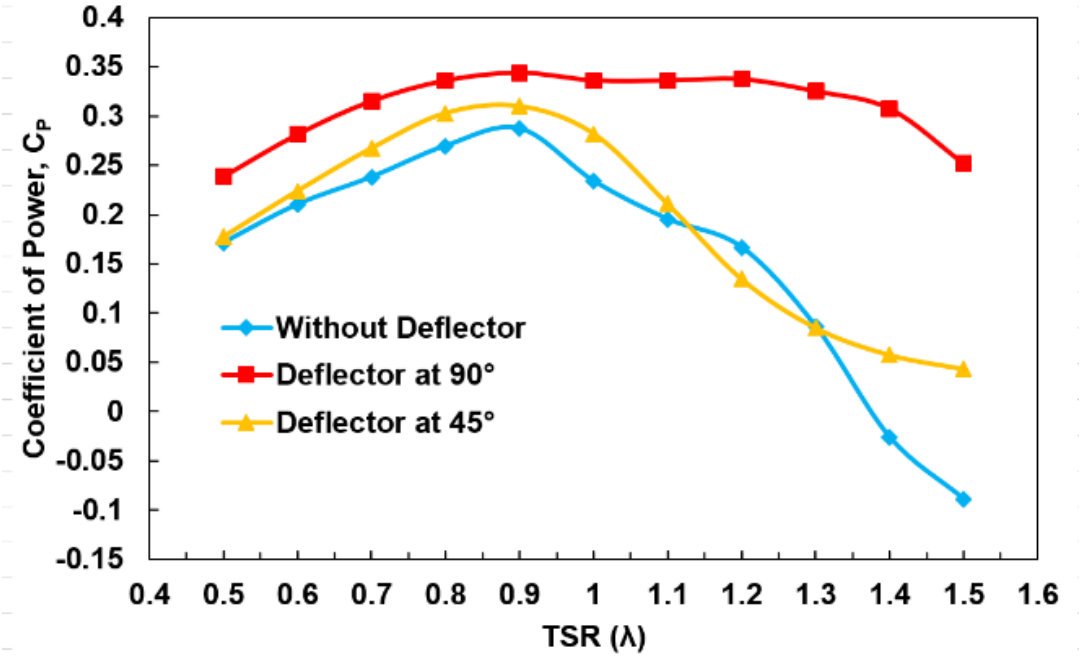

Fig. 4.28. Variation of C_p w.r.t. tip speed ratio for **25° twist angle of blade**

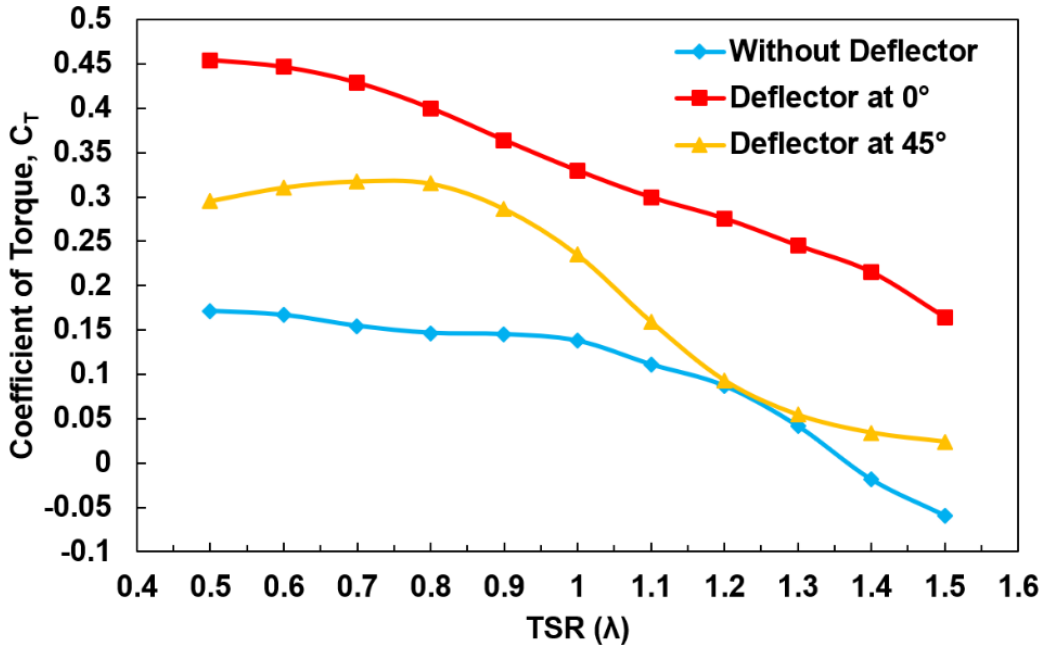

Fig. 4.29. Variation of C_t w.r.t. tip speed ratio for **25° twist angle of blade**

Table 4.10. provides the highest power coeff. (C_p), and tip speed ratio that corresponds for varying blade twist angles along with deflector configuration.

Table 4.10. Maximum power coefficient (C_p) corresponding to blade twist angle, deflector plate configuration, and tip speed ratio

Blade Twist Angle (°)	**Deflector plate configuration**	**Maximum Power Coefficient ($C_{p\ max}$)**	**Tip Speed Ratio**
0	w/o deflector plate	0.312	0.9
	deflector plate at 90°	0.351	0.9
	deflector plate at 45°	0.340	0.9
12.5	w/o deflector plate	0.341	0.9
	deflector plate at 90°	0.364	0.9
	deflector plate at 45°	0.337	0.9
25	w/o deflector plate	0.287	0.9
	deflector plate at 90°	0.344	0.9
	deflector plate at 45°	0.309	0.9

4.7. VARIATION OF POWER COEFF. (C_p) & TORQUE COEFF. (C_t) WITH RESPECT TO TWIST ANGLE OF BLADES CORRESPONDING TO DIFFERENT TSR

Fig. 4.30 - 4.35 illustrates change in power coeff. (C_p) and torque coeff. (C_t) w.r.t. twist angle of blades corresponding to different tip speed ratio along with different configuration of deflector plate. It is observed from Fig. 4.30-4.35 that when tip speed ratio increases, then power coeff. (C_p) and torque coeff. (C_t) but after tip speed ratio of 1.0 the power coeff. (C_p) and torque coeff. keeps on decreasing and if tip speed ratio is increased above 1.4 then coefficient of torque (C_t) becomes negative which shows inherent unsteady aerodynamic behaviour is taking place around the rotor if tip speed ratio is above 1.0. So, we may keep the tip speed ratio below 1.0 and operating SHT at tip speed ratio of above 1.4 is unfavourable.

4.7.1. Variation of C_p & C_t w.r.t. twist angle without deflector plate

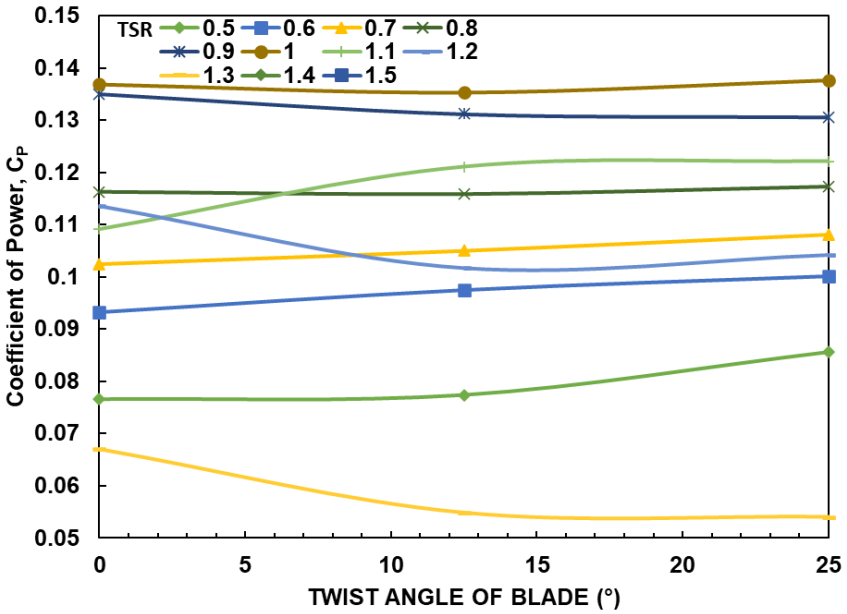

Fig. 4.30. Variation of **C_p** w.r.t. twist angle of blades corresponding to tip speed ratio of turbine **with no deflector plate**

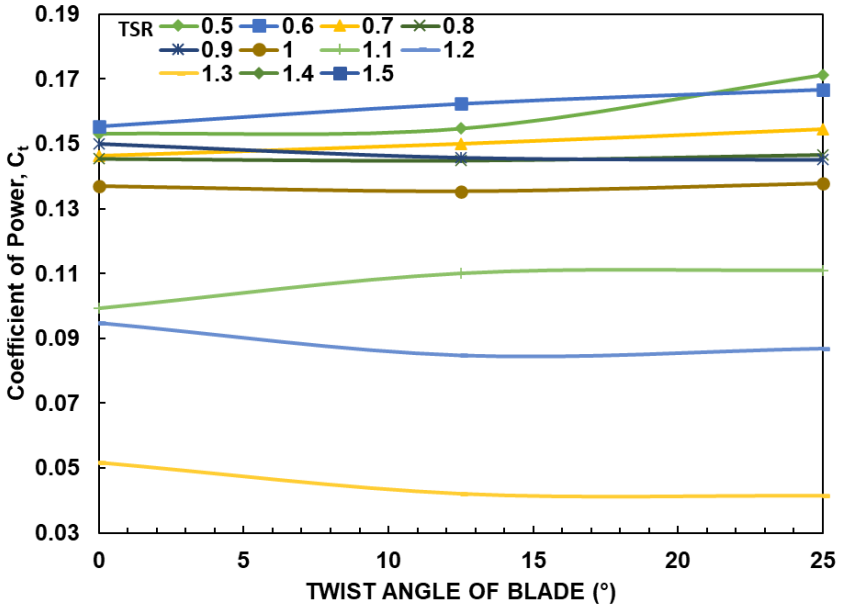

Fig. 4.31. Variation of $\mathbf{C_t}$ w.r.t. twist angle of blades corresponding to tip speed ratio for turbine **with no deflector plate**

4.7.2. Variation of C_p & C_t w.r.t. twist angle with deflector plate at 90˚

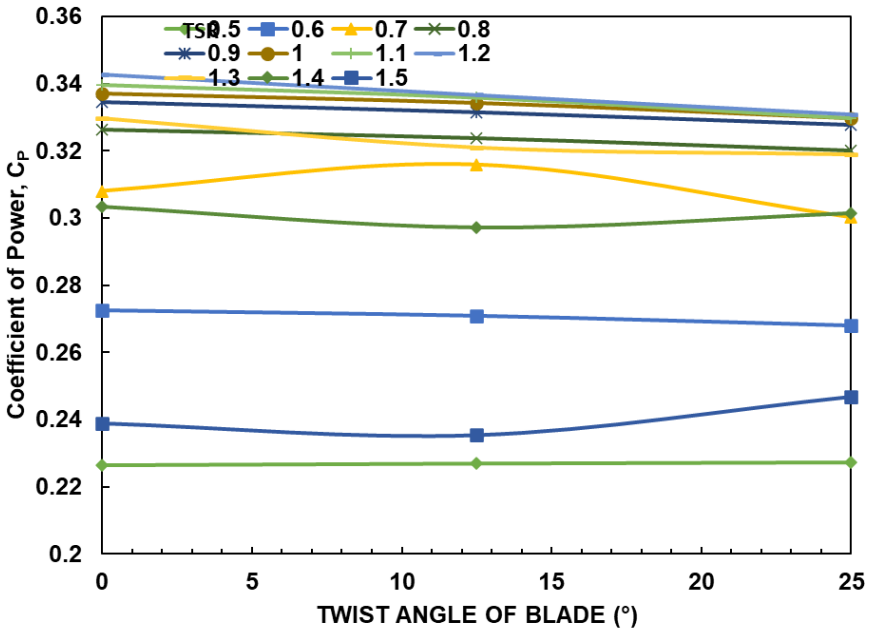

Fig. 4.32. Variation of $\mathbf{C_p}$ w.r.t. twist angle of blades corresponding to different tip speed ratio for turbine with **deflector plate at 90˚**

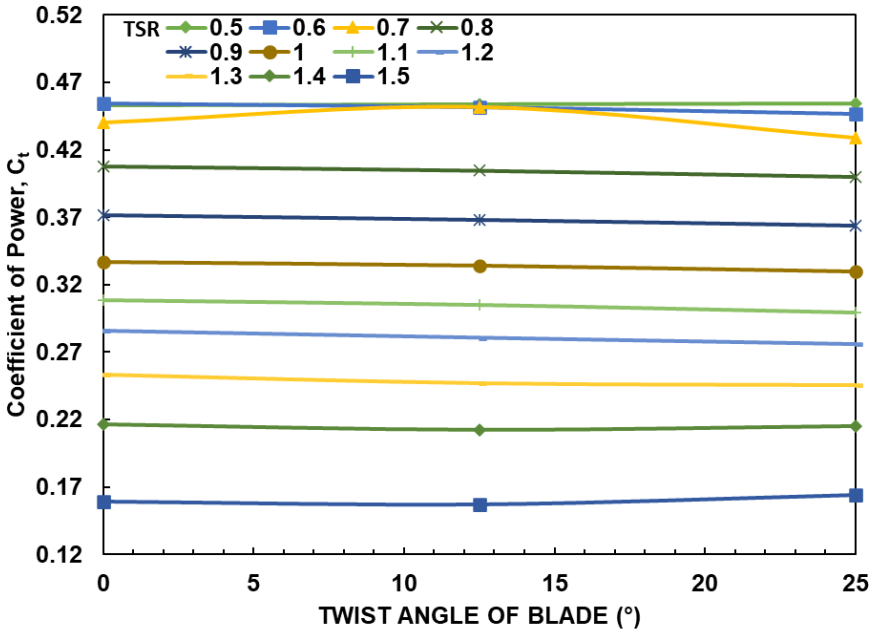

Fig. 4.33. Variation of $\mathbf{C_t}$ w.r.t. twist angle of blades corresponding to different tip speed ratio for turbine with **deflector plate at 90˚**

4.7.3. Variation of C_p & C_t w.r.t. twist angle with deflector plate at 45˚

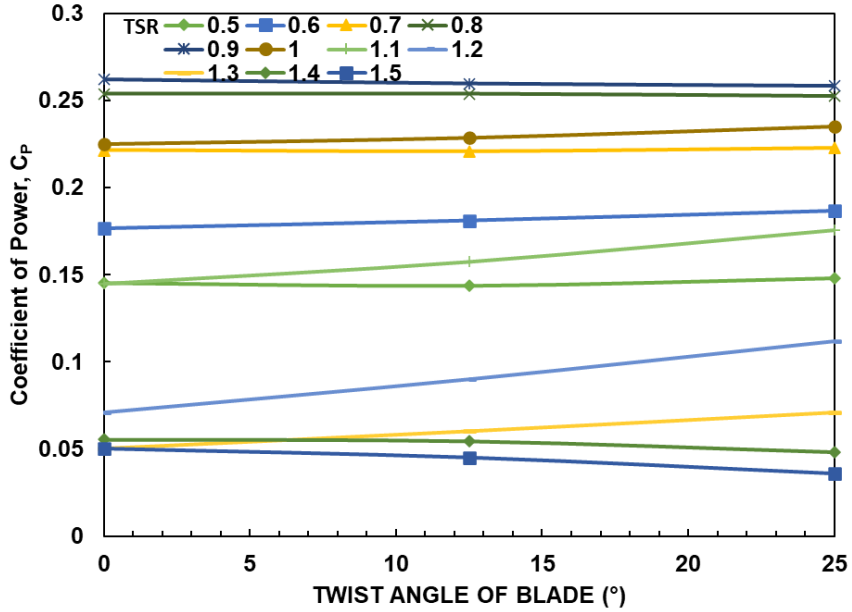

Fig. 4.34. Variation of $\mathbf{C_p}$ w.r.t. twist angle of blades corresponding to different tip speed ratio for turbine with **deflector plate at 45˚**

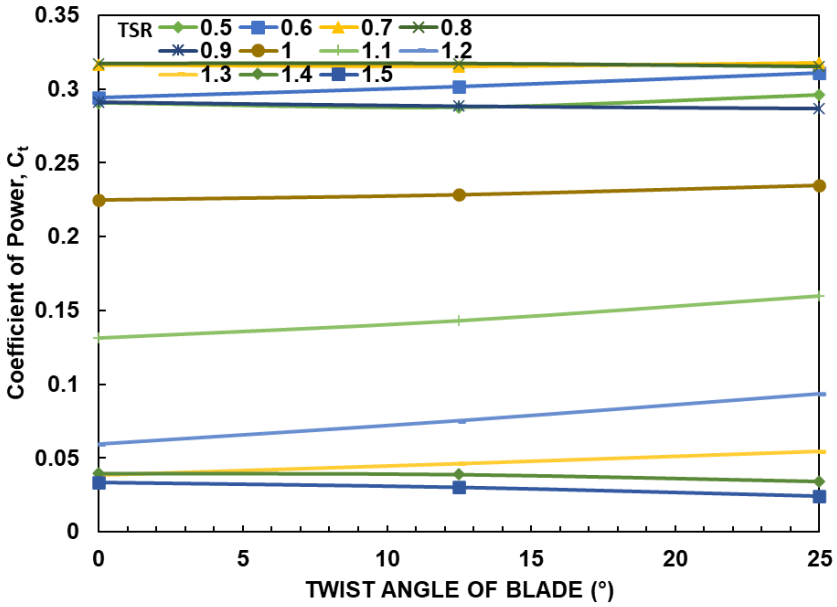

Fig. 4.35. Variation of C_t w.r.t. twist angle of blades corresponding to different tip speed ratio for turbine with **deflector plate at 45**°

4.8. VALIDATION

The results for SHK Turbine having twist angle of 0°, 6.25°, 25° with no deflector plate have been validated from Kumar et al. [20]. Tip speed ratio considered is 0.9 with 0.5 m/s as free stream velocity. The summarized table 4.10. is shown below:

Table 4.11. Validation of results obtained in this research

Twist Angle (°)	**Tip Speed Ratio**	**V1 (m/s)**	**Present Study - Power Coeff. (C_p)**	**Kumar et al. - Power Coeff. (C_p)**	**Error %**
0	0.9	0.5	0.312	0.31	0.64
12.5	0.9	0.5	0.341	0.34	0.29
25	0.9	0.5	0.282	0.28	0.71

CHAPTER 5

CONCLUSIONS

According to the simulation findings, the turbine's efficiency in terms of coeff. of power has max. C_p of 0.364 at a tip speed ratio of 0.9 at a 12.5° blade angle of twist with deflector plate at 90° and 0.5 m/s water velocity. The max. value of coeff. of torque C_t for the turbine's performance is 0.454 at tip speed ratio value 0.5 at blade twist angle of 25° with deflector plate at 90° and 0.5 m/s free stream velocity of water. It is noted that as the TSR value increases, coeff. of power (C_p) first increases and afterwards decreases but there is decrease in coefficient of torque (C_t), so it is recommender to keep the TSR in the range of 0.7-0.9 for improved efficiency of Savonius turbine.

Considering varying C_p based on twist angle of blade then we can observe that C_p may increase or decrease based on tip speed ratio value and deflector plate angle (δ). Example, SHT with deflector plate at 90° shows that for TSR = 0.7 the C_p value keeps on decreasing as we increase the twist angle but for TSR = 0.8 and TSR = 0.9 the C_p value first increases till blade twist angle of 12.5° and thereafter decreases. But for TSR = 1 the C_p value first decreases till blade twist angle of 12.5° and thereafter increases as we increase the blade twist angle. It is also observed from the analysis that when tip speed ratio is increased above 1.4 then coefficient of torque (C_t) becomes negative

which shows inherent unsteady aerodynamic behaviour. So we may concluded that operating SHT at tip speed ratio of above 1.4 is unfavourable.

The current study might be valuable for future research into performance of Savonius hydrokinetic turbines with different system parameters for example blade geometry, various stages, blade arc angle and operational factors such as blockage ratio and fluid velocity. The scope for further improvisation is still open to further study and development, and will undoubtedly help us meet rising power demand by achieving renewable energy.

References

[1] I. Loots, D. M. Van, B. Barta,S. V. Van, and J. Bhagwan, “A review of low head hydropower technologies and applications in a South African context,” *Renewable and Sustainable Energy Reviews*, vol. 50(C), pp. 1254 - 68, 2015.

[2] "World Energy Outlook 2019," International Energy Agency, Paris, 2019.

[3] “CO2 emissions Analysis - Global Energy Review,” International Energy Agency, Paris, 2021.

[4] “Renewable Capacity Statistics,” International Renewable Energy Agency (IRENA), Abu Dhabi, 2022.

[5] “Renewable Energy Policy Network for the 21st century (2018) - Global Status Report.” Renewables, Paris, 2018.

[6] T. Tanbhir, U. Nawshad, N. Islam, I. Sina, K. Syfullah, and R. Raiyan, “Micro hydro power: promising solution for off-grid renewable energy source,” *International Journal of Scientific and Engineering Research*, vol. 2(12), pp. 1 - 5, 2011.

[7] M. J. Khan, M. T. Iqbal, and J. E. Quaicoe, “River current energy conversion system: progress, prospects and challenges,” *Renewable and Sustainable Energy Reviews*, vol. 12, pp. 2177 - 2193, 200).

[8] H. J. Vermaak, K. Kusakana, and S. P. Koko, “Status of micro-hydrokinetic river technology in rural applications: A review of literature,” *Renewable and Sustainable Energy Reviews*, vol. 29, pp. 625 - 633, 2014.

[9] M. Balat, “Hydropower systems and hydropower potential in the European Union countries,” *Energy Sources, Part A: Recovery, Utilization and Environmental Effects*, vol. 28 (10), pp. 965 - 978, 2006.

[10] M. A. Kamoji, S. B. Kedare, and S. V. Prabhu, “Experimental investigation on the effect of overlap ratio and blade edge conditions on the performance of conventional Savonius rotor,” *Wind Engineering*, vol. 32(2), pp. 163 - 178, 2008.

[11] "Vertical wind turbine," [Online]. Available: http://energythic.com/view.php?node=201.

[12] S. Savonius, "The S-rotor and its applications," *Mechanical Engineering*, vol. 53(5), pp. 333 - 38, 1931.

[13] J. V. Akwa, H. A. Vielmo, and A. P. Petry, "A review on the performance of Savonius wind turbines," *Renewable and Sustainable Energy Reviews*, vol. 16(5), pp. 3054 - 3064, 2012.

[14] B. D. Altan, and M. Atilgan, "An experimental and numerical study on the improvement of the performance of Savonius wind rotor," *Energy Conversion and Management*, vol. 49(12), pp. 3425 - 3432, 2008.

[15] B. Wahyudi, S. Soeparman, S. Wahyudi, and W. Denny, "A simulation study of Flow and Pressure distribution patterns in and around of Tandem Blade Rotor of Savonius (TBS) Hydrokinetic turbine model," *Journal of Clean Energy Technologies,* vol. 1, pp. 286 - 291, 2013.

[16] R. Dagur, V. Singh, S. Grover, N. Sethi, and B. B. Arora, "Design of flying wing UAV and effect of winglets on its performance," *International Journal of Emerging Technology and Advanced Engineering*, vol. 8(3), pp. 414 - 28, 2018.

[17] U. K. Saha , and M. J. Rajkumar, "On the performance analysis of Savonius rotor with twisted blades," *Renewable Energy,* vol. 31(11), pp. 1776 - 88 2006.

[18] J. V. Akwa, H. A. Vielmo, and A. P. Petry, "A review on the performance of Savonius wind turbines," *Renewable and Sustainable Energy Reviews*, vol. 16(5), pp. 3054 - 64, 2012.

[19] U. K. Saha, S. Thotla, and D. Maity. "Optimum design configuration of Savonius rotor through wind tunnel experiments," *Journal of Wind Engineering and Industrial Aerodynamics*, vol. 96 (8–9), pp. 1359 - 75, 2008.

[20] A. Kumar, and R. P. Saini, "Performance analysis of a Savonius hydrokinetic turbine having twisted blades," *Renewable Energy,* vol. 108, pp. 502 - 522, 2017.

[21] L. Pham. "Riverine Hydrokinetic Technology: A Review," *Oregon Tech – REE516 Term Paper*, 2014.

[22] R. E. Sheldahl, L. V. Feltz, and B. F. Blackwell, “Wind tunnel performance data for two and three-bucket Savonius rotors,” *Journal of Energy*, vol. 2(3), pp. 160 - 64, 1978.

[23] Z. Zhao, Y. Zheng, X. Xu, W. Liu, and G. Hu, “Research on the Improvement of the Performance of Savonius Rotor Based on Numerical Study,” *In: Proceedings of international conference on sustainable power generation and supply (SUPERGEN)*, pp. 1 - 6, 2009.

[24] G. Kailash, T.I. Eldho, and S.V. Prabhu. “Performance study of modified Savonius water turbine with two deflector plates,” *International Journal of Rotating Machinery*, vol. 2012, pp. 12, 2012.

[25] M. A. Kamoji, S. B. Kedare, and S. V. Prabhu, “Experimental investigations on single stage modified Savonius rotor,” *Applied Energy*, vol. 86(7–8), pp. 1064 - 73, 2009.

[26] K. Golecha, T. I. Eldho, S. V. Prabhu, “Influence of the deflector plate on the performance of modified Savonius water turbine,” *Applied Energy*, vol. 88, pp. 3207 - 17, 2011.

[27] K. Golecha, T. I. Eldho, and S. V. Prabhu, “Performance study of modified savonius water turbine with two deflector plates,” *International Journal of Rotating Machinery*, vol. 2012, Article ID 679247, pp. 12, 2012.

[28] E. Kerikous, and D Thevenin, “Optimal shape of thick blades for a hydraulic Savonius turbine,” *Renewable Energy*, vol. 134, pp. 629 - 638. 2019.

[29] B. B. Arora, and B. D. Pathak, "Effect of geometry on the performance of annular diffuser," *International Journal of Applied Engineering Research 5*, vol. 20, pp. 2639 - 52, 2009.

[30] H Singh, B.B Arora, “Effect of Area Ratio on Flow Separation in Annular Diffuser,” *Advances in Fluid and Thermal Engineering*, vol. 2019, pp. 297 – 305, 2019.

[31] A. Grönman, J. Tianinen, and A. Jaatinen-Värri, “Experimental and analytical analysis of vaned Savonius turbine performance under different operating conditions,” *Applied Energy*, vol. 250, pp. 864 - 872, 2019.

[32] S. Iio, Y. Katayama, F. Uchiyama, E. Sato, and T Ikeda, “Influence of setting condition on characteristics of Savonius hydraulic turbine with a shield plate,” *Journal of Thermal Science*, vol. 20(3), pp. 224 - 228, 2011.

[33] S. Bhattacharjee, B. B. Arora, and V Kashyap, “Optimization of Race Car Front Splitter Placement Using CFD,” *SAE Technical Paper 2019-01-5097,* 2019.

[34] M. H. Mohamed, G. Janiga, E. Pap, and D. Thévenin, “Optimization of Savonius turbines using an obstacle shielding the returning blade,” *Renewable Energy*, vol. 35(11), pp. 2618 - 2626, 2010.

[35] H. Singh, and B. B. Arora, “Performance characteristics of flow in annular diffuser using CFD,” *International Journal of Turbo & Jet-Engines*, vol. 2021, pp. 1 - 11, 2021.